NTNU – Trondheim
Norwegian University of
Science and Technology

Hydraulic design of a Francis turbine that will be influenced by sediment erosion

Gjert Aaberge Dahl

Master of Energy and Environmental Engineering
Submission date: June 2014
Supervisor: Ole Gunnar Dahlhaug, EPT
Co-supervisor: Torbjørn Nielsen, EPT
Biraj Singh Thapa, EPT

Norwegian University of Science and Technology
Department of Energy and Process Engineering

NTNU
Norwegian University
of Science and Technology

Department of Energy
and Process Engineering

EPT-M-2014-21

MASTER THESIS

for

Gjert Aaberge Dahl

Spring 2014

Hydraulic design of a Francis turbine that will be influenced by sediment erosion
Hydraulisk design av Francis turbin utsatt for sediment erosjon

Background

Sediment erosion in Francis turbines is a large problem for river power plants near the Himalayas and the Andes Mountains. Due to high sediment concentration in the rivers the turbine components are exposed to erosion wear and must be maintained often. During monsoon periods, the sediment concentration is at its highest and the turbines are stopped to reduce the damage on the components. The turbines at Cahua Power Plant in Peru and Jhimruk Power Plant in Nepal are a good example on how the sediment erosion effects the power plant operation. These turbines need to be maintained annually due to high erosion wear. This result in a reduction of energy production and high maintenance cost. It is therefore of interest to design a new Francis turbine which is more resistant to sediment erosion. A cooperation between Kathmandu University and NTNU has started and aim to start manufacture Francis turbines that can withstand high sediment load. The development has focused on the erosion in the runner alone. In this study, the student will investigate the erosion in both guide vanes and runner.

Objective

The aim is to define a hydraulic design of a runner and guide vanes in a Francis turbine which can handle large sediment load

The following tasks shall be considered in the project work

1. Literature survey
   a. Hydraulic and mechanical design of Francis turbines
   b. Sediment erosion in Francis turbines and relevant materials/ coating

2. Software knowledge
   a. Get familiar with the CAD-tool; Pro-Engineer/ Creo

3. The student will carry out the hydraulic design of runner and guide vanes in a Francis turbine with focus on different parameters:
   a. Sediment concentration
   b. Water velocity
   c. Impingement angle of the sediment to the material surface

Within 14 days of receiving the written text on the master thesis, the candidate shall submit a research plan for his project to the department.

When the thesis is evaluated, emphasis is put on processing of the results, and that they are presented in tabular and/or graphic form in a clear manner, and that they are analyzed carefully.

The thesis should be formulated as a research report with summary both in English and Norwegian, conclusion, literature references, table of contents etc. During the preparation of the text, the candidate should make an effort to produce a well-structured and easily readable report. In order to ease the evaluation of the thesis, it is important that the cross-references are correct. In the making of the report, strong emphasis should be placed on both a thorough discussion of the results and an orderly presentation.

The candidate is requested to initiate and keep close contact with his/her academic supervisor(s) throughout the working period. The candidate must follow the rules and regulations of NTNU as well as passive directions given by the Department of Energy and Process Engineering.

Risk assessment of the candidate's work shall be carried out according to the department's procedures. The risk assessment must be documented and included as part of the final report. Events related to the candidate's work adversely affecting the health, safety or security, must be documented and included as part of the final report. If the documentation on risk assessment represents a large number of pages, the full version is to be submitted electronically to the supervisor and an excerpt is included in the report.

Pursuant to "Regulations concerning the supplementary provisions to the technology study program/Master of Science" at NTNU §20, the Department reserves the permission to utilize all the results and data for teaching and research purposes as well as in future publications.

The final report is to be submitted digitally in DAIM. An executive summary of the thesis including title, student's name, supervisor's name, year, department name, and NTNU's logo and name, shall be submitted to the department as a separate pdf file. Based on an agreement with the supervisor, the final report and other material and documents may be given to the supervisor in digital format.

☐ Work to be done in the Waterpower laboratory
☐ Field work

Department of Energy and Process Engineering, 14. January 2014

Olav Bolland
Department Head

Ole Gunnar Dahlhaug
Academic Supervisor

Research Advisors/ co-supervisors:

Torbjørn K. Nielsen, Professor	torbjorn.nielsen@ntnu.no
Biraj Singh Thapa, PhD-student	biraj.s.thapa@ntnu.no

Preface

This Master thesis is the result of the work performed by stud. techn. Gjert Aaberge Dahl at the Waterpower Laboratory, Department of Energy and Process Engineering at Norwegian University of Science and Technology during spring 2014. The work is a continuation of the Project thesis carried out in fall 2013, where the base theory and basic design methods for erosion resistant runners were covered.

The aim of the Master is to define several guide vane designs and compare the change in erosion tendency using CFD.

When the work on the Project thesis first started in August 2013 I had no experience with the different softwares necessary in this work. The first step was to define a reference model using the Matlab based design tool Khoj developed at the Waterpower Laboratory. The original design reference was the Tokke turbine in Norway, but several issues with the software made me change the reference design from Tokke to Jhimruk turbine in Nepal.

Learning the Ansys meshing and simulations system was a challenging process with a steep learning curve. Simple tasks that in the beginning could take an hour to perform would in the end of the work be finished in bare minutes. Through the work I have gained knowledge on both the simulation process and the meshing quality, understanding both how to create a mesh of high quality and what parameters that will affect the result.

The work has been both challenging and inspiring, as the different problems through the work went from impossible to solvable. There are several people I would like to thank for invaluable support through the process. First I would like to thank my supervisor professor Ole Gunnar Dahlhaug for his patience with my questioning. I would also like to thank my co-supervisors Torbjørn K. Nielsen and PhD-candidate Biraj Singh Thapa for their support. In addition to these, the PhD-candidates Bjørn Winter Solemslie, Peter Joachim Gogstad and Krishna Prasad Shrestha have been available for questions during the thesis period and Mette Eltvik in Voith and Kristine Gjøsæter in Energiselskapet Buskerud have been helpful during the process. At last I want to thank the students at the Waterpower Laboratory for their contribution both academically and socially.

Gjert Aaberge Dahl

Gjert Aaberge Dahl
Trondheim, June 10, 2014

Summary

High amount of sediments in the Himalayas are at present a large problem for power companies in Nepal, preventing them of utilizing the large amount of hydro power available in the area. In the Jhimruk power plant the sediment load makes it necessary to repair the system once a year, and the power plant is shut down if the concentration of sediments is exceeding 3000 ppm. Several different measures have been tried to minimize the wear on the system.

This Master thesis describes the theoretical definition of erosion and examines both designs and materials affecting erosion. The work is based on earlier work and strives for better design of Jhimruk power plant. The main objective of the thesis is to define different guide vane designs that affect and reduce sediment erosion in a Francis turbine. The work is carried out using several NACA designs for the guide vanes and implementing sediments in the flow to simulate sediment erosion. The assignment include utilization of several programs, including the Matlab-based design tool Khoj, the meshing tools Ansys Turbogrid and Ansys ICEM, and the CFD calculation tool Ansys CFX.

The simulations in Ansys CFX are done using the Tabakoff erosion model. The erosion on the reference parts show similar tendencies as previous work, while the new designs in general show heighten erosion tendency. The simulations show in general the same tendency for the reference runner and the optimal runner.

The results produced in this thesis show the difference in sediment erosion handling by different guide vane profiles, affecting the pressure distribution along the guide vanes and thus disrupting the inlet conditions on the runner. In this thesis the implementation of NACA 2412 enhancing the pressure difference across the guide vane shows the best effect of erosion reduction, while the design changes equalizing this pressure difference generally show an increased erosion tendency along the runner. The results are opposite of the expected results.

The implementation of the optimal runner design show that the use of NACA 4412 with pressure difference enhancing effect reduces the erosion maximum for the design changes.

Samandrag

Store mengder sediment i Himalaya-fjella er i dag eit stort problem for kraftselskap i Nepal, sidan det hindrar dei å utnytte seg av dei store vasskraftressursane som er tilgjengeleg i området. I Jhimruk kraftverk er sedimentlasta så stor at ein må reparere turbinane kvart år og kraftverket blir kopla ut ved sedimentlast tilsvarande 3000 ppm. Det er prøvd mange ulike tiltak for å redusere erosjonsproblema.

Denne masteroppgåva skildrar den teoretiske definisjonen av sedimentær erosjon og tek for seg både design og materialval som påverkar erosjonen. Oppgåva baserer seg på tidlegare oppgåver og streber mot å definere gode tiltak for å redusere erosjon. Hovudmålet med denne oppgåva er å definere ulike design for leieapparat som påverkar og reduserer sedimenterosjon i ein Francisturbin. Arbeidet er utført ved å nytte ulike NACA profil som leieapparat og implementere sediment i straumen for å simulere sedimentær erosjon. Oppgåva inkluderer bruken av fleire programvarer, som det Matlabbaserte designverktøyet Khoj, meshingprogramvarene Ansys Turbogrid og Ansys ICEM, og CFD kalkulatoren Ansys CFX.

Simuleringane i Ansys CFX er gjennomført ved å bruke Tabakoff-erosjonsmodellen, med observasjon av 5000 partiklar. Resultata frå Ansys CFX viser ein motsett tendens frå det som var forventa ut frå hypotese. Resultata viser generelt same tendens for både referanseløpehjulet og det optimaliserte løpehjulet.

Resultata oppnådd i denne oppgåva viser korleis ulik implementering av ulike design av ledeapparat påverkar den sedimentære erosjonen i ein Francisturbin. Resultata viser at særleg implementering av NACA 2412 med aukande trykkskilnad over bladet har god påverknad på erosjonen grunna homogen strøyming. Generelt viser resultata for den antekne positive designendringa ei auke av erosjonstendensane på løpehjulet. Resultata er motsett av den orginale hypotesa.

Ved bruk av optimalisert løpehjul viser testane at implementering av NACA 4412 med aukande trykkskilnad over bladet har ynskt effekt på erosjonen.

Contents

1 Introduction **1**
1.1 Hydropower in Nepal . . . 1
1.2 Hydropower in Norway . . . 2
1.3 Objective . . . 2

2 Previous work **3**

3 Wear **5**
3.1 Abrasive wear . . . 5
3.2 Erosive wear . . . 6

4 Sediments **9**
4.1 Sediment types . . . 9
4.2 Characteristics of sediment . . . 10
4.2.1 Size and shape . . . 10
4.3 Density of sediment in the flow . . . 11

5 Materials **13**

6 Hydraulic design **15**
6.1 Guide Vanes . . . 15
6.1.1 NACA Profiles . . . 16
6.1.2 Design . . . 17
6.2 Runner . . . 18

7 CFD **19**
7.1 Turbulence model . . . 19
7.2 Grid specifications . . . 20
7.2.1 Mesh independency . . . 22
7.2.2 Boundary conditions . . . 22
7.3 Simulation Process . . . 24
7.3.1 Sediment simulation . . . 25
7.4 Mesh size . . . 26
7.4.1 Mesh dependent erosion . . . 26

8 Results **29**
8.1 Main dimensions . . . 29
8.2 Guide vane design . . . 31
8.3 Pressure distribution . . . 32
8.3.1 Positive design changes . . . 32
8.3.2 Negative design changes . . . 34
8.4 Velocity profile . . . 35
8.4.1 Positive design . . . 35
8.4.2 Negative design . . . 40

8.5 Erosion 44
8.5.1 Positive design 44
8.5.2 Negative design 46
8.6 Optimal design change 48
8.6.1 Positive design 48
8.6.2 Negative design 49
8.7 Possible definition errors 50
8.7.1 Velocity vector difference 50
8.7.2 Velocity vector direction 50
8.7.3 Mesh dependent erosion 53

9 Discussion **55**
9.1 Pressure 55
9.1.1 Positive design 56
9.1.2 Negative design 56
9.2 Velocity 57
9.2.1 Positive design 57
9.2.2 Negative design 57
9.3 Erosion 58
9.3.1 Positive design 59
9.3.2 Negative design 59
9.3.3 Summary 60
9.4 Optimal design 61
9.5 Material choice 62
9.6 Possible simulation errors 62
9.7 Design flaws 64

10 Conclusion **67**

11 Further work **69**

A Basic design of a Francis turbines **I**

B CFD **V**
B.1 Basic equations V
B.2 Turbulence models V

C Khoj **VII**

D Erosion models **XIII**
D.1 Bergeron's model XIII
D.2 Tsuguo's model XIII
D.3 The IEC model XIII
D.4 Tabakoff's model XIV

E Mesh Independency **XV**

F Guide for sediment definition in CFX-Pre **XVIII**
F.1 Defining environment XVIII
F.2 Defining the Properties of Quartz XX
F.3 Defining the flow XXI

G Parameters from Khoj **XXV**

H Figures from CFX **XXVII**
H.1 Reference blade pressure XXVII
H.1.1 Positive design XXVII
H.1.2 Negative design XXX
H.2 Optimal design streamlines XXXIII
H.2.1 Positive design XXXIII
H.2.2 Negative design XXXVI
H.3 Velocity vector direction XXXIX

I Efficiency calculations **XL**

J ANSYS report **XLII**

List of Figures

1.1 Erosion on machinery in Kali Gandaki, Nepal (Photo: Kristoffer Vegdal Tabutiaux). 1
3.1 Four types of abrasive wear in a hydraulic flow (Stachowiak and Batchelor, 1993). 5
3.2 Four subcategories of erosive wear in hydraulic flows (Stachowiak and Batchelor, 1993). 6
4.1 Equipment at Kali Gandaki power plant, Nepal (Photo: Kristoffer Vegdal Tabutiaux). 10
4.2 Effect of particle size on mode and rates of erosive wear. (Hojo et. al., 1986). 11
5.1 Erosion tendency at different impingement angles at $30m/s$ velocity (Stachowiak and Batchelor, 1993). 13
6.1 Secondary flows on guide vanes(Kristine Gjøsæter, 2011). . . 15
6.2 Curvature of the guide vane profiles used in the work. 17
6.3 Design flaw in Turbogrid at the trailing edge of NACA 4412. 17
7.1 SST-function, adapted from Ansys release notes (Thapa, 2011). 19
7.2 ATM Optimized topology for the reference runner for a structured mesh produced in Turbogrid. 20
7.3 Properties outside of mesh specifications for runner blade, Ansys Turbogrid. 21
7.4 Wall function of turbulence, adapted from Ansys manual(Gogstad, 2012). 22
7.5 Computational domain of the work in Ansys CFX. 23
7.6 Mesh properties, Ansys Turbogrid. 24
7.7 Merged mesh 25
7.8 Mesh sizes from Turbogrid. 27
8.1 Pressure distribution in the system, positive design changes. . 32
8.2 Pressure distribution at guide vane outlet, positive designs. . 33
8.3 Pressure distribution in the system, negative designs. 34
8.4 Pressure distribution at guide vane outlet, negative designs. . 35
8.5 Velocity streamlines at guide vanes, positive design changes. . 36
8.6 Velocity streamlines at runner blade, positive design changes. 37
8.7 Velocity lines along the blade, pressure side, positive design changes. 38
8.8 Velocity lines along the blade, suction side, positive design changes. 39
8.9 Velocity streamlines at guide vane, negative design changes. . 40
8.10 Velocity streamlines at runner blade, negative design changes. 41
8.11 Velocity lines along the blade, negative design changes. 42
8.12 Velocity lines along the blade, negative design changes. 43
8.13 Erosion density along the guide vane in order $10^{-5}[kg/(m^2s)]$. 44
8.14 Erosion density along the blade in order $10^{-5}[kg/(m^2s)]$. . . . 45
8.15 Erosion density along the guide vane in order $10^{-5}[kg/(m^2s)]$. 46

8.16 Erosion density along the blade in order $10^{-5}[kg/(m^2s)]$. . . . 47
8.17 Erosion density along the blade in order $10^{-5}[kg/(m^2s)]$, optimal blade, positive guide vane design. 48
8.18 Erosion density along the runner blade in order $10^{-5}[kg/(m^2s)]$, optimal blade, negative guide vane design. 49
8.19 Difference of pressure distribution with different velocity vector inlet conditions. 50
8.20 Different velocity vector definitions. 51
8.21 Comparison of erosion result with different velocity vector. . . 52
8.22 Erosion tendency along guide vane in order $10^{-5}[kg/(m^2s)]$. . 53
8.23 Erosion density along the blade in order $10^{-5}[kg/(m^2s)]$. . . . 53
9.1 Alignment of pressure lines at guide vanes, red lines as reference. 55
9.2 Erosion on runner blade close to shroud, Kali Gandaki (Photo: Kristoffer Vegdal Tabutiaux). 63
9.3 Mesh related errors for outlet region in NACA 0012 result . . 65
A.1 Velocity triangles of a Francis turbine IV
C.1 First tab of Khoj. VII
C.2 Second tab of Khoj: Main Dimensions. VIII
C.4 Definition of the GH-plane. VIII
C.3 Third tab of Khoj: Axial View. IX
C.5 Fifth tab of Khoj: Distribution. IX
C.6 Sixth tab of Khoj: Radial View. X
C.7 Seventh tab of Khoj: Blade Thickness. XI
C.8 Eight tab of Khoj: Labyrinths. XI
C.9 Ninth tab of Khoj: Runner Cascade. XII
C.10 Tenth tab of Khoj: Summary. XII
E.1 Independency test nodes XV
E.2 Simulated pressure by node count XVI
E.3 Independence test(Thapa, 2011) XVI
H.1 Pressure distribution at runner blade, pressure side, positive designs. XXVII
H.2 Pressure distribution at runner blade, suction side, positive designs. XXVIII
H.3 Pressure distribution at guide vane outlet, standard label, positive design changes. XXIX
H.4 Pressure distribution at runner blade, pressure side, negative designs. XXX
H.5 Pressure distribution at runner blade, suction side, negative designs. XXXI
H.6 Pressure distribution at guide vane outlet, standard label, negative design changes. XXXII
H.7 Velocity streamlines at optimal blade, radial view. XXXIII
H.8 Velocity streamlines at optimal blade, pressure side. XXXIV
H.9 Velocity streamlines at optimal blade, suction side. XXXV
H.10 Velocity streamlines at optimal blade, radial view. XXXVI

H.11 Velocity streamlines at optimal blade, pressure side. XXXVII
H.12 Velocity streamlines at optimal blade, suction side. XXXVIII
H.13 Velocity result for correct boundary vector. XXXIX

List of Tables

4.1 Sediment classification. 9
5.1 Material description for hydraulic machinery (Batchelor et.al., 1993). 14
6.1 NACA profiles used for guide vanes. 16
7.1 Specifications of sediment(Eltvik 2013). 25
8.1 Main dimensions for Jhimruk turbine from Khoj. 29
8.2 Node count of different designs. 30
8.3 y^+ evaluation of designs 30
8.4 CFX results for reference blade. 31
8.5 Guide vane angles for the designs. 31
A.1 Overview main paramters I
A.2 NPSH constants (Brekke, 2003) II
E.1 Independence test XV
E.2 Boundary layer refinement control data, TurboGrid XVII
F.1 Turbo mode XX
F.2 Sediment definition. XXI
F.3 Defining sediment in flow, table 1. XXII
F.4 Defining sediment in flow, table 2. XXIII
F.5 Defining sediment in the flow, table 3. XXIII
F.5 Defining sediment in the flow, table 3. XXIV
G.1 Turbine data, Khoj. XXV
G.2 CFX data, Khoj. XXVI
I.1 CFX Results for optimal blade design XL
I.2 Manual efficiency calculation XLI

Nomenclature

Symbols

Symbol	Description	Unit
C	Absolute velocity	m/s
D	Diameter	m
E	Erosion tendency	m^3/s^3
g	Gravity	m/s^2
G	Length of streamline in axial plane	m
H	Length of streamline in radial plane	m
i	Factor	-
k	Factor	-
k	Kinematic turbulent energy	J/kg
n	Rotational speed	rpm
p	Pressure	Pa
P	Power	W
q	Load	kg/s^2
Q	Flow rate	m^3/s
r	Radius	m
u	Peripheral velocity	m/s
U	Rotational velocity	m/s
w	Relative velocity	m/s
y^+	Non-dimentional height	-
Z_p	Number of poles in the generator	-

Greek Letters

Symbol	Description	Unit
β	Blade angle	$^\circ$
ϵ	Kinetic turbulent energy dissipation	m^2/s^3
η	Efficiency	-
θ	Tangential angle	$^\circ$
μ	Viscosity	$kg/(s \cdot m)$
ν	Kinematic viscosity	m^2/s
ρ	Density	kg/m^3
τ	Shear stress	Pa
ω	Kinetic energy Specific Dissipation Rate	m^2/s^3
ω	Rotational velocity	rad/s

Subscript

Symbol	Description
f	Factor
i	X-coordinate
j	Y-coordinate
m	Meridional
t	Tendency
U	Radial
W	Relative
in	Inlet
out	Outlet
tot	Total
τ	Friction

Abbreviations

Acronyms	Meaning
ATM	Atmosphere
ADB	Asian Development Bank
ATM	Automatic Topology and Meshing
BEP	Best Efficiency Point
CFX	Name of Ansys Program, slang for Computial Fluid "Dynamix"
CFD	Computitional Fluid Dynamics
DNS	Direct Numerical Solution
FSI	Fluid Structure Interaction
GUI	Graphical User Interface
IEC	The International Electrotechnical Commission
ICEM	Integrated Computer Engineering and Manufacturing
NACA	National Advisory Committee for Aeronautics
NPSH	Net Positive Suction Head
NTNU	Norwegian University of Science and Technology
PPM	Parts Per Million
RMS	Root Mean Square
RPM	Rounds Per Minute
SST	Shear Stress Transport

1 Introduction

1.1 Hydropower in Nepal

Nepal is at present a developing country and is experiencing a large demand for electrical energy. The access to electrical energy plays a major role in a sustainable development of a country.

The energy consumption per inhabitant in Nepal is one of the lowest in the world. In the rural areas of the country the access to electrical energy is nearly non-present. However, the demand for power have increased steadily with an annual average growth of 8,5 % for several years, according to Asian Development Bank (ADB)[1]. Nepal, with its location in the Himalayas, has a large amount of hydro power potential which is capable to meet the growing demand. The potential is estimated to be close to 83 000 MW, with about 43 000 MW defined as economical feasible[2]. Today, only 1,7 % of this potential is developed.[3]

Hydro power is in general a very efficient way of extracting energy from natural resources. The extraction is sustainable and dependable, but the equipment is expensive and troublesome to replace. The equipment installed must therefore be designed to minimize wear.

(a) Runner erosion (b) Guide vane erosion

Figure 1.1: Erosion on machinery in Kali Gandaki, Nepal (Photo: Kristoffer Vegdal Tabutiaux).

The Jhimruk Power Plant in Nepal has previously been object for several research papers and master theses, and is therefore well documented. The turbine is known for the large amount of sediments present in the system and the large wear issues of the design. The issue has been researched on several other occasions, and several design changes have already been proposed to minimize the wear on the runner. Only minor research has presently been carried out on design changes of the guide vanes to reduce the wear on the machinery.

The results in this report are based on the known data from Jhimruk power plant in Nepal. The pictures are however from the much larger power plant Kali Gandaki i Nepal, where the Waterpower Laboratory was visiting on their yearly excursion in 2014.

1.2 Hydropower in Norway

Norwegian hydro power is worldwide known, and has been essential for several developing countries such as Nepal and Chile. The Norwegian tradition of hydro power can be followed further back in history, but the first utilization of hydro power in electricity production is dated as early as 1891 with the county owned power plant in Hammerfest, and have been continuously developed since then. The Norwegian system is near free of sediment problems due to the geology and geography of the country. Due to the increasing demand and lack of new production facilities the existing stations are presently being utilized so the sediments previously filtered from the stream now run through the turbine, creating new consideration when redesigning the current machinery. This makes the erosion consideration previously deemed unnecessary in Norway a necessity.[4]

1.3 Objective

This project is a continued research on erosion issues in hydraulic machinery. The main objective of the thesis is to define certain design changes on guide vanes to minimize erosion damage on guide vanes and runner of the turbine. This is done by designing different guide vanes using known NACA profiles with different attributes to achieve different pressure distribution along the guide vanes. This should reduce the pressure difference across the guide vanes as well as equalize the pressure distribution along the trailing edge of the guide vanes. The hypothesis is that this pressure equalization should remove the secondary flows across the guide vanes and reduce the creation of vortexes in the flow. These effects should contribute to the total reduction of erosion on both guide vanes and runner blades.

Necessary and helpful tools in the thesis has been the design tool Khoj and the CFD simulation software Ansys CFX, including the meshing software Ansys ICEM.

2 Previous work

Sediment erosion is a well documented field, and many books and papers have been written on the subject. There are however relative few papers regarding sediment erosion in hydraulic machinery. The scarceness of literature on the subject may be due to the nature of Francis design, which often is based on experience and being subject to copyright rules. The design theory is fortunately similar to pump impeller design, which is well described in theory.

Professor Emeritus Hermod Brekke at NTNU has been and still is one of the most influential persons in hydro power industry, and has performed a remarkable amount of research on sediment erosion in hydraulic machinery. The research includes hydraulic design, material properties and development of erosion resistant coatings. He has also contributed with a chapter (Design of Hydraulic Machinery Working in Sand Laden Waters) in the book *Abrasive Erosion & Corrosion of Hydraulic Machinery* by Duan and Karelin, published in 2002.[5, 6]

In the last decade the focus on sediment erosion in hydraulic machinery has become a large area of research at the Waterpower Laboratory at NTNU, Trondheim. Several research papers on both master and PhD level have been published. The process started with Jonas Jessen Ruud finishing his master thesis *Sediment handling problems at Jhimruk Power Plant* in 2004, and Dr. Bhola Thapa finishing his doctoral thesis *Sand Erosion in Hydraulic Machinery* the same year.[7, 8]

In 2008, Mattias Rögnen finished his master thesis *Design of a High Head Francis Turbine Exposed to Sand Erosion*, which started the procedure of reducing the velocity components in the system. This process was further investigated by Hallvard Meland in 2010.[9, 10]

Ola Gjølme performed a CFD analysis and a stress analysis test of the Francis turbine in Cahua power plant in Peru in 2008. This turbine was used as reference for the project and master thesis of Mette Eltvik in 2010, where she compared the erosion damage on the old turbines from Cahua with her CFD analysis with two-dimensional fluid particle flow.[11, 12]

In 2010, Hari Prasad Neopane finished his doctoral thesis *Sand Erosion in Francis Turbines*, which includes experimental tests, CFD analysis and field studies of sediment erosions. Neopan and Thapa are both considered very important contributors to the research field of sediment erosion in hydraulic machinery through these theses.[1, 7]

Kristine Gjøsæter finished her master thesis *Hydraulic Design of Francis*

Turbine Exposed to Sediment Erosion in 2011. She performed CFD analyses on different new turbine designs for a new turbine in Jhimruk power plant in Nepal. Gjøsæter was part of the Francis turbine design team of spring 2011, which included Biraj Singh Thapa(*Hydraulic design of Francis Turbine Exposed to Sediment Erosion*), Helene P. Erichsen (*Mechanical Design of Francis Turbine Exposed to Sediment Erosion*) and PhD. candidate Mette Eltvik. This team started the creation process of the Matlab-based hydraulic design tool Khoj, which was a major part of both project and master thesis for Gjøsæter.[13, 14, 15, 16]

Peter Joachim Gogstad finished his master thesis *Hydraulic Design of Francis Turbine Exposed to Sediment Erosion* in 2012, which continued the work started by Gjøsæter. In the thesis he carried out simulations for several new designs for runner and guide vanes for a new turbine in the La Higuera power plant in South America. He also further developed the design software Khoj and made it possible to export the resulting design into the 3D-modeling software Creo 2.[17]

In 2013, Mette Eltvik finished her doctoral thesis *Sediment Erosion in Francis Turbines* using the Jhimruk power plant in Nepal as reference. The thesis includes CFD simulations, CFD mesh investigations and FSI (Fluid Structure Interaction) analysis of the designs created to minimize sediment erosion, as well as considerations about methodology and erosion model theory.[16]

3 Wear

Wear is a general term which consists of different mechanisms causing deformation of solids or material loss. The mechanisms may be classified into three different categories: Mechanical, chemical and thermal actions. These are considered the main cause for material separation due to erosion. Stachowiak and Batchelor[18] classify three types of mechanical wear: Abrasive, erosive and cavitation wear. Abrasive and erosive wear are caused by particles in the flow, while cavitation is due to pressure drop along the blade, causing vapor bubbles to implode on the surface and creating water jets that cause the wear.[1]

3.1 Abrasive wear

Stachowiak and Batchelor further define four different types of abrasive wear, shown in figure 3.1: Cutting wear, fracture, fatigue by repeated ploughing and grain pullout.

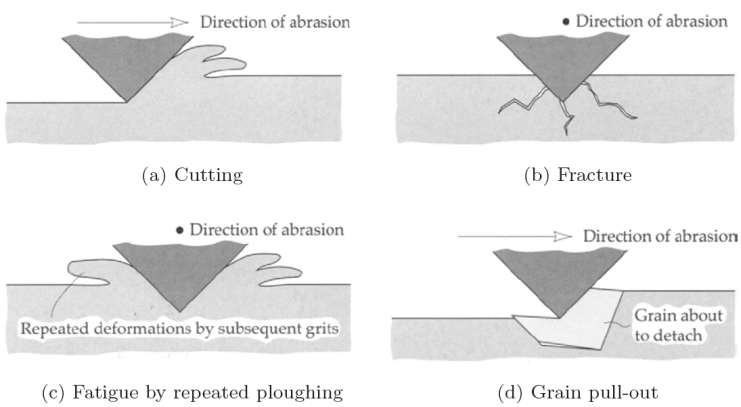

Figure 3.1: Four types of abrasive wear in a hydraulic flow (Stachowiak and Batchelor, 1993).

Cutting occurs when the particles in the flow are of higher hardness than the surface, grinding the surface and remove material, causing wear[19]. This is illustrated in figure 3.1a. For brittle surfaces like ceramic coating the material may crack or fracture, as shown in figure 3.1b. In this case, the wear is due to fracturing convergence.

For more ductile surfaces and directly hitting flow, the surface may be deformed due to repeatedly ploughing of the flow, causing metal fatigue. This

is shown in figure 3.1c.

The last kind of abrasive wear, shown in figure 3.1d, is most applicable to ceramic coating, which has relative weak boundary between the grains[1]. In this case, the particles remove the whole grain in the process.

According to Neopane[1], abrasive wear is possibly the least problematic kind of wear in hydro power systems. His report claims that turbine material hardness greater than 1.2 removes the problem almost completely.

3.2 Erosive wear

Erosive wear involves several wear mechanisms, which are largely decided by impact velocity, particle size, particle material and angle of impingement[1, 18]. The mechanisms are defined loosely by empirical connections to the process and practical considerations rather than understanding of the erosive process.

In opposition of abrasive wear, which requires hard particles, erosive wear may be of either hard or soft particles. With hard particles the erosion is similar to the abrasive wear. With soft particles the wear is due to continuously stress on the surface[1]. The mechanism is further divided into four subcategories, given in figure 3.2. These categories are similar to the ones defined for abrasive wear.

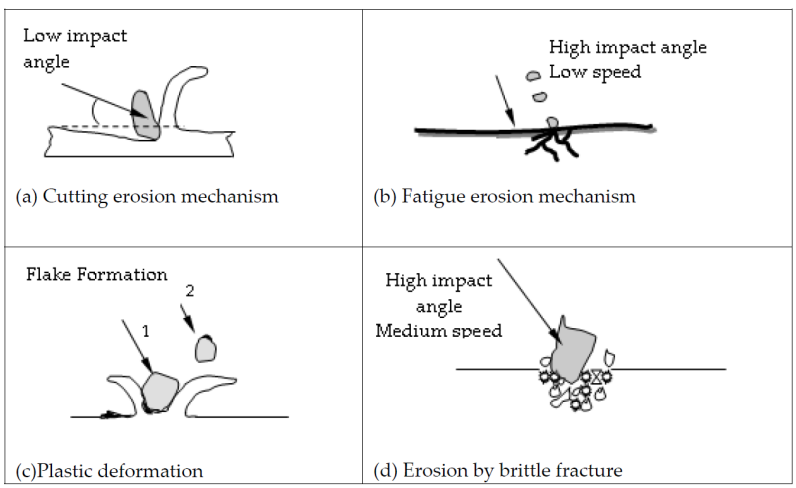

Figure 3.2: Four subcategories of erosive wear in hydraulic flows (Stachowiak and Batchelor, 1993).

In figure 3.2a the erosion cutting mechanism is presented. The particle

strikes the surface with a low impact angle and erodes the surface by cutting away material.

Fatigue mechanism occurs when the erosive particles attack at low speed and high angle. The mechanism is similar to wear due to surface fatigue on rolling surfaces. The surface cannot be deformed and instead becomes strained and weak, causing it to fracture. The mechanism is shown in figure 3.2b.

Figure 3.2c shows plastic deformation on a surface. This kind of deformation takes place around the impact area after the particle connects with the surface with medium speed at large impact angle. With repeatedly impact from particles the material will detach.

When a particle strikes a brittle surface with medium speed and high impact angle, the surface fracture rather than deform, as shown in figure 3.2d. The probability for fracturing increases with the sharpness of the particle.

This subject is further covered in the project thesis by Dahl.[20]

4 Sediments

The different erosion types described in section 3 is caused by different types of sediment. There are many types of sediment and not all are relevant for this thesis. Different measures are used for different kinds of sediments, and the measures are decided according to many different specifications of the sediments.

4.1 Sediment types

There are several types of sediments in a flow, and they erode the turbine in different ways. The different types of sediment are listed in table 4.1.

Table 4.1: Sediment classification.

Particle	Clay	Silt	Sand	Gravel	Cobble	Boulders
Size (mm)	<0.002	0.002 - 0.06	0.06 - 2	2 -60	60 - 250	>250

Of the sediments listed in table 4.1, only a few is regarded a problem in this thesis. The largest ones, boulders and cobbles, are removed from the stream by the thrash racks at the inlet, as shown in figure 4.1a. Some cobble may come through the refuse gate and those particles should be removed in the sand traps of the system, as shown in figure 4.1b. Clay and silt are normally too soft and small to erode the turbine in large degree, and this wear is largely decided by material choice. The eroding material is therefore normally sand, as shown in table 4.1[1, 21]. This is the assumption used in this thesis.

(a) Trash rack at Kali Gandaki (b) Sand trap at Kali Gandaki

Figure 4.1: Equipment at Kali Gandaki power plant, Nepal (Photo: Kristoffer Vegdal Tabutiaux).

4.2 Characteristics of sediment

According to Neopane[1] the subject of particle characteristics are an important but relatively poorly researched subject regarding erosive wear. From earlier research it is known that hard particles erode in a larger degree than soft particles[18]. It is however impossible to isolate the hardness as the sole meaningful parameter regarding erosion, ignoring size and shape.

4.2.1 Size and shape

From table 4.1 the size of sand particles is listed. The size area is rather large and is normally classified further as fine (0.06 - 0.2 mm), medium (0.2 - 0.6 mm) and coarse (0.6 - 2 mm).[1, 21]

Size and shape of sediments are focus of much research, and many have studied the phenomenon. Based upon information available from literature surveys done by Truscott[22], Beregoron[23] and Wiedenroth[24] it is assumed that the absolute wear rate increase with grain size and sharpness. Wellinger[25] states that wear due to sliding and grazing abrasion is directly proportional with grain size, but is independent of size for direct impact[1]. Particle size of 0.2 mm and above are special harmful to a hydro power system, even with low hardness[1]. It has been found that particles with hardness as low as 5 on Moh's scale[26] cause wear, which for smaller particles is not the case. Similarly, particles of greater hardness but of finer size (0.05 - 0.1 mm) tend to erode the underwater parts.

Tests with different types of particles of size spanning 8.75 μm to 127 μm shows that with larger particles the erosive type changes from ductile to brittle. The erosive peak move from 30° to 80° impingement angle and also raise the erosive tendency for all materials, as shown in figure 4.2[1, 27]. The figures are produced using eroding agents of silicon carbide at 152 m/s.

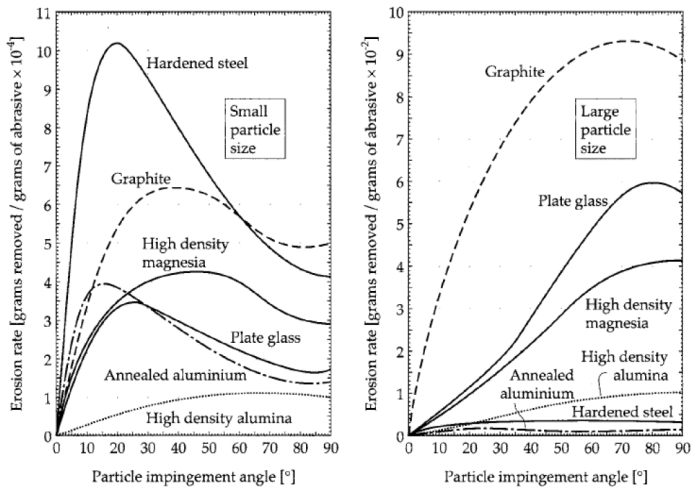

Figure 4.2: Effect of particle size on mode and rates of erosive wear. (Hojo et. al., 1986).

It is considered known that even if a particle is hard, it may not do severe erosive damage if it is blunt. A much more pressing attribute of the sediment is the shape. A blunt particle, without corners and edges, do much less damage than a sharp particle with flat surfaces and edges. In the nature most particles have such edges and the consideration done in this paragraph is mainly of academic nature[1]. However, the particles in this thesis are defined with set diameter and spherical shape, so the erosive effect must be evaluated based on this fact.

4.3 Density of sediment in the flow

The amount of sediments in the flow is important when estimating the wear. In Jhimruk power plant the estimated sediment flow rate is 500 ppm of the flow. The flow is 60 % quartz and 90% of the flow are below 0.1 mm. Based on this data and the evaluation of size and shape of the particles, the sediment is viewed as pure quartz at 0.1 mm in this thesis.[16]

5 Materials

The erosive wear rate of different materials is given by the material characteristics and the mechanism of erosive wear, and it is therefore difficult to define the optimal turbine material in a general way.[15]

Steel has historically been the preferred metal when constructing hydro turbines[28, 29]. Steel is a very hard and durable material, but it is brittle and vulnerable to corrosion. Other materials such as lead, copper/copper-alloys and aluminium/aluminium-alloys are on the other hand too easily deformed. In modern design, materials such as stainless steel, titanium, and nickel-alloys are preferred due to their superior hardness and low brittleness, combining the wanted qualities from the previous mentioned materials.[15, 20]

The erosion depends on several factors such as the impingement angle, as mentioned in Chapter 4. The effects of different impingement angles are shown in figure 5.1. The angles are 15° and 90°, respectively, and the abrasive used is 1 mm diameter silicon carbide particles. The impingement velocity is 30 m/s.[15, 18]

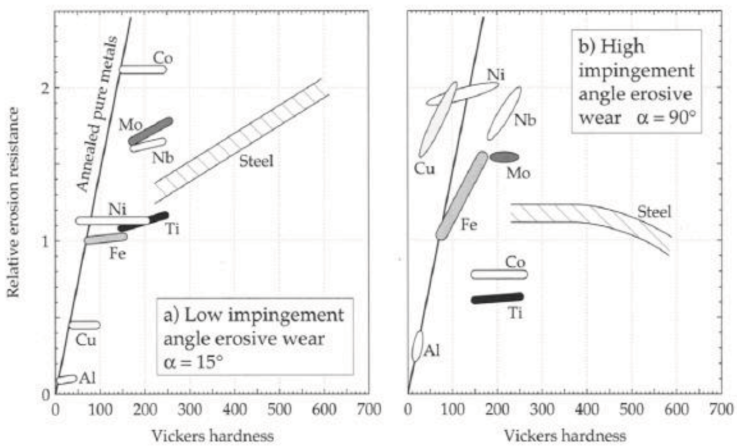

Figure 5.1: Erosion tendency at different impingement angles at $30m/s$ velocity (Stachowiak and Batchelor, 1993).

It can be seen in figure 5.1 that the impingement angle is crucial for the erosion tendency of the material. It shows that the different metals have very different resistance with different conditions.

According to Erichsen[15], the literature written on the subject suggest that

ductile steel is in total the most wear resistant material available. The effect of hardening the steel to martensite is only beneficial with very low impingement angles, and has a negative effect on high impingement angles. For some specific steel alloys, strengthening of the material is effective against erosion, but as a general rule ductility should be enhanced in steel rather than hardness in order to improve wear resistance.[15]

In the approach of developing new ceramic or metallic materials resistant of erosion, the idea is mainly to either design the material so hard that the impact particle is unable to damage the surface, or to make the material tough and elastic, causing the kinetic energy of the particle to dissipate on impact.[15, 18]

Roughly, the different materials used for hydro turbines may be listed as in table 5.1[1].

Table 5.1: Material description for hydraulic machinery (Batchelor et.al., 1993).

Material	Relative qualities regarding erosive wear resistance
Metals	Large range of toughness and hardness to suit any particles or impingement angle. Prone to high temperature corrosion and softening effects, corrosive media also harmful.
Ceramics	Very hard and increasingly tougher grades available. Resistant to high temperatures and corrosive media. Poor erosive wear resistance when brittle mode prevails.
Polymers	Though polymers and rubbers provide good erosion resistance even in corrosive media. Usage is restricted by a relative low temperature limit.

6 Hydraulic design

The different choices regarding the hydraulic design of the different parts of the system are covered in this section. The parts simulated in this thesis are the guide vanes and the runner of the Francis turbine located in Jhimruk power plant in Nepal.

6.1 Guide Vanes

The purpose of the guide vanes is to alter the direction of the flow so the water enters the runner at the optimal angle, utilizing the maximal amount of energy from the flow. The process leads to a certain loss in energy as the guide vanes force the flow in a different direction. This loss is troublesome as it lower the head of the stream and leads to abrasive and erosive wear.

As the guide vanes force the flow in new directions, several issues are presented. In order to change the flow, the vanes experience a pressure difference along the construction, causing flow issues at the outlet of the guide vanes. The vortexes caused by the pressure difference cause repeated wear along the blades.

Another reaction to this pressure difference is the secondary flows across the guide vanes. The large pressure in the system expands the steel casing of the turbine parts, creating a passage between the guide vane and the hub and shroud. This gap makes it possible for the water to pass through the guide vane, creating greater vortexes and also eroding the guide vane surface facing the hub or shroud. This erosion further widens the gap, causing larger cross flow and in the end makes the guide vanes useless.

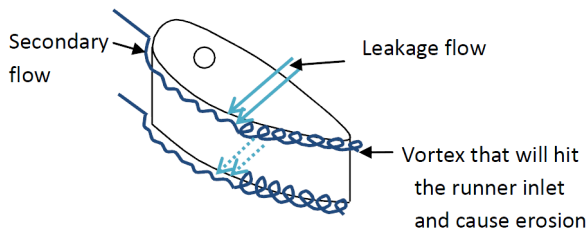

Figure 6.1: Secondary flows on guide vanes(Kristine Gjøsæter, 2011).

This effect may be lessened by changing the design of the guide vanes. By using different NACA profiles with certain specifications the effect may be lessened such that the pressure difference is lowered to the point where no secondary flows are present.

6.1.1 NACA Profiles

NACA profiles are airfoil shapes developed by the National Advisory Committee for Aeronautics for use in aircraft wings. These airfoils are similarly used in several kinds of machinery, like aircraft engines, both propels and jet engines, as well as wind turbines and hydraulic turbines.

The NACA name is generally followed by a series of digits identifying the individual profile. The digits are the input variables for a series of equations used to calculate the given profile, making it very easy to duplicate the given airfoil for further use. The NACA classification system has sections defined by 4, 5 or 6 digits[30, 31]. Historically the 4 digit system is used on wind turbines, and are therefore chosen for this thesis.

In the four digit system the first integer indicates the maximum value of the mean camber line ordinated in percent of the chord. The second integer indicates the distance from the leading edge to the maximum camber in tenths of the chord. The last two digits determine the maximum section thickness in percent of the chord[31]. The airfoils used in this thesis are given in table 6.1.

Table 6.1: NACA profiles used for guide vanes.

NACA-Profiles
NACA 0012
NACA 1412
NACA 2412
NACA 4412

The profiles presented in table 6.1 are chosen based on the known usage of the NACA 0012 in earlier projects and in Khoj[14]. The different profiles given in the table are of the same thickness, while all but the reference (NACA 0012) are identical save for the maximum value of the mean camber line. The curvature difference may be seen in figure 6.2.

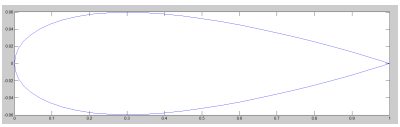

(a) NACA 0012 (reference)

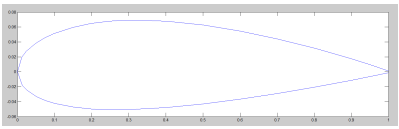

(b) NACA 1412

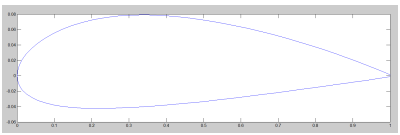

(c) NACA 2412

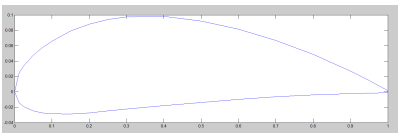

(d) NACA 4412

Figure 6.2: Curvature of the guide vane profiles used in the work.

The profile NACA 0012 is the reference design of this thesis. The design is symmetrical and is currently used in many installed systems. When installing such airfoil with angle of attack of 0° there will be no pressure difference across the curvature, as the velocity would be the same at both sides. When using an angle of attack of over 15° the distance to the trailing edge is not equal and a pressure difference appear.[31]

The designs have some issues from the creation in Khoj. The designs for 6.2b and 6.2d have a design flaw at the trailing edge, shown in figure 6.3. As one can see in figure 6.2d is the design flaw not there in the Matlab representation of the curvature. The flaw must therefore either be in the transformation from Matlab to Turbogrid or the representation in Turbogrid, both difficult to investigate properly.

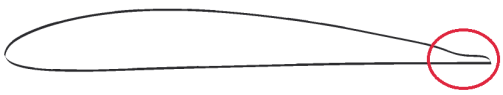

Figure 6.3: Design flaw in Turbogrid at the trailing edge of NACA 4412.

6.1.2 Design

The guide vanes are designed using the data description of the different NACA profiles through Khoj, and meshed using Ansys Turbogrid. Some alterations are done to the outlet of the mesh, executed using Ansys ICEM.

The different designs are implemented in two ways: One implementation to decrease pressure difference across the guide vanes, seeking pressure equalization. The other implementation is to increase the pressure difference across the guide vane. This test is to visualize the effect of pressure difference across the guide vanes. As the first implementation is believed to reduce the vortex creation through the system it is referred to as positive design changes. The second implementation is believed to increase the vortex creation and is referred to as negative design changes.

6.2 Runner

The runner is similarly to the guide vanes designed using the Matlab design tool Khoj, using main dimensions from Jhimruk power plant in Nepal. As the main focus of the thesis is the design of guide vanes, the runner is of reference design from Khoj, further explained in Appendix C.

In addition to the reference design, an optimize design using the discoveries of Mette Eltvik and Kristine Gjøsæter is presented to see the combined effect of the runner and guide vane design changes.[13, 16, 20]

7 CFD

CFD is a recognized tool for analysis of hydraulic machinery. There are several different systems available, and in this thesis the three dimensional Navier-Stokes solver Ansys CFX 15.0 has been used. Ansys software is a high-performance general purpose fluid dynamics program for solving fluid flow problems using several different turbulence models[32]. The program has been chosen due to the availability of experienced personnel, available literature and personal experience with the software.

7.1 Turbulence model

Turbulence may be solved using many different models, all based on the Navier-Stokes equations. Solving the Navier-Stokes equations numerically (DNS) demands a large amount of computational recources, which can easily be avoided in this case by using two-equation models. In general there are two classical two-equation models used: the k-ϵ model and the k-ω model. These models are used in different types of calculations.

The k-ϵ model is widely used in the industry due to its numerical robustness and general stability. The area of validity is unfortunately limited to the free stream region, called the logarithmic region. This makes it unsuitable for these simulations as they include analysis of the viscous region close to the wall. The k-ω model is on the other hand very stable and accurate in the viscous region. The model is unfortunately very sensitive in the free stream region and demands large computer resources.[13]

To cover both regions in an efficient way the Shear-Stress-Transport model is used (SST). This model was originally proposed by Menter[33] and use both calculations by using k-ω in the viscous region and the k-ϵ in the free stream region between the blades. The concept is shown in figure 7.1.

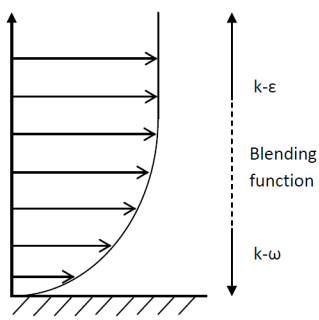

Figure 7.1: SST-function, adapted from Ansys release notes (Thapa, 2011).

A closer examination of the basic turbulent analysis is given in Appendix B.[17]

7.2 Grid specifications

A well-defined grid is essential for producing plausible results when simulating fluid dynamics, and the accuracy and convergence of the solution are affected by which properties that are chosen. Mesh orthogonality, expansion and aspect ratio are often used as measures of mesh quality.

Ansys Turbogrid is a meshing software designed for turbo machinery. The meshing is done by using the in-built system ATM Optimized (Automatic Topology and Meshing). This is an automatic meshing algorithm designed for turbo machinery given in Turbogrid, and ANSYS, Inc. claim the structured mesh produced is of high quality, as shown in figure 7.2. This statement is assumed valid in this report, and this assessment is confirmed by earlier experiments.[13, 16, 17]

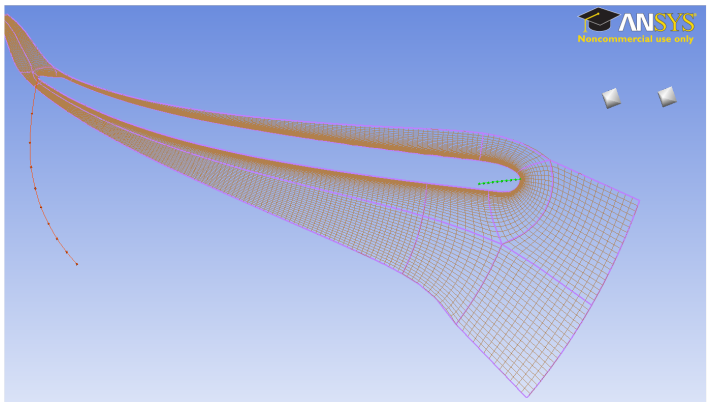

Figure 7.2: ATM Optimized topology for the reference runner for a structured mesh produced in Turbogrid.

Using the automatic generated mesh provide a solution for negative volumes that occurs when manually creating the mesh[13]. However, the automatic mesh produce certain cells which exceeds the mesh criteria set in Turbogrid. These areas are shown in figure 7.6. The variables exceeding the mesh criteria are not essential for the mesh durability and do not compromise the mesh accuracy.

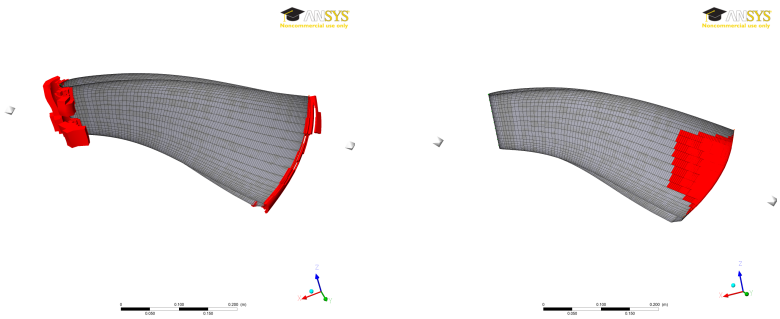

(a) Values outside range for maximum element volume ratio

(b) Values outside range for maximum edge length ratio

Figure 7.3: Properties outside of mesh specifications for runner blade, Ansys Turbogrid.

From previous projects the meshes are generated without using the 'cut-off and square' option as this choice yield best results for the trailing edge and the leading edge.[13]

The mesh resolution is defined by the wanted y^+ value. The y^+ parameter is a non-dimensional distance defined from the wall to the nearest mesh node, in turbulence theory defined as a non-dimensional wall distance for a wall-bounded flow[34]. The function is defined in equation 7.1.

$$y^+ = \frac{\rho \cdot \Delta y \cdot u_\tau}{\mu} \qquad [-] \tag{7.1}$$

Δy is the distance from the wall to the first node, u_τ is in the literature defined as the friction velocity, given in equation 7.2.

$$u_\tau = (\frac{\tau_w}{\rho})^{\frac{1}{2}} \qquad [N/m^2] \tag{7.2}$$

τ_w is defined as the wall shear stress.

Theoretically, a mesh resolution of $y^+ \sim 1$ is required for SST simulations to account for the physics of the flow through the viscous sub layer[14]. This is difficult to achieve for a Francis runner blade. An alternative is to not resolve the near-wall flow completely, but using a wall function approach on the flow close to the wall instead. Thapa[14] writes that the wall function method assume a velocity profile for the near-wall region, as shown in figure 7.4. The method allows use of a much coarser mesh, since the boundary layer no longer needs resolving.

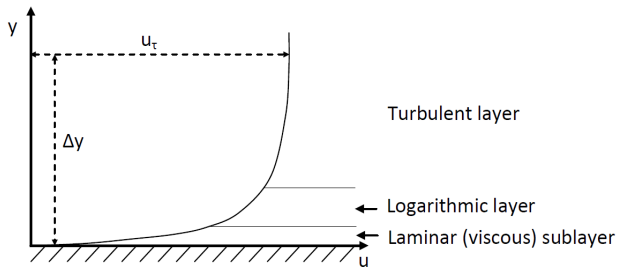

Figure 7.4: Wall function of turbulence, adapted from Ansys manual(Gogstad, 2012).

The idea is researched in several papers. Menter[33] discovered that the computed shear stress in a Couette flow varied with less than 5 % when changing the resolution of the mesh from $y^+ \sim 0.2$ to $y^+ \sim 100$. Due to this observation and others similar to it, covered in the master thesis by Biraj Singh Thapa[14], an y^+ value under 100 is considered valid in this paper.

7.2.1 Mesh independency

The generated solution is dependable only if it is independent of the mesh. In order to satisfy these criteria a mesh independency test is needed. An example of this kind of test is listed in the literature[35]. For the mesh to be independent three criteria must be met:

- Residual RMS Error values have reduced to an acceptable value (typically 10^{-4} or 10^{-5})
- Monitor points for the values of interest have reached a steady solution
- The domain has imbalances of less than 1% of the variables.

If these criteria are met and the results are the same for different meshes, then they are independent of the mesh. When the mesh independency is defined, the coarsest independent mesh is chosen to minimize the simulation time, as the result should be the same.

In this report the independency test defined in the project thesis by Dahl[20] is used as basis. The test shows that the mesh is independent at 250 000 nodes. For further explanation, see Appendix E.

7.2.2 Boundary conditions

In Ansys CFX-Pre the flow parameters are defined, as well as the boundary conditions of the system. The blades, shroud and hub are defined as walls. The flow may be simulated as either viscous or inviscid, and the different

approach is defined by the boundary conditions along the walls. For viscous solutions a no-slip condition along the wall must be chosen, which indicate zero velocity along the wall and a boundary layer between the wall and the free stream region between the blades. Inviscid flow is a simplified case of a viscous flow, which disregards the boundary layer between the wall and the free stream. Inviscid flow is defined by setting the wall specification to free slip, which indicates that the velocity along the wall is similar to the free stream region. This removes the friction loss at the blade, increasing the efficiency slightly.

In Francis simulations it is recommended to use flow rate as input parameter, and static pressure as outlet parameter. The static pressure is set to 1 atm[36]. The rotational speed ω must be defined negative to let the machine work as a turbine rather than a pump.

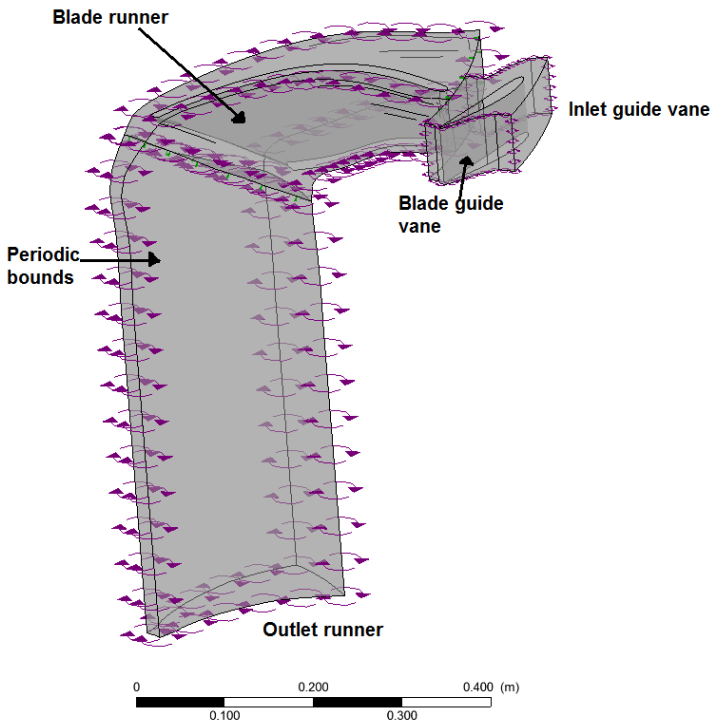

Figure 7.5: Computational domain of the work in Ansys CFX.

The inlet velocity vector is calculated in Khoj. This parameter is calculated

for a blade with no thickness. Earlier experiments[13, 14, 17] used a small Matlab code running CFX in batch mode to calculate the right inlet velocity angle. As this script proved insufficient in this project due to guide vane intervention, the head of the system is set by manually adjusting the angle of the guide vanes. As this is done without using any iteration method, the head of the different designs are of slightly different magnitude. The actual head of the system does not affect the wanted result and the inaccuracy is therefore deemed satisfactory.

7.3 Simulation Process

To simulate the combined system the different parts must be meshed. This is done separately using Ansys Turbogrid for each part, as shown in figure 7.6a and 7.6b. The process yields a structured mesh for each part.

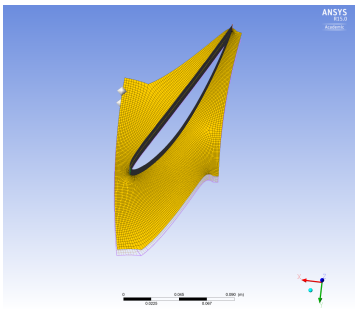

(a) Guide vane mesh from Turbogrid.

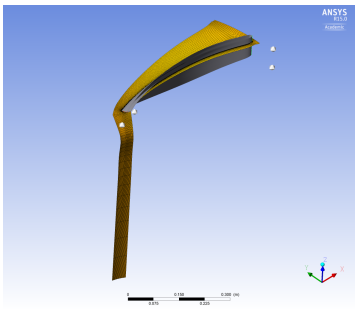

(b) Runner mesh from Turbogrid.

Figure 7.6: Mesh properties, Ansys Turbogrid.

Next the meshes are merged in CFX. The merging process is somewhat troublesome, as the produced meshes have several regions that must be defined separately. It should be noted that the guide vanes and the outlet region of the blade are stationary parts while the runner itself is a rotational part. The outlet region of the runner has in addition some non-physical issues. The mesh of the blade section yields both a shroud and a hub for the outlet region, when only a shroud is present in the real world. As Ansys is unable to remove the hub from the outlet region, the part should be modelled as a free slip wall. The merged pieces of the design is shown in figure 7.7.

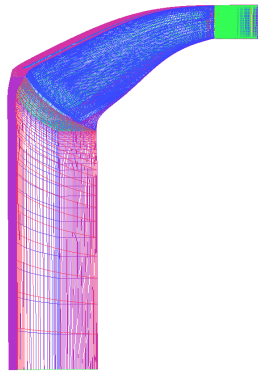

Figure 7.7: Merged mesh

7.3.1 Sediment simulation

The sediments used in the system are based on the sediments present in the Jhimruk power plant, mentioned in chapter 4. The simulated sediments are 100 % quartz with specifications given in table 7.1.[16]

Table 7.1: Specifications of sediment(Eltvik 2013).

Name	Value	Unit
Sediment	Quartz	-
Molar mass	60.08	g/mol
Density	2,65	g/cm^3
Particle size	0,1	mm
Shape factor	1	-
Particle track	5000	-
Mass flow	3	kg/s

The sediments are implemented using the description given in Appendix F. The sediment flow is set after discussion with PhD-candidate Biraj Singh Thapa[37]. The sediment characteristics are defined in the PhD-thesis by Mette Eltvik.[16]

The wear is calculated by using the Tabakoff erosion model.[38] This model and several other different erosion models were considered by several earlier projects at the Waterpower laboratory, and the Tabakoff model was deemed the best for hydraulic turbine simulation[13, 16, 39]. The different models are roughly explained in Appendix F[13] .

7.4 Mesh size

In earlier projects the calculated erosion has tended to be smaller than anticipated. Following research carried through at the Waterpower Laboratory there have emerged several theories of why this reaction is so small compared to the expected result, and one of them is the mesh coarseness. Previous researches have assumed that fine mesh is essential to achieve plausible results. Later inspections have questioned this logic. Sediments in the flow are designed to a certain diameter and research done at the Waterpower Laboratory indicates that the mesh size cannot be smaller than this diameter. In mesh calculations the cells are calculated individually and if the sediments are larger than the cell no motion will be registered. Another issue is the physics regarding the boundary layer. As the velocity close to the wall converges to zero, there are registered low kinetic energi in the cells close to the wall. If the cells near the wall are too small, the velocity along the wall will be close to zero and the particles in the stream will have only a small amount of kinetic energy, which cause little erosion.[16]

The mesh independency must however be taken into consideration. Previous tests [13, 16, 20, 39] yields a mesh independency for the runner at 250 000 nodes. This makes the lowering of mesh quality beyond this limit unsuitable for research. The accuracy of the results where coarse meshes are used must therefore be investigated.

7.4.1 Mesh dependent erosion

Different meshes may produce different result regarding erosive nature. The theory is tested by using different meshes for one guide vane in the thesis, where both runner and guide vane are meshed both coarse and fine, and the erosive tendency is compared.

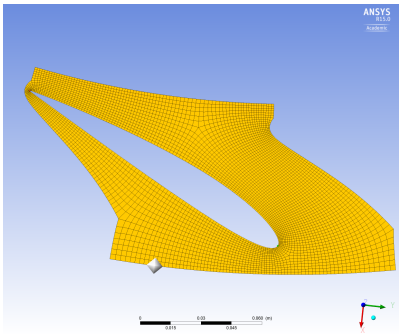

(a) Coarse mesh

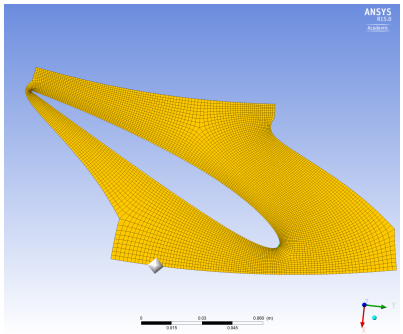

(b) Fine mesh

Figure 7.8: Mesh sizes from Turbogrid.

The test has three possible outcomes:

1. The erosion is larger for coarse mesh
2. The erosion is similar/identical for the different meshes.
3. The erosion is smaller for the coarse mesh

The first option indicates that the theory is correct and that a fine mesh is contra productive for sediment simulation. The erosion is not registered as the particles are larger than the grid size at the wanted positions. Further research should therefore consider the coarsest mesh possible to minimize the need for computer resources and still have independent mesh.

The second point show that the mesh is of little relevance for sediment simulations, as both the fine mesh and the coarse mesh in this thesis are equally sufficient/insufficient of simulating the erosive damage. Wanted mesh should therefore be the smallest available and still having independent mesh.

The last option suggests that the reduction of mesh size reduce the credibility of the test, and therefore show that a coarser mesh is not possible for this simulation.

8 Results

8.1 Main dimensions

The main dimensions for the turbine are defined using Khoj, as described in section 6.2. The resulting parameters for the system are given in table 8.1.

Table 8.1: Main dimensions for Jhimruk turbine from Khoj.

	Variable	**Value**	**Unit**
General	P	4,5	MW
	H	201,5	m
	Q	2,35	m^3/s
	n	1000	rpm
	Ω	0,322	-
Inlet	U_1	46,60	m/s
	C_{U1}	40,72	m/s
	C_{m1}	13,26	m/s
	C_1	42,82	m/s
	β_1	66,49	$\circ$
	W_1	14,50	m/s
	D_1	1,89	m
	B_1	0,097	m
Outlet	$D_{2,korr}$	0,54	m
	$U_{2,korr}$	28,27	m/s
	C_{U2}	0,00	m/s
	C_{m2}	13,13	m/s
	C_2	16,41	m/s
	β_2	24,90	$\circ$
	W_2	31,17	m/s

The different guide vane designs have shown no impact on these values and are identical for each part of the main design changes.

As defined in section 6.1.2 the following results are divided into two different design sets, where the first is believed to affect the system in a positive manner while the second is believed to have a negative effect on the system, as explained in section 6.1.2. For easily separate the different sets they will be referred to as the positive and negative design changes. This way of defining the sets is based on the hypothesis and has no connection with the actual results.

The node count and y^+ values of the different designs are presented in table 8.2 and 8.3.

Table 8.2: Node count of different designs.

	Design	Node count	Element count
Runner	Runner (Reference) Runner(Coarse) Runner(Optimal)	290315 31766 295306	267120 26273 272100
Reference	NACA 0012	286254	261630
Coarse	NACA 0012	74734	63430
Positive design	NACA 1412 NACA 2412 NACA 4412	259656 258881 253704	241920 241200 236280
Negative design	NACA 1412 NACA 2412 NACA 4412	256990 261950 262756	239790 243360 243510

Table 8.3: y^+ evaluation of designs

	Design	y^+ value [-]
Runner	Runner (ref) Runner(coarse) Runner(Optimal)	22,47 159,688 24,04
Reference	NACA 0012	114,844
Coarse	NACA 0012	162.06
Positive design	NACA 1412 NACA 2412 NACA 4412	44,29 43,293 39,66
Negative design	NACA 1412 NACA 2412 NACA 4412	30,77 82,62 129,45

From section 7.2 it is given that the limit for the y^+ value is exceeded for several of the designs given in table 8.3. The error may be explained by the mesh coarseness for two of the designs, but the high values for NACA 4412 negative and the reference NACA 0012 is more difficult to verify. The design parameters are identical for all of the designs and should yield similar values. As the errors are of such small magnitude the specifications are deemed satisfactory for this thesis after consulting with professor Ole Gunnar Dahlhaug[40].

The results of the different designs are given in table 8.4.

Table 8.4: CFX results for reference blade.

Result table	Reference	Positive design			Coarse	Negative design			
	NACA 0012	NACA 1412	NACA 2412	NACA 4412	NACA 0012	NACA 1412	NACA 2412	NACA 4412	unit
Rotation Speed	-104,72	-104,72	-104,72	-104,72	-104,72	-104,72	-104,72	-104,72	rad/s
Inlet Volume Flow Rate	2,36	2,36	2,36	2,36	2,36	2,36	2,36	2,36	m^3/s
Reference Density	997,00	997,00	997,00	997,00	997,00	997,00	997,00	997,00	kg/m^3
Reference Diameter	0,20	0,20	0,20	0,20	0,20	0,20	0,20	0,20	m
Output Power	4,45	4,49	4,54	4,53	4,45	4,37	4,49	4,50	MW
Capacity Coefficient	2,72	2,72	2,72	2,72	2,72	2,72	2,72	2,72	
Head Coefficient	4,38	4,40	4,47	4,48	4,38	4,37	4,40	4,40	
Power Coefficient	11,49	11,60	11,74	11,71	11,49	11,29	11,62	11,65	
Total-to-Total Head	200,35	201,22	204,54	205,04	200,31	199,61	201,38	201,20	m
Total-to-Total Efficiency %	0,965	0,971	0,972	0,961	0,965	0,951	0,971	0,973	
Nozzle Loss Coefficient	0,26	0,17	0,26	0,24	0,21	0,16	0,14	0,12	
Nozzle Efficiency %	95,08	96,41	94,72	94,70	95,27	96,64	97,03	97,54	

It is important to note that the efficiency of the systems are manually calculated as the intern calculation in Ansys CFX yielded improbable result. The calculations are done using parameters listed in table 8.4 and I.2, the whole calculation is given in Appendix I. The calculations of the efficiency is done for a system consisting of guide vanes and runner only, causing the the magnitude of the result.

The calculations for the design changes using optimal blade are given in Appendix I.

8.2 Guide vane design

The different designs are chosen to achieve BEP for the runner, which include correct head and flow rate. As the different designs at the same running angle induce different head on the runner, the guide vane angles are different for the different designs. The different inlet angles affect the investigated phenomenon in small extent, but the simulations are less credible due to increased error sources. The angles of the guide vanes are listed in table 8.5.

Table 8.5: Guide vane angles for the designs.

	Guide vane	Khoj angle [°]	Real angle [°]
Reference	NACA 0012	88	18,84
Positive design	NACA 1412	86,5	18,4
	NACA 2412	86,5	18.4
	NACA 4412	84	17.18
Negative design	NACA 1412	89	19,55
	NACA 2412	89,5	19,78
	NACA 4412	91,5	20,72

The different values changed in Khoj do not reflect the real values of the guide vanes inlet position. The source code in Khoj does not state how to change this position, so the solution in this thesis has been to change one of the calculation variables used to set the opening. The real value of the opening is then found by measurement using Ansys ICEM.

8.3 Pressure distribution

The results regarding the pressure distribution on the guide vanes are presented in the following section. The definitions of positive and negative design changes are given in section 6.1.2.

8.3.1 Positive design changes

In figure 8.1 the positive design changes are presented, with the reference design given in figure 8.1a.

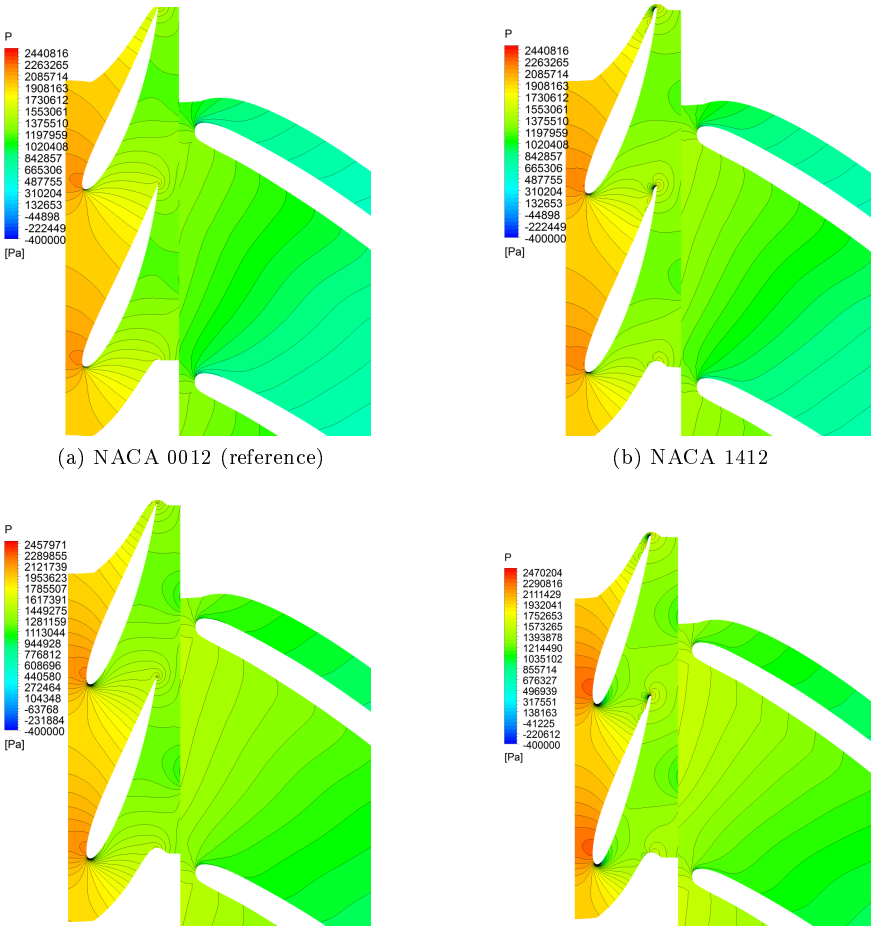

(a) NACA 0012 (reference)

(b) NACA 1412

(c) NACA 2412

(d) NACA 4412

Figure 8.1: Pressure distribution in the system, positive design changes.

As mentioned in section 6.1 is the symmetrical NACA 0012 the reference

guide vane. One can see from figure 8.1a that the pressure distribution at the trailing edge of the guide vane show a tendency for large pressure difference, which may cause vortexes.

The pressure difference across the guide vane gets more equalized at the trailing edge for each design, but the pressure distribution between the guide vanes gets more disordered for designs further from the reference. The inlet pressure is mostly unaltered by the design change, which is as expected.

The pressure distribution of the outlet region of the guide vanes are presented in figure 8.2.

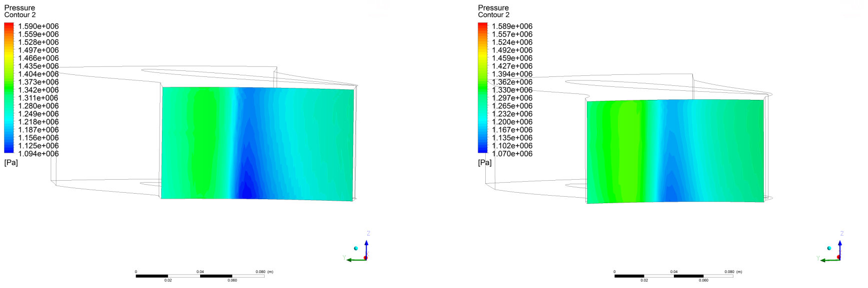

(a) NACA 0012 (reference)

(b) NACA 1412

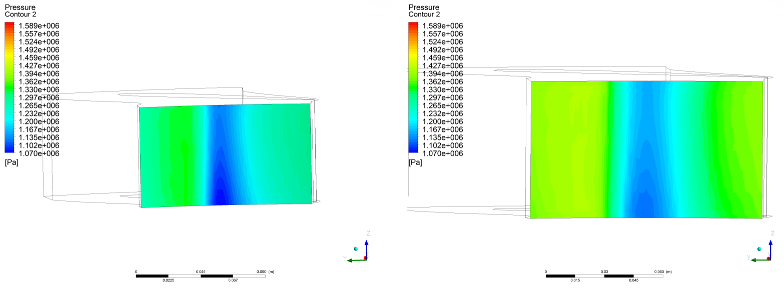

(c) NACA 2412

(d) NACA 4412

Figure 8.2: Pressure distribution at guide vane outlet, positive designs.

The figures given in figure 8.2 show minor changes in the pressure distribution at the guide vane outlet for the positive designs. The figures are differently labelled than the results in figure 8.1, as to visualize the pressure distribution with more precision. For same labeling as figure 8.1, see figure H.3 in Appendix H.

8.3.2 Negative design changes

The results regarding pressure distribution for the negative design changes are given in figure 8.3.

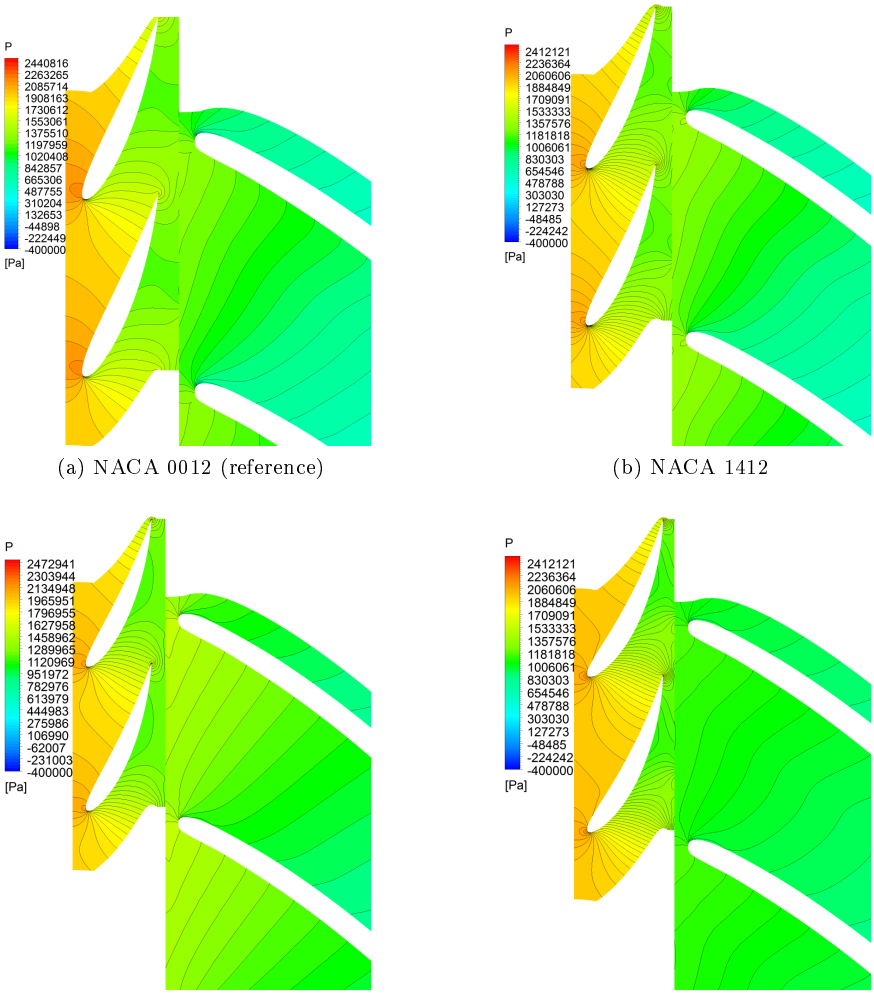

(a) NACA 0012 (reference)

(b) NACA 1412

(c) NACA 2412

(d) NACA 4412

Figure 8.3: Pressure distribution in the system, negative designs.

In contrast with the positive design changes is the pressure difference increased by negative implementations. The velocity is increased at the suction side and decreased on the pressure side, increasing the pressure difference across the blade. The pressure distribution along the guide vanes is

however much improved through the design, as one can see from the pressure lines in the presentations in figure 8.3.

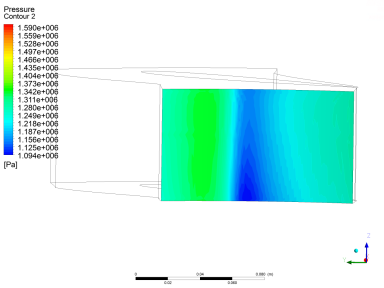

(a) NACA 0012 (reference)

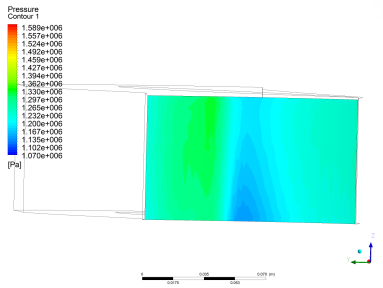

(b) NACA 1412

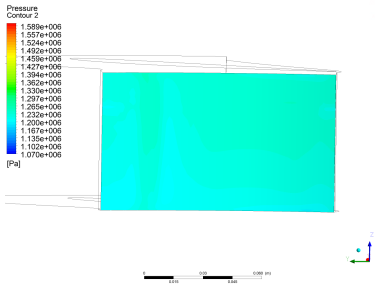

(c) NACA 2412

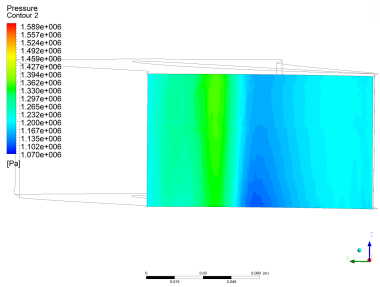

(d) NACA 4412

Figure 8.4: Pressure distribution at guide vane outlet, negative designs.

The outlet of the guide vane region is shown in figure 8.4 with same labeling as figure 8.2. The improved pressure distribution along the guide vanes clearly improve the outlet pressure distribution of the guide vanes, which is obvious for the NACA 2412 negative design, given in figure 8.4c.

8.4 Velocity profile

To fully be able to evaluate the parameter changes in the system the velocity streamlines must be examined. The streamlines are found at the guide vanes and the runner blades for each design.

8.4.1 Positive design

The results for the positive design changes are shown in figure 8.5 and 8.6, 8.7 and 8.8 for guide vane and runner, respectively.

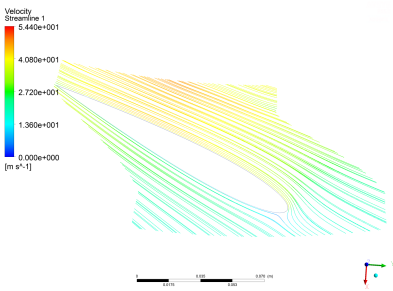

(a) NACA 0012 (reference)

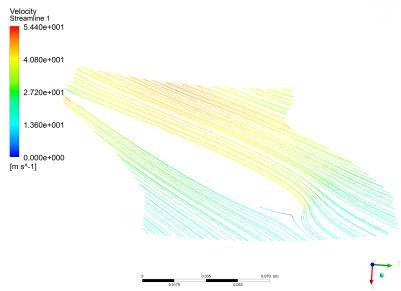

(b) NACA 1412

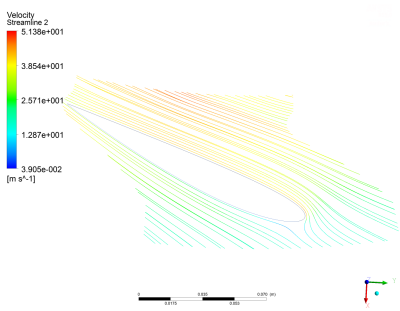

(c) NACA 2412

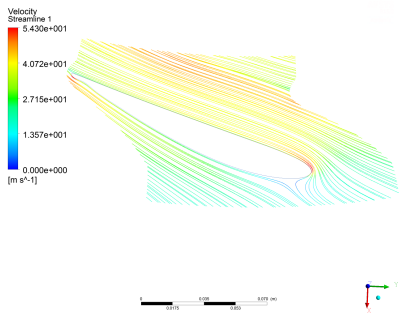

(d) NACA 4412

Figure 8.5: Velocity streamlines at guide vanes, positive design changes.

The resulting velocities for the positive guide vane designs yield a surprising tendency. The outlet velocity field seems to become less uniform as the design become more radical. This may cause increased vortex creation. The velocity difference across the guide vanes are reduced through the design changes, which is as expected from the hypothesis.

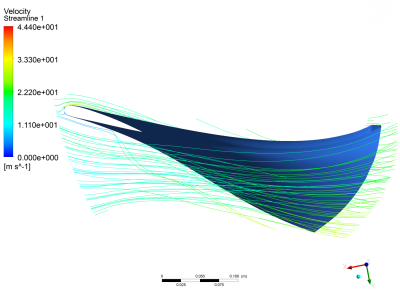

(a) NACA 0012 (reference)

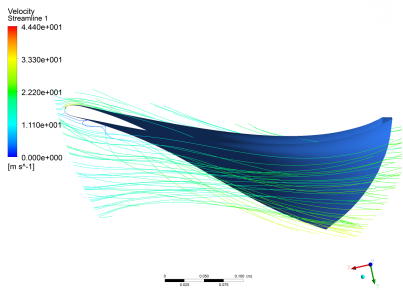

(b) NACA 1412

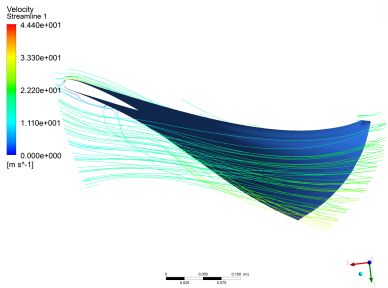

(c) NACA 2412

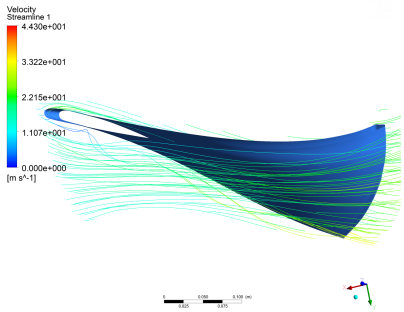

(d) NACA 4412

Figure 8.6: Velocity streamlines at runner blade, positive design changes.

The streamlines on the blade show an increased density of vortexes along the pressure side of the blade, indicating an increase in erosion tendency.

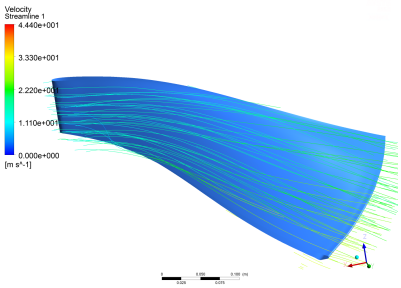

(a) Naca 0012 (reference)

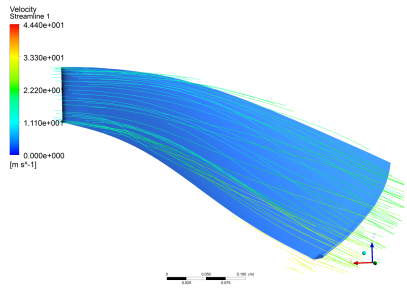

(b) Naca 1412

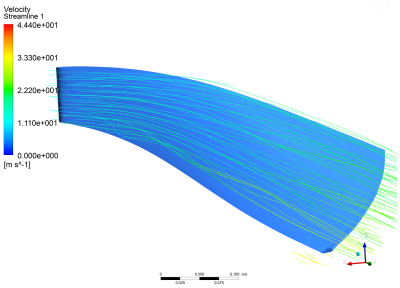

(c) Naca 2412

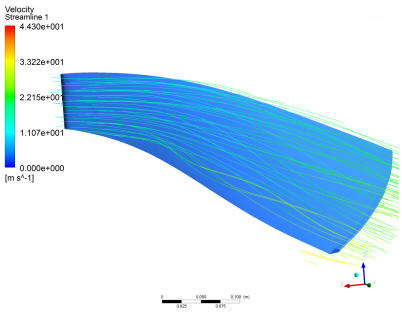

(d) Naca 4412

Figure 8.7: Velocity lines along the blade, pressure side, positive design changes.

From figure 8.7 the streamlines seem to flow denser in specific regions, indicating that more sediments will be present in these regions.

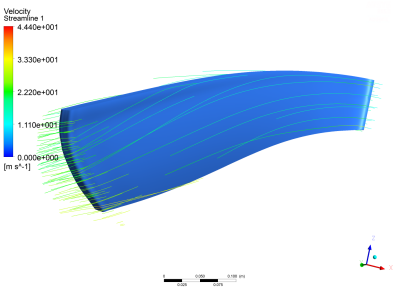

(a) Naca 0012 (reference)

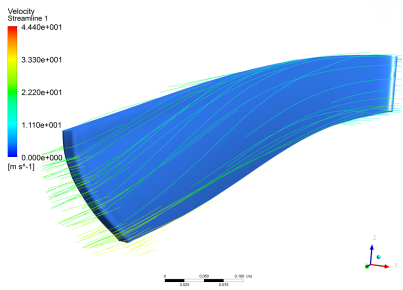

(b) Naca 1412

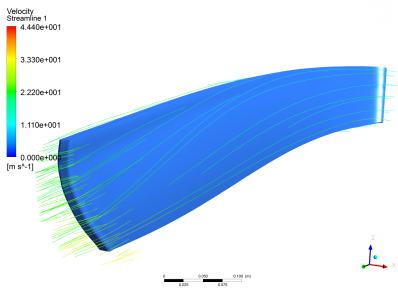

(c) Naca 2412

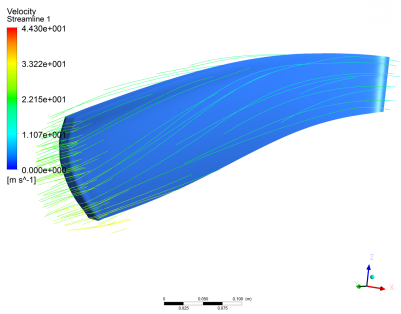

(d) Naca 4412

Figure 8.8: Velocity lines along the blade, suction side, positive design changes.

The streamlines on the both the pressure side and the suction side of the blade indicate a clear tendency of the flow following the blade curvature through the design, causing denser water flow at the lower parts of the blade close to the shroud. Some streamlines do however cross the blade almost horizontally, increasing the particle density in the area closer to the hub, shown in figure 8.7b, 8.7c and 8.7d.

8.4.2 Negative design

The results for the negative design changes are given in figure 8.9 and 8.10, 8.11 and 8.12 for guide vane and runner, respectively.

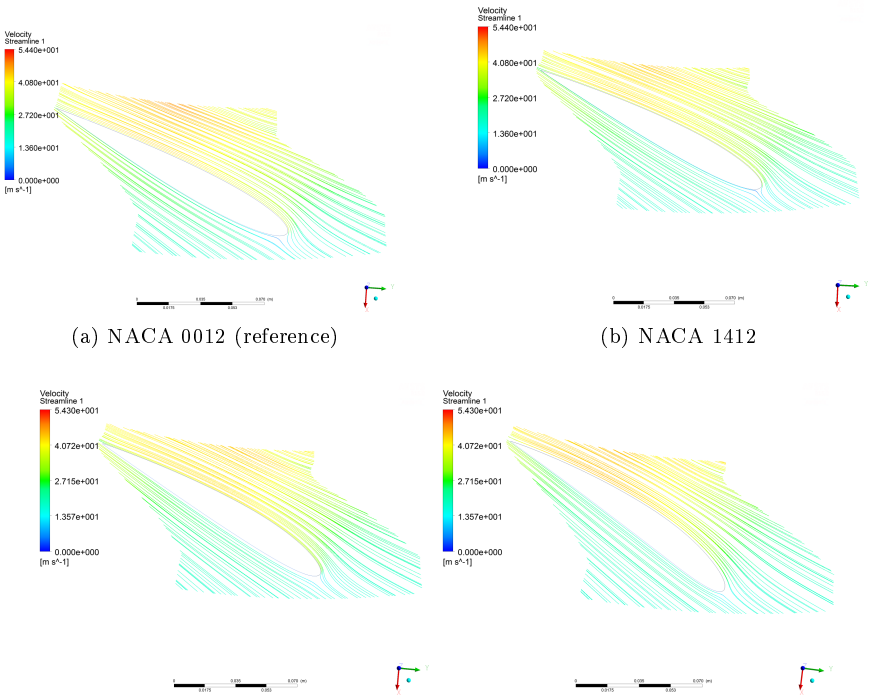

(a) NACA 0012 (reference)

(b) NACA 1412

(c) NACA 2412

(d) NACA 4412

Figure 8.9: Velocity streamlines at guide vane, negative design changes.

The result for the negative design change is opposite of the positive design change, which is as expected. The resulting velocity field of the outlet region shows a clear indication of smoothing, making the velocity field close to uniform. This tendency seem to increase up to a certain point, where the balance is shifted and a new high-speed region is defined, shown in figure 8.9d. The velocity distribution along the guide vane is as expected, as the velocity difference across the blade become larger as the designs become more radical.

The streamlines on the runner blade are shown in figure 8.10, 8.11 and 8.12.

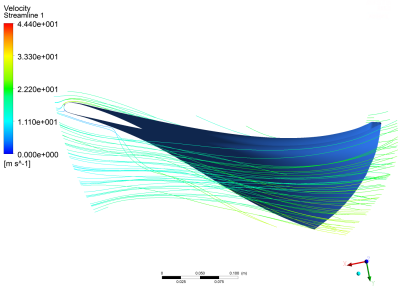

(a) NACA 0012 (reference)

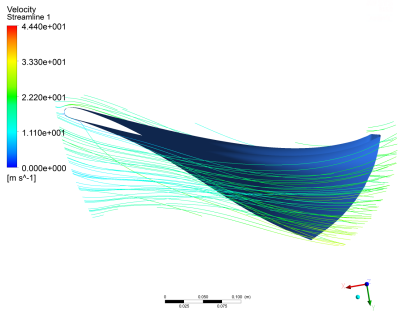

(b) NACA 1412

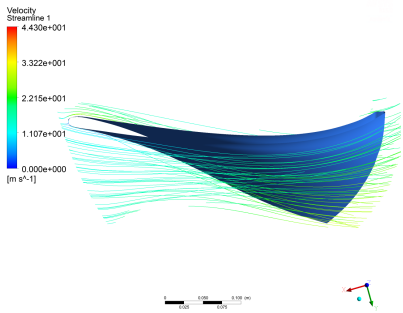

(c) NACA 2412

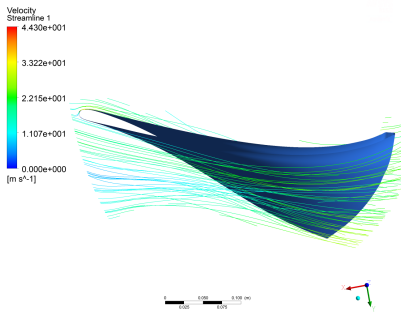

(d) NACA 4412

Figure 8.10: Velocity streamlines at runner blade, negative design changes.

The streamlines of the negative design show a clear decrease of stream vortexes with more radical design changes. The change is clear from figure 8.10.

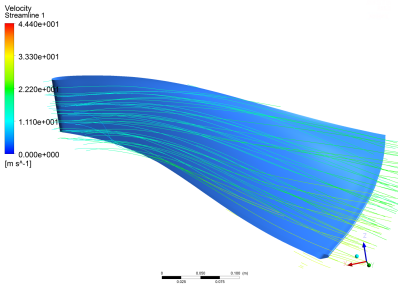

(a) Naca 0012 (reference)

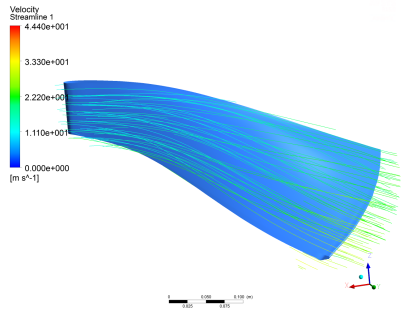

(b) Naca 1412

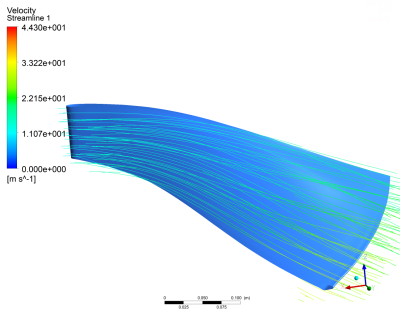

(c) Naca 2412

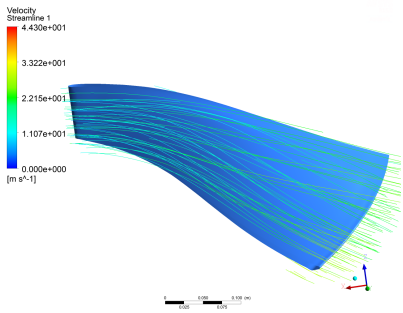

(d) Naca 4412

Figure 8.11: Velocity lines along the blade, negative design changes.

The streamlines in figure 8.11 show an increased density of streamlines at the higher part of the blade, close to the hub. This indicates an increased load on these parts of the blade, decreasing the load on the areas close to the shroud.

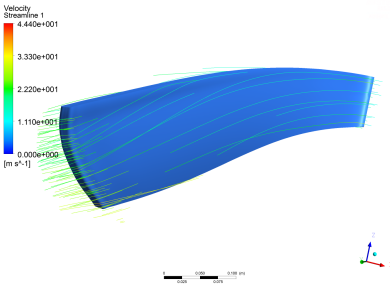

(a) Naca 0012 (reference)

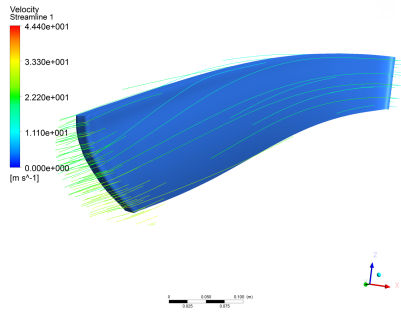

(b) Naca 1412

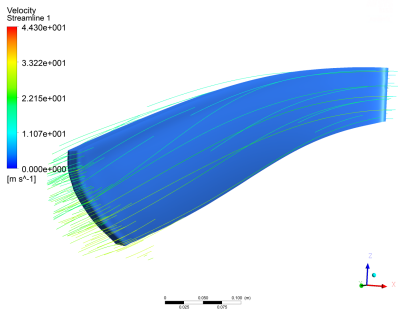

(c) Naca 2412

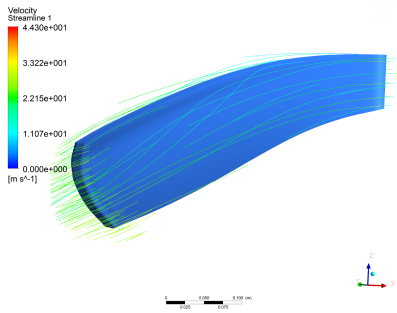

(d) Naca 4412

Figure 8.12: Velocity lines along the blade, negative design changes.

The streamlines on both the suction and pressure side of the blade for these design changes seem more promising than for the positive design changes. The streamlines are less affected by vortexes and thus the erosion tendency should be decreased for these design changes. This result is surprising, as the hypothesis predicted a different result.

8.5 Erosion

As explained in section 7.3.1 is the sediment erosion modeled using the Tabakoff erosion model. The results from these simulations are shown in the figures 8.13, 8.14, 8.15 and 8.16.

8.5.1 Positive design

The erosive tendency of the positive design changes presented in figure 8.1 are shown in figure 8.13 and 8.14 for guide vane and runner, respectively.

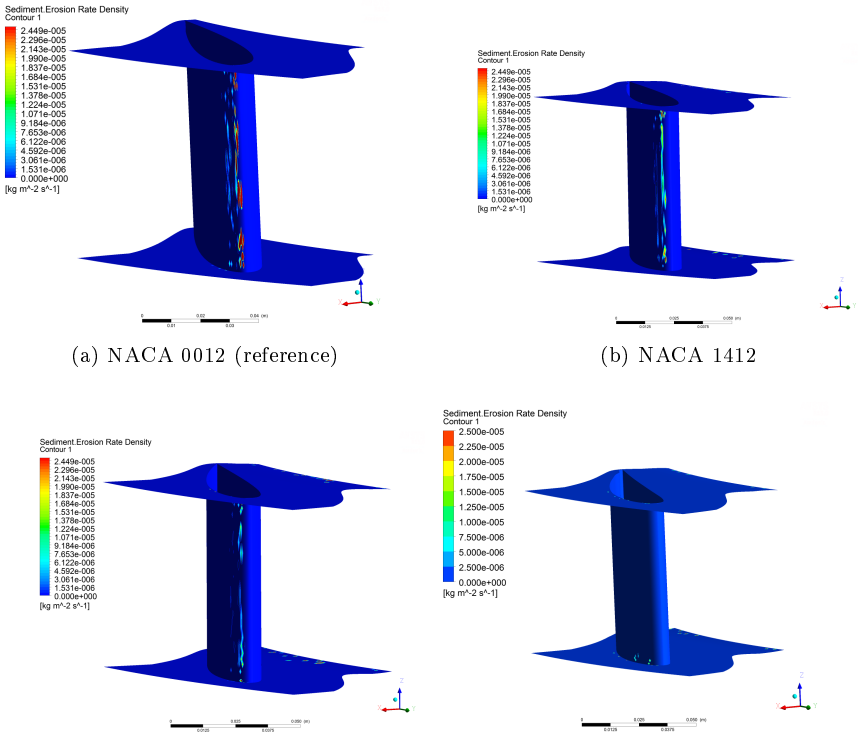

(a) NACA 0012 (reference)

(b) NACA 1412

(c) NACA 2412

(d) NACA 4412

Figure 8.13: Erosion density along the guide vane in order $10^{-5}[kg/(m^2s)]$.

The results of the guide vanes yield a much improved result regarding erosion density, which is as expected from the initial hypothesis. For the NACA 4412 profile the erosion is almost abolished, given in figure 8.13d.

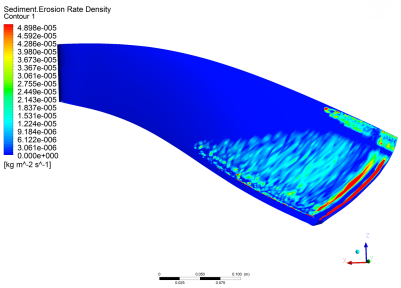

(a) NACA 0012 (reference)

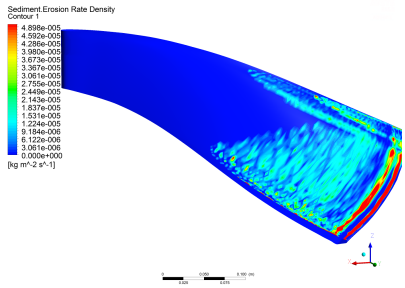

(b) NACA 1412

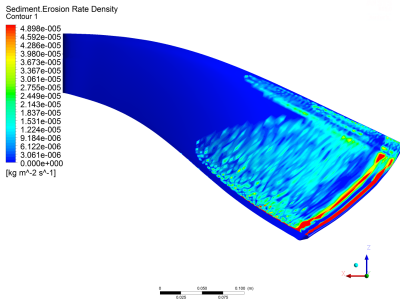

(c) NACA 2412

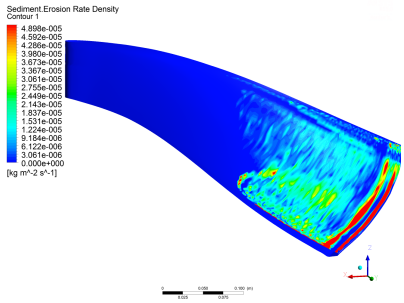

(d) NACA 4412

Figure 8.14: Erosion density along the blade in order $10^{-5}[kg/(m^2s)]$.

The results show an increase in the erosive tendency, with a relative clear indication of further degeneration with more drastic design changes. This result is the opposite of the predicted behaviour.

8.5.2 Negative design

Figure 8.15 and 8.16 show the erosion tendencies from the designs presented in figure 8.3, which is the negative design changes.

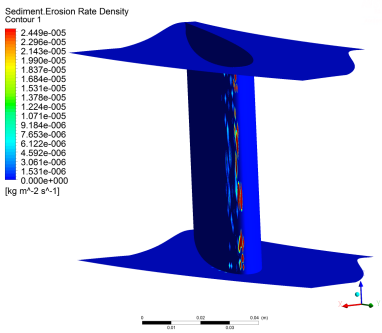

(a) NACA 0012 (reference)

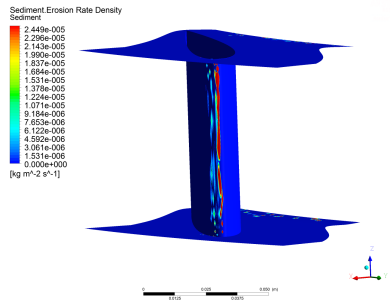

(b) NACA 1412

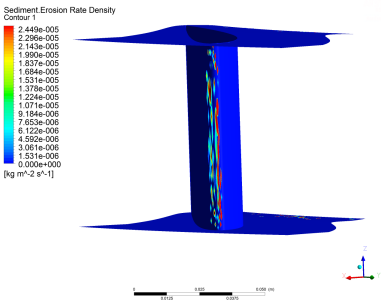

(c) NACA 2412

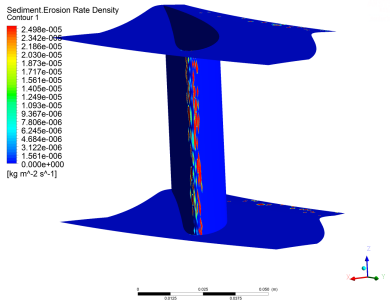

(d) NACA 4412

Figure 8.15: Erosion density along the guide vane in order $10^{-5}[kg/(m^2 s)]$.

In contrast to the positive guide vane design changes are the guide vanes with negative design changes exposed to more sediment erosion, especially on the leading edge. The tendency will be further discussed.

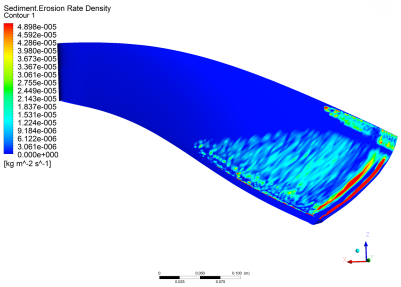

(a) NACA 0012 (reference)

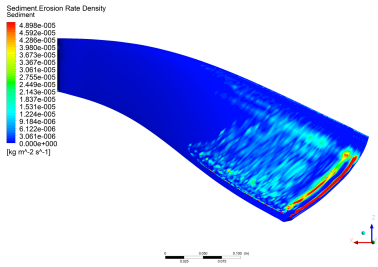

(b) NACA 1412

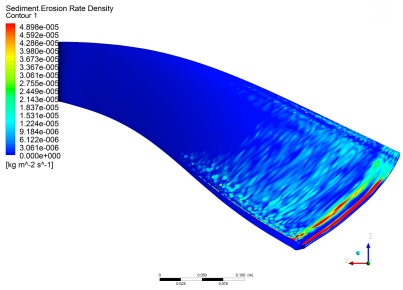

(c) NACA 2412

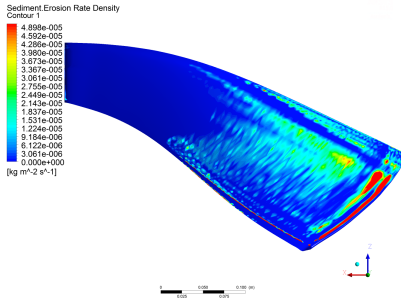

(d) NACA 4412

Figure 8.16: Erosion density along the blade in order $10^{-5}[kg/(m^2 s)]$.

The negative design change show a tendency of erosion reduction for NACA 1412 and NACA 2412 in figure 8.16b and figure 8.16c respectively, while the tendency of NACA 4412 show a extensive increase regarding erosion tendency, given in figure 8.16d.

8.6 Optimal design change

The design changes carried out on the guide vanes show different results regarding erosion on the runner blade. As several different measures have been done in order to reduce this tendency on the blade itself, the following figures show how the combination of the design changes affects the erosion. The velocity streamlines on the blades are given in Appendix H.

8.6.1 Positive design

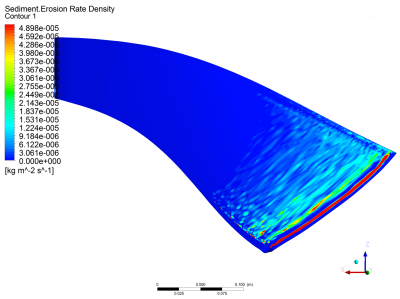

(a) NACA 0012 (reference), optimal blade design

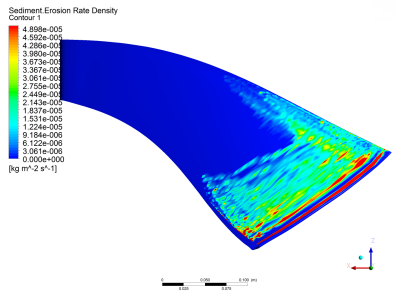

(b) NACA 1412 positive design, optimal blade.

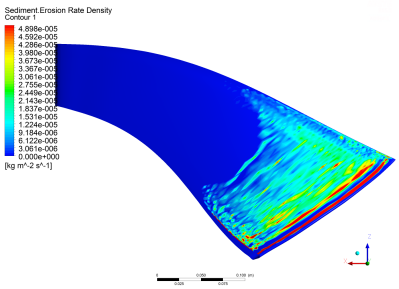

(c) NACA 2412 positive design, optimal blade.

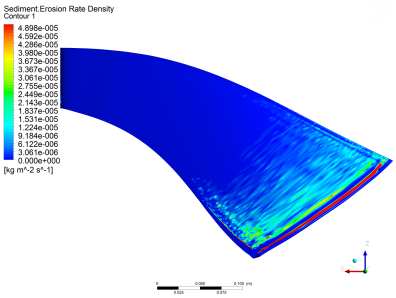

(d) NACA 4412 positive design, optimal blade.

Figure 8.17: Erosion density along the blade in order $10^{-5}[kg/(m^2s)]$, optimal blade, positive guide vane design.

The results from the positive design changes show an improvement regarding erosion tendency for NACA 0012 and NACA 4412, with a reduction in both eroded area and erosion density. The results regarding NACA 1412 and NACA 2412 do in opposition show a large increase in both eroded area and erosion density, which indicate that the optimized runner is ineffective for these designs.

8.6.2 Negative design

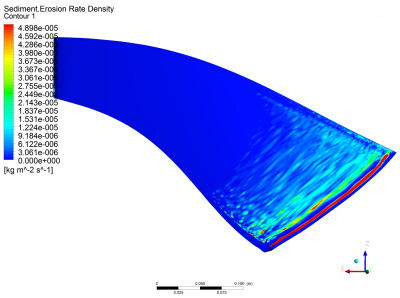

(a) NACA 0012 (reference), optimal blade design

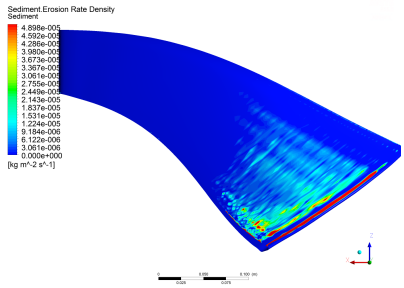

(b) NACA 1412 negative design, optimal blade.

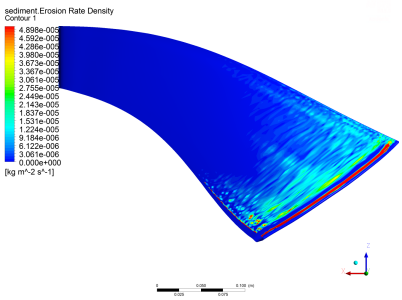

(c) NACA 2412 negative design, optimal blade

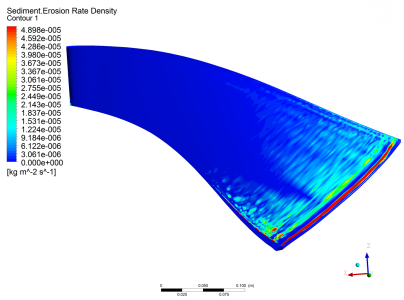

(d) NACA 4412 negative design, optimal blade.

Figure 8.18: Erosion density along the runner blade in order $10^{-5}[kg/(m^2s)]$, optimal blade, negative guide vane design.

The negative designs have a more continuous result, with decrease in both eroded area and erosion density for all profiles.

From figure 8.17 and 8.18 it is clear that the different designs affect the erosion, but the effect is not unambiguous. Further research should be done on these designs, as the results indicate that there is present some errors in the simulations.

8.7 Possible definition errors

8.7.1 Velocity vector difference

As briefly discussed in section 7.2.2 the inlet velocity vector is an important parameter affecting the pressure distribution and can alter the results of this thesis drastically. The impact is shown in figure 8.19.

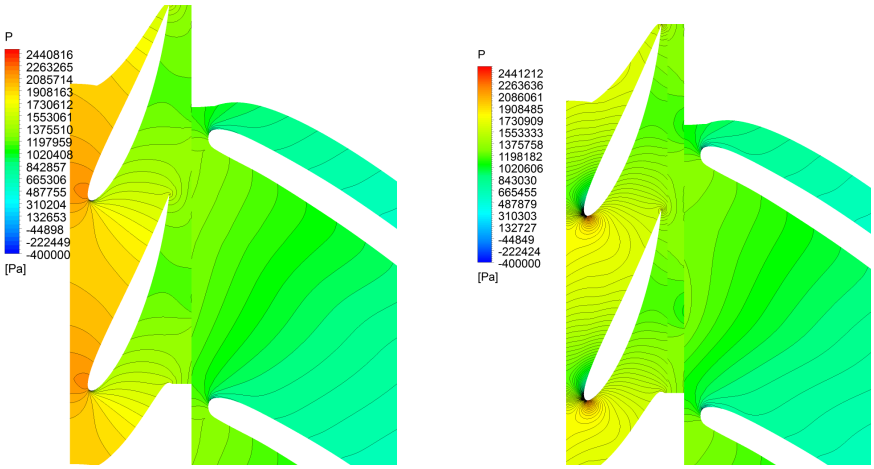

(a) NACA 0012 (reference)

(b) NACA 0012 (different inlet velocity vector)

Figure 8.19: Difference of pressure distribution with different velocity vector inlet conditions.

The velocity vectors are constant in this thesis so the results are unaffected by this parameter. The results given in figure 8.19 show the impact of changing the inlet velocity vector can have on a system and indicate the possible error of the simulations.

8.7.2 Velocity vector direction

In Ansys CFX-Pre the flow rate of the system and the velocity vector is defined, as discussed in section 7.2.2. These parameters are defining the inlet conditions of the system, and may therefore have large impact on the simulations. At the end of the work it appeared that the inlet velocity vector should be defined negative, which was not done for these simulations[41]. The difference is shown in figure 8.20.

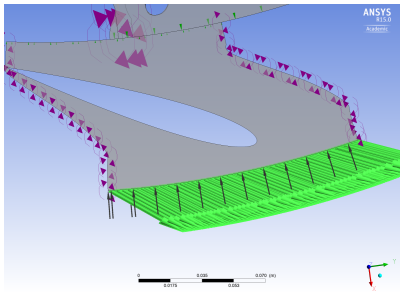

(a) Incorrect defined velocity vector

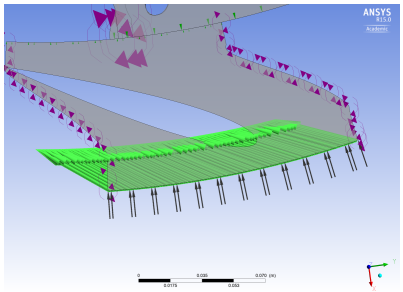

(b) Correct defined velocity vector

Figure 8.20: Different velocity vector definitions.

The incorrect vector shown in figure 8.20a is the definition used for the results given earlier, indicating that the results in this thesis may be thoroughly wrong. The vector indicates that the flow is flowing out of the inlet, rather than into it, as shown in figure 8.20b. Some test were carried out, and the results are shown in figure 8.21.

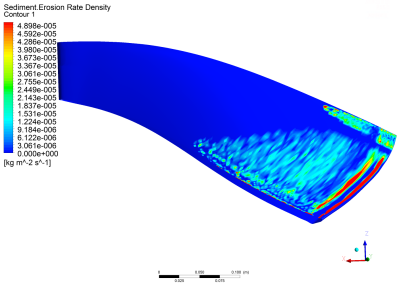

(a) NACA 0012 erosion, incorrect velocity vector

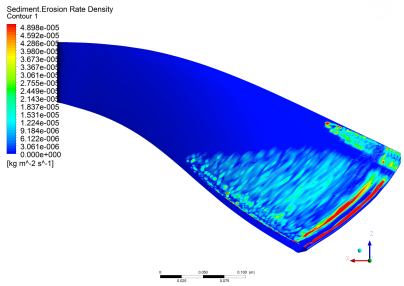

(b) NACA 0012 erosion, correct velocity vector

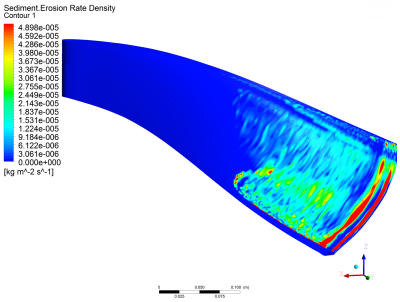

(c) NACA 4412 erosion, positive design, incorrect velocity vector

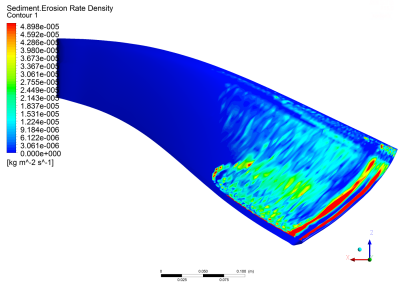

(d) NACA 4412 erosion, positive design, correct velocity vector

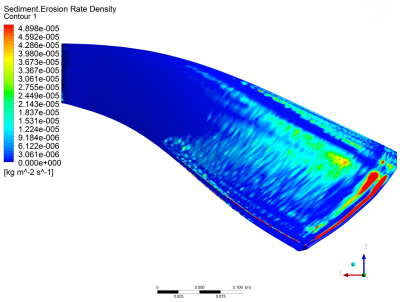

(e) NACA 4412 erosion, negative design, incorrect velocity vector

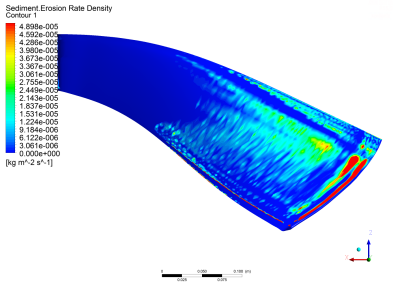

(f) NACA 4412 erosion, negative design, correct velocity vector

Figure 8.21: Comparison of erosion result with different velocity vector.

The figures show little difference in the registered erosion tendency. The streamlines on the correct system are given in Appendix H.

8.7.3 Mesh dependent erosion

A possible problem listed in section 7.4 is the mesh size regarding sediment registration. To test the assessment a coarse mesh of the profile NACA 1412 and the reference blade is created and tested for identical circumstances. The results are given in figure 8.22 and 8.23.

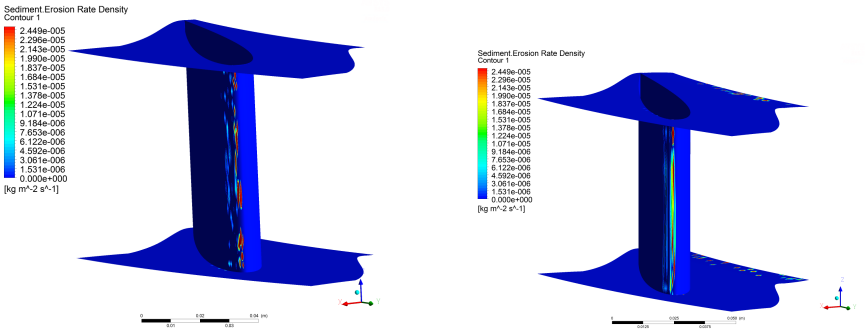

(a) NACA 0012 (reference, 250 000 nodes)

(b) NACA 0012 (coarse, 70 000 nodes)

Figure 8.22: Erosion tendency along guide vane in order $10^{-5}[kg/(m^2s)]$.

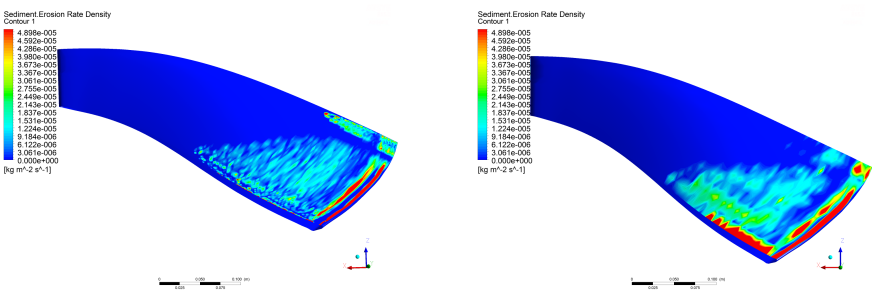

(a) NACA 0012 (reference, 250 000 nodes)

(b) NACA 0012 (coarse, 30 000 nodes)

Figure 8.23: Erosion density along the blade in order $10^{-5}[kg/(m^2s)]$.

From figure 8.22 and 8.23 it is possible to see the difference between a fine and a coarse mesh regarding the erosion. For both the guide vane and the runner the difference is very clear, but the tendencies are similar. For the runner especially is the tendency of the erosion clear as the resolution of the coarse mesh yields only an estimate of the general erosion compared to the finer mesh. The coarse mesh does however seem to predict more erosion than

the fine mesh, especially close to the shroud. This may be caused by the coarseness of the mesh, but on the fine mesh hardly any erosion is present at this position at all. In real life the erosion tendency on this position on the blade is a large problem. From this the coarse mesh may actually show more probable erosion tendency than the fine mesh. More research should be done on this subject.

9 Discussion

9.1 Pressure

The pressure is evaluated using two effects registered in the system. The first is the pressure difference across the guide vane, where the wanted effect is an equalization of the pressure, ideally resulting in no pressure difference across the blade. The second effect is the pressure field along the blade, which may affect flow stability and vortex production.

The inlet pressure distribution shows a magnitude difference between the pressure side and the suction side of the blade, which is caused by the inlet velocity vector of the flow. The velocity vector is identical for each guide vane in the flow, causing an equal pressure on the inlet. As the guide vanes are not aligned, the pressure lines are equally misaligned, as shown in figure 9.1

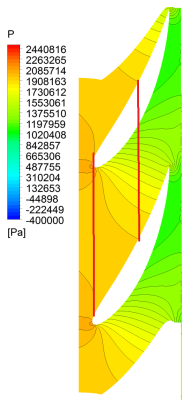

Figure 9.1: Alignment of pressure lines at guide vanes, red lines as reference.

As the pressure must be identical on each guide vane and the pressure field is changing along the blade, the pressure must be higher on the pressure side of the trailing edge than for the suction side. This pressure difference is caused by the centripetal force, caused by the circular movement of the stream.[42]

The result achieved from the simulations shows a stable pressure distribution for the reference design, shown in figure 8.1a. This is as expected given that the pressure difference along the sides is caused by the inlet angle and that a symmetrical airfoil does not have any effect on the pressure equalization. The pressure equalization is enhanced by the positive new designs, as shown in figure 8.1 and reduced with the negative design changes, shown in figure 8.3.

9.1.1 Positive design

The pressure equalization is minor as the design changes are rather small, but it is a clear tendency on the trailing edge of the blades that the pressure is more equalized. This pressure equalization is unfortunately connected to a different, negative effect of the design change. Figure 8.1b, 8.1c and 8.1d show that the pressure distribution between the guide vanes become increasingly disordered and unpredictable. This effect disturbs the flow in such degree that the positive effect of the equalization at the trailing edge is cancelled. The change may be explained with the pressure equalization, as the pressure on both sides of the blade is equalized. This effect causes the flow direction to be altered, as the flow normally is controlled by the pressure difference along two blades, with direction normal to the pressure lines, as shown in figure 8.1a. With the pressure lines increasingly altered through the design changes the flow is disrupted and a less uniform flow is the result. The tendency is most clear for NACA 4412, shown in figure 8.1d.

The pressure fields of the guide vane outlet region for the positive designs are given in figure 8.2. The figures show minor changes in the pressure field on the outlet for the different designs, but some tendencies can be observed. The general pressure difference seem to increase for the more radical designs, but the pressure difference from hub to shroud seem to decrease as the design becomes more radical. The reduced pressure difference from hub to shroud reduces the velocity in negative z-direction. This indicates a less uniform flow, but with higher density of streamlines close to the hub compared to the reference design.

9.1.2 Negative design

The implementation of the negative designs enhances the pressure difference across the guide vanes, which in real life causes larger secondary flows. Without the secondary flows the pressure changes further stabilize the pressure distribution and equalize the flow between the guide vanes, as shown in figure 8.3. The pressure distribution in figure 8.3d is especially neat, as it maximizes the pressure difference across the blade. This design should though experience increased vortexes in the flow as the pressure distribution at the trailing edge of the guide vanes are increasingly disturbed.

The pressure fields of the guide vane outlet region for the negative designs are given in figure 8.4. The figures show very small differences in the pressure field, indicating a uniform outlet condition. The pressure difference both generally and from hub to shroud seem to be reduced for the design changes. The negative implementation of NACA 2412 display an extreme uniform pressure distribution, shown in figure 8.4c. This outlet show an almost total uniform pressure field, despite the more detailed labeling used for these figures. The pressure distribution may be a calculation curiosity,

as a pressure field this uniform is unlikely for any design. However, this result will to a high extent affect the erosion result for this profile, and the results regarding both pressure field and the velocity distribution at the outlet indicate that the uniform result in figure 8.4c is correct and it is therefore considered valid in this thesis. The pressure difference is increased for NACA 4412, given in figure 8.4d, indicating that the tendency have reached its maximum for NACA 2412.

9.2 Velocity

To further examine the stream in both guide vanes and runner, the velocity fields in both areas are examined. The velocity fields are evaluated on similar parameters as the pressure, the velocity difference across the guide vane and the velocity distribution at the outlet of the guide vane.

As previously discussed is the centripetal force present at the guide vanes and causes the high pressure on the trailing edge, pressure side. This centripetal force should also be present at the trailing edge of the guide vanes, applying a force on the streamlines in circular direction. The force is presented as a bending of the streamlines in tangential direction.[40] The results given in figure 8.5a does however not show any bending tendency in the streamlines, and the force is therefore not affecting the stream after the guide vane inlet. This is a factor that may affect the results in this thesis in its absence.

9.2.1 Positive design

The velocity streamlines of the positive guide vane designs are described in figure 8.5. The subfigures show a connection between development in the velocity distribution and the pressure distribution for the design changes. The difference in velocity between NACA 0012 in figure 8.5a and NACA 4412 in figure 8.5d shows an extensive increase of velocity along the pressure side of the guide vane, reducing the pressure difference across the guide vane. The increased velocity at the pressure side of the blade also causes the velocity at the trailing edge and outlet of the guide vane region to increase in some areas. This makes the outlet region less uniform and causes the creation of more vortexes, opposing the effect from the pressure equalization. This is clear from the figurers 8.6, 8.7 and 8.8. One can clearly see the increase of vortexes from NACA0012 in figure 8.6a to NACA 4412 in figure 8.6d, which probably appear due to the velocity distribution and pressure distribution in the respective guide vanes. The figures show that the pressure distribution and the velocity distribution correlate, which is as expected.

9.2.2 Negative design

The results for the negative designs show similar connection between the velocity distribution and the pressure distribution as the positive designs,

given in figure 8.3 and 8.9. The velocity at the outlet of the guide vane region get less uniform as the design change, while the velocity difference across the blade increases. This correlates to the increasing pressure difference across the blade shown in figure 8.3, which is as expected from airfoil theory.[31]

The velocity distributions for the negative designs at the outlet are more uniform than for the positive velocity changes, shown in figure 8.5 and 8.9 respectively, which causes the pressure distribution to be more uniform. These results are according to the observations done for the pressure distribution. The velocity field for NACA 2412 is particularly uniform, given in figure 8.9c, which supports the result from the outlet pressure distribution. The transformation from figure 8.9a to 8.9c may be explained from the velocity transformation on the pressure side of the guide vane. The highest velocities in the outlet region of the reference guide vane are present for the streamlines in the middle of the flow. This area is less affected by the guide vanes and has therefore more kinetic energy and higher velocity. As the guide vane design is altered, larger parts of the flow are affected and the region shift. The previously high-speed region is because of the design changes increasingly affected by the streamlines from the pressure side of the guide vane, which experiences a decrease in velocity. This reduces the velocity in the high-speed region. A previously low-speed region is likewise affected by the altered design, causing an increase in the velocity in this region. For the NACA 2412 profile, the effect of the velocity reduction in the high-speed region and velocity increases in the low-speed region are of such magnitude that they equalize each other, causing a relative uniform velocity field for this specific design.

When observing the NACA 4412 profile it is clear that the balancing effect is tipped, and that the high-speed region is moved closer to the trailing edge of the guide vane, causing similar effect as the reference design in a different region. The effect is clearly shown in the streamlines in the runner, shown in figure 8.10, 8.11 and 8.12. In opposition of the positive design changes is the reduction of circular behaviour in the streamlines obvious, which clearly indicates a reduction in the creation of vortexes at the trailing edge of the guide vanes. The best streamlines are presented in the NACA 2412 profile, which is as expected from pressure and velocity results at the guide vane.

9.3 Erosion

From the results concerning pressure and velocity distribution, the erosion tendencies can be evaluated.

9.3.1 Positive design

The erosion tendencies for the positive designs are presented in figure 8.13 and 8.14 for guide vane and runner, respectively. The erosion on the guide vanes shows little resemblance to the pressure and velocity distributions, as the erosion seems to be reduced proportional with the design changes. The pressure field shows an increased pressure difference at the leading edge in figure 8.1, while the velocity field in figure 8.5 show an increasing velocity difference. These parameters correlate and indicate an increased erosion tendency at this point, which is the opposite of the simulated result.

The erosion on the runner blade show more correlation with the pressure and velocity results, while the results are in opposition of the initial hypothesis. In figure 8.14 the increase of erosion in both magnitude and eroded area is shown. The hypothesis indicates that the design changes should reduce the creation of secondary flows and vortexes and thus reduce the erosion. The different result may be caused by the velocity distribution at the outlet, which is discussed earlier. This effect, combined with the disturbed pressure distribution discussed previously, causes the flow to increase the vortex production in such degree that the reduction of vortexes due to pressure equalization is cancelled.

The results in figure 8.14 show an increase of erosion in the known eroded area, but the design changes also increase the erosion on the higher part of the blade. These results indicate a change in the flow direction. The streamlines along the blade are shown in figure 8.7 and several streamlines change their initial course when changing the design. Especially the NACA 2412 profile shows an increase of streamlines travelling almost horizontally through the runner, shown in figure 8.7c. The tendency may be explained from figure 8.2, showing the pressure distribution at the outlet of the guide vanes. The reference pressure distribution shows a clear pressure difference from the higher part of the region to the lower part, increasing the velocity in negative z-direction. The effect is clearly reduced for the design changes, and the NACA 2412 profile show the smallest amount of pressure levels, indicating the lowest pressure difference from hub to shroud in the stream. This tendency is broken for the NACA 4412 profile, where the pressure levels have increased and cause less erosion close to the hub. These results are given in figure 8.14c and 8.14d.

9.3.2 Negative design

The results given in figure 8.15 show the erosion tendency of the negative design changes on the guide vanes. The guide vanes show the opposite erosion tendency compared to the positive designs, given in figure 8.13. The results show a clear increase in erosion tendency on the leading edge proportional to the design change. Again the results are in opposition to the expected

result, given by the pressure and velocity distributions. As seen in the pressure distribution in figure 8.3 and the velocity distribution in figure 8.9, both the pressure difference and the velocity difference is decreasing proportional to the design change, indicating a reduction in the erosion on the leading edge.

The erosion tendencies on the runner blade with negative design guide vanes are given in figure 8.16. The results are, like the positive design changes, according to the results of the pressure and velocity if not according to the initial hypothesis. The results given in figure 8.16 indicate a reduction of erosion density on the blade but an increased eroded area for the profiles NACA 1412 and NACA 2412 in figure 8.16b and 8.16c, respectively. The erosion is multiplied for NACA 4412 in figure 8.16d. The erosive tendencies may be explained from the pressure and velocity distributions, similar to the positive design changes.

The negative designs alter the velocity fields of the outlet region of the guide vanes, causing the outlet region to become more uniform, presented in figure 8.9. The velocity equalization at the outlet observed for NACA 1412 and NACA 2412 causes the flow to travel more smooth and uniform, reducing the vortex creation at the trailing edge of the guide vanes and thus causing less erosion on the runner blade. This tendency may be explained from the streamlines presented in figure 8.11. The figure shows a much more homogenous distribution of the streamlines along the blade for both NACA 1412 and NACA 2412, with some areas with increased streamline density. The balance is tipped for the NACA 4412 profile, causing the flow to again create vortexes at the trailing edge of the guide vane. The altered position of the velocity peak, given in figure 8.9d, causes the flow to create vortexes with different effect than before. The change leads the flow to move more horizontally along the blade, with certain fields with much increased streamline density, shown in figure 8.12d. This effect causes the erosion density to be higher closer to the hub, while the erosion close to the shroud is harshly reduced.

9.3.3 Summary

Both the positive and negative design changes on the guide vane show surprising results regarding erosion tendency at the trailing edge. The primary parameters used to predict erosion indicate opposite reaction from the simulated results in both cases, making the conclusion of the tendency difficult to determine. As the particle density and flow rate is unaltered for the different designs, there are no clear reason why the erosion behaves as shown in figure 8.13 and 8.15. The erosion may be caused by direct collision between the flow and the guide vane, but this theory implies that the erosion on the leading edge is constant. As the results for both negative and positive design

show either increase or decrease of erosion, the connection is improbable. The tendency should be investigated further.

The erosion tendencies on the runner blades are according to the velocity streamlines on the blades, which are as expected. The positive designs show increased erosion for the design changes while the negative design changes overall show decreased erosion development. This result is surprising. The erosion tendency on the runner blades shows a relative clear coherence with the pressure and velocity distribution at the guide vanes and at the runner blade, verifying the results. This is opposite to the results for the guide vane, and the results are opposite of the initial hypothesis regarding the effect of guide vane design change. The results for the runner blades may be explained by the lack of secondary flows, as previously discussed. From the results gained in this thesis it is clear that the assumed negative designs are decreasing the erosion tendency while the assumed positive designs are increase it for the reference blade.

9.4 Optimal design

The usage of an erosion-minimizing runner yields some surprising results, especially regarding the positive results. The erosion on the runner using the optimized design mentioned in section 6.2 is drastically altered by using different guide vane designs, as shown in figure 8.17 and 8.18.

The implementation of the positive design changes with the optimized blade is given in figure 8.17, and show a very inconsistent result. While both NACA 0012 and NACA 4412 show a clear reduction in erosion in both erosion density and eroded area, the profiles NACA 1412 and NACA 2412 show a clear increase in both erosion density and eroded area. From the pressure distribution and velocity fields of these guide vanes there is a clear indication of vortex creation, as discussed earlier. The non-uniform situation at the guide vane outlet for these designs seems to affect the optimized runner in a negative way, as the erosion in clearly increased. There are done no other changes in the system and the results are therefore only affected by the runner change. The phenomenon should be further investigated.

The negative design changes show a more explainable development, with an decreasing eroded area size and increased erosion density. The profile NACA 4412 seems to be the best design with erosion density concentrated in a smaller area than the reference design, and with an increasing tendency closer to the leading edge. This result is not identical with the results from the reference runner design, but show a similar tendency.

9.5 Material choice

The results presented in this thesis indicate that it is possible not only to reduce the erosion tendency by changing the hydraulic design of the machinery, but to concentrate the erosion tendency on a smaller area. Ideally the erosion should be totally removed, but this idea is close to impossible. With the erosion concentrated in a small area, it can however be harshly reduced by material choice.

As commented in section 5 are different materials wear resistant for different conditions and different sediment materials. Many materials are especially sensitive to the impingement angle of the sediment, shown in figure 5.1. If the wear is limited to a small area, the impingement angle will be close to constant for the region. The limitation of erosion possibilities should make it possible to choose the most wear resistant material for a given angle, without worrying about wear damage at different positions of the system. The results in this thesis do still cover a fairly large area, making the theory only partly executable. The results for the negative design with an optimal blade given in figure 8.18 are generally the best option from these simulations, as they have reduced erosion and the eroded area is mainly close to the trailing edge. Since the choice of material can almost abolish the erosion of a specific impingement angle, the main parameter should be eroded area.The NACA 1412 profile, negative design presents itself as the best option for combination with the reference runner. This is because the erosion tendency is located in a smaller area than the other profiles, even if the erosion tendency is clearly larger for the area. The best profiles for the optimized blade are the NACA 1412, negative design, and the NACA 4412, positive design. The profile show an clear reduction of eroded area, if not necessarily reduction in erosion tendency in said area.

It should be noted that several other issues may be present regarding erosion tendency and the theory of the impingement angle is not thoroughly covered in this thesis. More research must be carried out on the subject.

A different approach of the same idea is to implement different types of coating on strategic areas of the blade, each specifically created to resist certain sediments and impingement angle. The drawback with such precision application of coating is that it will be very expensive and will not necessarily improve the erosion tendency.

9.6 Possible simulation errors

The results in this thesis are gotten by setting several parameters constant, so that the simulations will include as few variables as possible. Among these parameters are the mesh size and inlet velocity vector. As the design

change of the guide vanes are the focus, the parameters can be set constant. To enlighten any possible problems with these constants, some research is done to see what impact the change of these two parameters would have on the simulations.

In figure 8.19 the inlet velocity vector of the system is altered, so the pressure field along the guide vane is improved in terms of the secondary flows and vortex creation. The result shows a clear improvement of the pressure distribution across the blade, which should remove the secondary flows almost completely. The pressure distribution through the guide vane seems orderly, which indicates an uniform pressure distribution at the outlet. The pressure distribution does seem suboptimal on the guide vane inlet, which may cause vortex creation. If the pressure distribution at the inlet does not cause vortex creation the inlet conditions could indicate an almost perfect guide vane for preventing both secondary flows and trailing edge vortexes. The design is however not tested for other guide vane angles. The inlet conditions may not show such promising results for other guide vane openings and therefore could be unsuited for operational situations.

As mentioned in section 7.4 a current theory is that the mesh size close to the blade may affect the erosion result as these cells may be smaller than the particles, causing the calculations to ignore the effect. Figure 8.22 and 8.23 partly prove the theory, as the coarser mesh show a different erosion tendency. The erosion for the coarse mesh is similar in both magnitude and spread on the blade, but the coarser mesh show in addition an increase of erosion close to the shroud. This erosion is small in the simulation using fine mesh, while experience show that erosion close to the shroud is a large problem, shown in figure 9.2. The test shows that coarser meshes may simulate erosion more correctly, but low resolution makes precise estimation difficult. As only one test was carried out, the results are not necessarily correct and should be viewed as a strengthening of the theory only.

Figure 9.2: Erosion on runner blade close to shroud, Kali Gandaki (Photo: Kristoffer Vegdal Tabutiaux).

9.7 Design flaws

The guide vanes in this thesis are created by using data sheets acquired from the internet site "NACA Profile Archive".[43] Two of these profiles (1412 and 4412) are defined by only 40 data points, which make the curvatures rather coarse. As a result the curvatures of these designs have some flaws at the trailing edge, given in figure 6.3. The origin of the flaws is unknown, but since they do not appear on the outline created by Matlab in figure 6.2, the origin must be in the conversion from Matlab vectorial type to the .curve file type used in Turbogrid. The errors may cause flow complications at the trailing edge and may compromise the simulations for these designs. Some of the surprising results achieved in this thesis may be caused by the design flaw, as some of the most surprising results are for the NACA 1412 and NACA 4412 profiles. For the negative design changes presented in figure 8.3 the effect is present in a similar way, but as the flaw here is present at the suction side of the blade, the disfigurement have less impact on the pressure distribution of the flow, causing less vortex production and thus less erosion. These problems partly explain the surprising tendencies in both velocity and pressure distribution.

The flaw is however a rather small disfigurement, and should not create such large reaction. A similar reaction is in addition recorded for NACA 2412 in figure 8.1c, which does not have any design flaw. The tendency is smaller here, but given that it is present show that several other issues are causing the vortex production, and supporting the conclusion towards the abandonment of the theory.

In these simulations, no gap between hub/shroud and guide vane is simulated. The implementation of this gap in several meshes is too comprehensive and not well suited for a master thesis. The lack of such effect makes the changes in erosion tendency insufficient compared to a real system, as the results will be affected by the reduction of secondary flows from the positive design changes. In addition the negative design changes will suffer under the increase of secondary flows. These assumptions are made from the indications given by the pressure distributions across the blade. A further study including secondary flows must be carried out in order to verify the effect of guide vane design change.

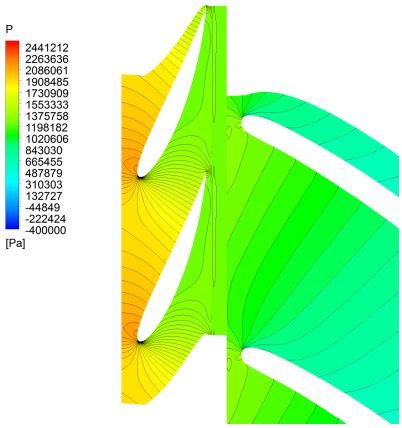

(a) NACA 0012 with outlet region, pressure

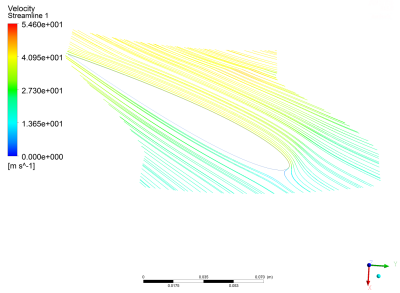

(b) NACA 0012 with outlet region, velocity

Figure 9.3: Mesh related errors for outlet region in NACA 0012 result

A different flaw in the design is the resulting guide vane from Turbogrid. The designs do sometimes lack a proper outlet region, making it difficult to simulate them. Turbogrid provides a solution for the problem by adding an alternative outlet on the mesh, creating a different region. This region creates a buffer between the runner and the guide vane, which somehow removes the effects from the guide vane. In this thesis the problem is present at the NACA 0012 profile, giving abnormal good results for both pressure distribution and velocity distribution at the trailing edge, shown in figure 9.3a and 9.3b. The problem is due to the lack of communication between the mesh interface regions. The problem should be investigated further, since the achieved results are probable and thus not easily discovered. The solution used in this thesis is to import both regions of the guide vanes in ICEM and create a merged region, which becomes very similar to regular meshes from Turbogrid with functioning outlet region. This approach should remove the difference in mesh and thus create more comparable results.

10 Conclusion

The main conclusion is that changing the guide vane design shows clear indications of change in the erosion tendency in the system, but with opposite effect of the expected from theory.

The design changes in this thesis show that the implementations of positive design changes improve the pressure distribution across the guide vanes, but disturb the pressure distribution between the guide vanes in equal or greater degree. These effects create a non-uniform velocity field at the outlet of the guide vanes, causing an increase in erosion tendency. The velocity field becomes less uniform as the design changes, increasing the erosion tendency. From the results in 8.14 the profile NACA 4412 show most erosion when secondary flows are not included.

The negative design changes show in opposition an increase in the pressure difference across the guide vanes, but improve the pressure distribution between the guide vanes. For the profile NACA 2412 the improvement is stabilizing the velocity distribution at the guide vane outlet in such degree that the region is close to uniform. The uniform pressure distribution greatly improves the erosion tendency on the runner blade. This effect cause the negative implementation of NACA 2412 to be the best alternative to reduce the erosion tendency at the runner blades in this thesis, where secondary flows are not included.

The erosion tendency on the guide vanes for the positive designs shows a clear reduction for the design changes, and the negative designs show an equal increase in erosion tendency. The recorded results for both the negative and positive designs are as expected, but the pressure and velocity distribution indicate that the tendency should be opposite. There is not found any clear explanation of this phenomenon.

When implementing an optimal runner blade in the simulation the improved erosion tendency on the runner blade is further improved, which is as expected. The best result is achieved for the negative implementation of NACA 4412. The results from the positive design changes yield some results that are inconsistent with the comparable results for the reference blade.

The results for both reference runner and optimal runner indicate that the erosion can be harshly reduced by material choice, as the eroded area is reduced. The most promising results in this thesis are the NACA 1412 negative design for reference runner and NACA 2412 negative design and NACA 4412 positive design for optimal runner.

The tests show that using coarser mesh when simulating erosion may produce more realistic results. The resolution of the results makes the results coarse and inaccurate, but the estimated tendencies show a clear connection with the observerd results at Kali Gandaki. Too few tests were carried out to conclude otherwise than to strengthen the theory.

11 Further work

The work in this thesis is the basis for further study of the guide vane design of Francis turbines. The main focus of the work has been to implement different guide vane designs in order to reduce sediment erosion, where the main focus parameter has been to reduce pressure difference across the guide vanes. The simulations have taken into consideration the connection between erosion on runner and guide vane design, which is a connection that is not well documented previously. The results show little resemblance with the initial hypothesis of the thesis, but several other conditions should be investigated further.

The effect of the secondary flows and how the pressure equalization across the guide vanes affects this flow are important for erosion estimation and should be documented. Meshes should therefore be developed that include a space between hub and shroud and guide vane, allowing a small water flow to pass across the blade. When this is accomplished, the effect of the secondary flows can be compared to the effect of the disturbed pressure distribution observerd in this thesis.

A part load test and a full load test should be carried out on the present designs. The designs in this report are simulated using BEP, and simulations on part load and full load may produce different results of erosion along the blade. An attempt of full load simulation was carried through, but simulation issues as creation of walls in the flow made the results invalid. Further research on both the wall complications and the part load/full load effect on the design changes should be conducted.

The pressure distributions show promising results when using different NACA profiles, which is according to airfoil theory[31]. Further investigation using more radical shaped guide vanes should be tested, as the equalization of pressure should be the goal. As more radical designs of NACA profiles are rather different from the current design, other flow complications like the pressure distribution disturbance and velocity field disturbance could occur and should be documented.

The effect of different runner blade designs should be investigated further. The focus has been to reduce the erosion on the blade by changing guide vane design and only briefly testing of other runner designs has been performed. As the few results in this thesis show, there is a clear possibility that the guide vane design may further enhance the erosion durability of the system when using different runner designs.

The design changes may affect which materials that are fitted for the specific turbine, as the sediment impact may have changed. This should be tested

and documented. The results in this thesis indicate that certain design changes may demand specific materials as the catchment decide a specific impingement angle for the design.

To further improve the sediment simulation other sediments should be added. The sediments in Jhimruk are only 60 % quartz and the other parts should be defined. This may change the simulated wear and change the investigation approach.

Stay vanes, draft tube and casing should be added for a complete simulation of the system. As the sediments are carried through the whole system, the design of the first parts, like casing, stay vanes and guide vanes may affect the wear on the runner and in the draft tube significantly.

The issue is not directly related to the work but the program Khoj should be reprogrammed. The tool is made in Matlab and the user is dependent on the access to the source code to ensure a reliable result. The user has access to the code, but the system is difficult to understand and not sufficiently explained. This makes alterations and new implementations in the program difficult. The implementation of the calculations should therefore be redone. The system should be reorganized in a way that the main calculations follow a clear path in the system, maybe a linear script showing the whole setup. The main script describes the calculation cells in the system, and labels each file to its role, with GUI in separate files with similar labelling. The advanced extra calculations to improve the designs implemented in the program today should still be present, as it makes the program more accurate, but should be extracted in clearly marked function file as adaptation calculations, which should be possible to remove from the process without destroying the functionality of the program.

References

[1] Hari Prasad Neopane. *Sediment Erosion in Hydro turbines.* PhD thesis, Norwegian University of Science and Technology, Department of Energy and Process Engineering, 2010.

[2] Nepal Electrical Authority. Annual report of nepal electricity authority 2012, 2012. Extracted 14.12.13.

[3] Hydroelectricity Investment & Development Company Limited. Nepal hydropower overview, 2013. Extracted 18.12.13.

[4] Biraj Singh Thapa, May 2014.

[5] C. Duan and V.I.A. Karelin. *Abrasive Erosion & Corrosion of Hydraulic Machinery.* Series on hydraulic machinery. Imperial College Press, 2002.

[6] Hermod Brekke. *Pumper og turbiner.* NTNU, Vannkraftlaboratoriet, 2003.

[7] Bhola Thapa. *Sand Erosion in Hydraulic Machinery.* PhD thesis, Norwegian University of Science and Technology, Faculty of Engineering Science and Technology, 2004.

[8] Jonas Jessen Ruud. Sediment handling problems jhimruk hydroelectric center nepal. Master's thesis, Norwegian University of Science and Technology, 2004.

[9] Mattias Rögnen. Design of a high head francis turbine exposed to sand erosion. Master's thesis, Norwegian University of Science and Technology, 2008.

[10] Hallvard Meland. A new design of a francis turbine in order to reduce sediment erosion, 2010.

[11] Ola Gjølme Thorvaldsen. Styrkeberegning i løpehjul i francisturbiner. Master's thesis, Norwegian University of Science and Technology, June 2008.

[12] Mette Eltvik. Sediment erosion in francis turbine. Master's thesis, Norwegian University of Science and Technology, June 2009.

[13] Kristine Gjøsæter. Hydraulic design of francis turbine exposed to sediment erosion, 2011.

[14] Biraj Singh Thapa. Hydraulic design of francis turbine to minimize sediment erosion. Master's thesis, Katmandu University, 2012.

[15] Helene Palmgren Erichsen. Mechanical design of francis turbine exposed to sediment erosion, 2011.

[16] Mette Eltvik. *Sediment erosion in Francis turbines*. PhD thesis, Norwegian University for Science and Technology, 2013.

[17] Peter Joachim Gogstad. Hydraulic design of francis turbine exposed to sediment erosion, 2012.

[18] G.W. Stachowiak and A.W. Batchelor. *Engineering Tribology*. Tribology series. Elsevier Science, 1993.

[19] G.V. Samsonov. *Handbook of the physicochemical properties of the elements*. Instituto de Fomento Industrial, 1968.

[20] Gjert Aaberge Dahl. Hydraulic machinery exposed to sediment erosion. Master's thesis, Norwegian University of Science and Technology, 2013.

[21] Dagfinn K Lysne, Brian Glover, Haakon Støle, and Einar Tesaker. *Hydraulic design*. Norwegian University of Science and Technology, Department of Hydraulic and Environmental Engineering, 2003.

[22] G.F. Truscott. A literature survey on abrasive wear in hydraulic machinery. *Wear*, 20(1):29 – 50, 1972.

[23] P. Bergeron. Similarity conditions for erosion caused by liquids carrying solids in suspension application to centrifugal pump impellers, 1950.

[24] W Wiedenroth. 'the influence of sand and gravel on the characteristics of centrifugal pumps, some aspects of wear in hydraulic transportation installations. In *Proceedings of First Int. Conference on the Hydraulic Transportation of Solids in Pipes, AL King, MJ Rowat and HS Stephens, Eds., BHRA Fluid Engineering, Cranfield, Bedford, UK*, pages E1–28, 1970.

[25] K. Wellinger, H. Uetz, and M. Gürleyik. Gleitverschleissuntersuchungen an metallen und nichtmetallischen hartstoffen unter wirkung körniger stoffe. *Wear*, 11(3):173 – 199, 1968.

[26] Anne Marie Helmenstine. Mohs scale of hardness, identify rocks & minerals using hardness. http://chemistry.about.com/od/geochemistry/a/mohsscale.htm.

[27] GL Sheldon and I Finnie. On the ductile behavior of nominally brittle materials during erosive cutting. *Journal of Engineering for industry*, 88(4):387–392, 1966.

[28] Asis Mazumda Priyabrata Adhikary, Pankaj Kr Roy. Selection of hydroturbine blade material: Application of fuzzy logic (mcda). *International Journal of Engineering Research and Applications (IJERA)*, 2013.

[29] Torbjørn Nilsen. The choice of materials for turbines. Lecture material, January 2007.

[30] Jeff Scott. Naca airfoil series, August 2001.

[31] J.F. Manwell, J.G. McGowan, and A.L. Rogers. *Wind Energy Explained: Theory, Design and Application*. Wiley, 2010.

[32] Inc. Ansys. Product information.

[33] Florian R Menter. Two-equation eddy-viscosity turbulence models for engineering applications. *AIAA journal*, 32(8):1598–1605, 1994.

[34] CFD Online. Dimentionless wall distance, 2011.

[35] LEAP Support Team. Tips & tricks: Convergence and mesh independence study, January 2012.

[36] David Apsley. Turbulence modeling. Url, 2011. Extracted 12.12.2013.

[37] Biraj Singh Thapa, April 2014.

[38] G Grant and W Tabakoff. Erosion prediction in turbomachinery resulting from environmental solid particles. *Journal of Aircraft*, 12(5):471–478, 1975.

[39] Biraj Singh Thapa. Personal conversation, October 2013.

[40] Ole Gunnar Dahlhaug, May 2014. Waterpower Laboratory.

[41] Krishna Prasad Shrestha, June 2014. Waterpower Laboratory.

[42] The Physics Classroom. The centripetal force requirement, June 2014.

[43] Airfoil tools, 2014.

[44] *Hydraulic machines guide for dealing with abrasive erosion in water (draft)*, 2008. Technical report.

[45] Ole Gunnar Dahlhaug. Personal conversation, December 2013. Blade angle distribution.

[46] Harish Tr. Turbogrid. http://www.scribd.com/doc/159090303/Turbo-Grid, August 2013. Unofficial tutorial.

A Basic design of a Francis turbines

This section describes the calculation of the main parameters of a Francis turbine. The calculations are based on the description from "Pumper og Turbiner".[6]

Certain parameters of the system must be known or otherwise measured, like the head and the flow rate. These parameters are used to dimension the turbine. An overview of these parameters are given in table A.1. First

Table A.1: Overview main paramters

	Description	Variable	Value	Unit
General	Head	H	Known	m
	Flow rate	Q	Known	m^3/s
	Rotational speed	n	Unknown	rpm
Inlet	Rotational velocity	U_1	Unknown	m/s
	Absolute radial velocity	C_{U1}	Unknown	m/s
	Absolute meridional velocity	C_{m1}	Unknown	m/s
	Absolute velocity	C_1	Unknown	m/s
	Blade angle	β_1	Unknown	$\circ$
	Relative velocity	W_1	Unknown	m/s
	Diameter	D_1	Unknown	m
	Inlet Height	B_1	Unknown	m
Outlet	Diameter	D_2	Unknown	m
	Rotational velocity	U_2	Chosen	m/s
	Absolute radial velocity	C_{U2}	Unknown	m/s
	Absolute meridional velocity	C_{m2}	Unknown	m/s
	Absolute velocity	C_2	Unknown	m/s
	Blade angle	β_2	Chosen	$\circ$
	Relative velocity	W_2	Unknown	m/s

the submerging of the turbine is calculated. This value is decided to prevent cavitation in the system. The submerging is given by equation A.1.

$$NPSH_R = a\frac{C_{m2}^2}{2 \cdot g} + b\frac{U_2^2}{2 \cdot g} \qquad [m] \tag{A.1}$$

a and b are chosen variables, from experience chosen as described in table A.2. $NPSH_R$ has to fulfil the following requirement to avoid cavitation:

$$NPSH_R < h_{atm} - h_v a - H_s \qquad [m] \tag{A.2}$$

Where h_{atm} is the atmospherically pressure, h_{va} is the vapor pressure and H_s is the submerging of the turbine. A negative value of H_s implies that the turbine is set below tail water level.

Table A.2: NPSH constants (Brekke, 2003)

Parameter	Turbine	Pump
a	1,05 < a < 1,15	1,6 < a < 2,0
b	0,05 < b< 0,15	0,2 < b < 0,25

From here the values β_2 and U_2 must be chosen for the system. Normally the values for β_2 is between 13°and 19°, and U_2 is between 35 m/s and 40 m/s. The coherence shown in equation A.3 is used in equation A.1.

$$C_{m2} = U_2 \cdot tan(\beta) \qquad [m/s] \tag{A.3}$$

Then the submerging is defined.

Further the outlet diameter must be defined. The definition in equation A.4 is used.

$$C_{m2} = \frac{4 \cdot Q^*}{\pi \cdot D_2^2} \Rightarrow D_2 = \sqrt{\frac{4 \cdot Q^*}{\pi \cdot C_{m2}}} \qquad [m] \tag{A.4}$$

The diameter is then used in combination with the outlet velocity to find the rotational speed.

$$n = \frac{U_2 \cdot 60}{\pi \cdot D_2} \qquad [rpm] \tag{A.5}$$

As the rotational speed must be synchronized with the grid (50 Hz), the rotational speed must be refined by the number of poles in the generator.

$$n = \frac{3000}{Z_p} \qquad [rpm] \tag{A.6}$$

To keep the chosen blade angle the diameter D_2 must be corrected to D_{corr}. The correction is done by first defining $C_{m2,corr}$ from equation A.4 and define the correlation shown in equation A.7.

$$\frac{C_{m2,corr}}{C_{m2}} = (\frac{D_2}{D_{2,corr}})^2 = \frac{U_{2,corr}}{U_2} \qquad [-] \tag{A.7}$$

Given that β_2 is constant and $C_{U2} = C_{U2,corr} = 0$ the coherences given in equation A.8 is used.

$$tan(\beta) = \frac{C_{m2}}{U_2} = \frac{C_{m2,corr}}{U_{2,corr}} \qquad [-] \tag{A.8}$$

The coherence in equation A.8 leads to equation A.9.

$$D_{2,corr} = (\frac{n \cdot D_2^3}{n_{korr}})^{(\frac{1}{3})} \qquad [m] \tag{A.9}$$

If Z_P is already chosen, one may skip equation A.4 to A.5 and calculate the correct values directly.

The correct value of C_{m2} may now be calculated from equation A.3 using $U_{2,corr}$. Control of the calculated values of C_{m2} and $NPSH_R$ should be done using A.7 and A.1. The values of W_2, C_{U2} and C_2 is now possible to calculate by using geometry, as shown in figureA.1.
The inlet velocity is now defined by the Euler turbine equation, given in equation A.10.

$$\eta = \frac{1}{g \cdot H}(U_1 \cdot C_{U1} - U_2 \cdot C_{U2}) = 2 \cdot (\underline{U}_1 \cdot \underline{C}_{U1} - \underline{U}_2 \cdot \underline{C}_{U2}) \qquad [-] \quad \text{(A.10)}$$

The parameter $\underline{M} = \frac{M}{\sqrt{2 \cdot g \cdot H}}$ is a dimensionless parameter used in turbine design, where M is any variable.

By definition the turbine is operating at best point when the outlet velocity C_{U2}=0. From this equation A.10 is reduced to equation A.11. As η is chosen and U_1 is given, the value of C_{U1} is calculated.

$$\eta = 2 \cdot (\underline{U_1} \cdot \underline{C_{U1}}) \qquad [-] \qquad \text{(A.11)}$$

To find D_1 equation A.12 is used.

$$D_1 = \frac{2 \cdot \underline{U_1}}{\underline{\omega}} = \frac{2 \cdot \underline{U_1}\sqrt{2 \cdot g \cdot H}}{n \cdot \pi/30} \qquad [m] \qquad \text{(A.12)}$$

where $\underline{\omega} = \frac{n \cdot \pi/30}{\sqrt{2 \cdot g \cdot H}}$ is the rotational velocity of the turbine.

To find the last parameters C_{m1} and B_1 the assumptions given in equation A.13 and A.14 are made.

$$C_{m1} \cdot A_1 = Cm2 \cdot A_2 \qquad [m/s] \qquad \text{(A.13)}$$

$$C_{m2} = 1.17 \cdot C_{m1} \qquad [m/s] \qquad \text{(A.14)}$$

These assumptions leads to the definition of the inlet area A_1 and outlet area A_2, which coherence is given in equation A.15.

$$B_1 \cdot D_1 \cdot \pi = \frac{1.1 \cdot \pi \cdot D_2^2}{4} \qquad [m^2] \qquad \text{(A.15)}$$

From the calculated parameters, W_1 and β_1 may be found through geometry, as shown in figure A.1. Then all the main parameters of a turbine are calculated.

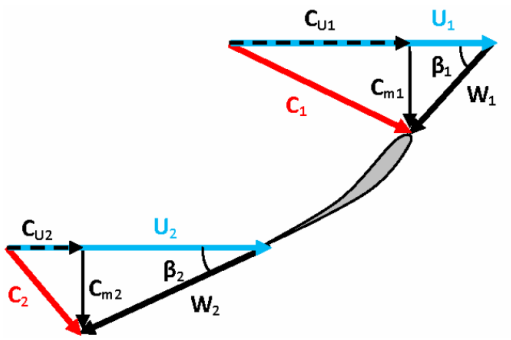

Figure A.1: Velocity triangles of a Francis turbine

B CFD

B.1 Basic equations

Fluid dynamics is based on the three fundamental principles of Newtons 2. law, mass conservation and energy conservation. These equations are solved as partial differential equations in the CFD solver as they are difficult to solve analytically.

The Continuity equation:

$$\frac{\partial \rho}{\partial t} + \Delta(\rho U) = 0 \tag{B.1}$$

The Momentum Equation:

$$\frac{\partial(\rho \cdot U)}{\partial t} + \Delta(\rho \cdot U \cdot U) = -\Delta p + \Delta \cdot \tau + S_M \tag{B.2}$$

Where τ is the stress tensor and S_M is the momentum source.

The Total Energy equation:

$$\frac{\partial \rho \cdot h_{tot}}{\partial t} - \frac{\partial \rho}{\partial t} + \partial(\rho \cdot U \cdot h_{tot}) = \partial(\Lambda \partial T) + \partial(U \cdot \tau) + U \cdot S_M + S_E \tag{B.3}$$

h_{tot} is the total enthalpy, $\partial(U \cdot \tau)$ is the viscous term, $U \cdot S_M$ is work due to external momentum sources and S_M is the energy source.

B.2 Turbulence models

For the CFD analysis certain turbulence models must be evaluated.

The famous k-ϵ model is the most common model used in CFD to simulate turbulent conditions. The model is a two-equation model which gives a general description of turbulence using transport equations. It is valid for the free stream region, but the model does not function well for the viscous layer.[13] The first variable determines the energy in the turbulence and is called turbulent kinetic energy, k. The second variable is defining the turbulent dissipation, which defines the dissipation of turbulent energy in the flow. The variable is described as ϵ.

The two equations is given in equation B.4 and eq B.5.

$$\frac{\partial(\rho \cdot k)}{\partial t} + \frac{\partial(\rho \cdot k \cdot u_i)}{\partial x_i} = \frac{\partial}{\partial x_i}[\frac{\mu_t}{\sigma_k}\frac{\partial k}{\partial x_j}] + 2 \cdot \mu_t \cdot E_{ij} \cdot E_{ij} - \rho \cdot \epsilon \tag{B.4}$$

$$\frac{\partial(\rho \cdot \epsilon)}{\partial t} + \frac{\partial(\rho \cdot \epsilon \cdot u_i)}{\partial x_i} = \frac{\partial}{\partial x_i}[\frac{\mu_t}{\sigma_k}\frac{\partial k}{\partial x_j}] + 2 \cdot \mu_t \cdot E_{ij} \cdot E_{ij} \cdot C_{1\epsilon}\frac{\epsilon}{k} - C_{2 \cdot \epsilon} \cdot \rho \cdot \frac{\epsilon^2}{k} \tag{B.5}$$

The k-ω model is less used than k-ϵ, and has a different area of use. Unlike k-ϵ, it works best at the viscous layer near the wall. The parameter k describes, like in the $k - \epsilon$ model, the kinetic turbulent energy. The second parameter ω describe the kinetic energy specific dissipation.

The two equations in the model is the following:

$$\frac{\partial k}{\partial t} + U_j \frac{\partial k}{\partial x_j} = P_k + \beta^* \cdot k \cdot \omega + \frac{\partial}{\partial x_j}[(\nu + \sigma_k \nu_T) \cdot \frac{\partial k}{\partial x_j}] \tag{B.6}$$

$$\frac{\partial \omega}{\partial t} + U_j \frac{\partial \omega}{\partial x_j} = \alpha \cdot S^2 - \beta \cdot \omega^2 + \frac{\partial}{\partial x_j}[(\nu + \sigma \cdot \nu_T) \cdot \frac{\partial \omega}{\partial x_j}] + 2 \cdot (1 - F1) \cdot \sigma_{\omega 2} \cdot \frac{1}{\omega} \frac{\partial k}{\partial x_i} \frac{\partial \omega}{\partial x_i} \tag{B.7}$$

Both these equations are used in the SST-model proposed by Menter[33] and makes the model an attractive alternative for these kinds of simulations.

C Khoj

Khoj is a Matlab based design tool created at the Hydro Power Laboratory at NTNU, Trondheim. The tool is made by MSc Kristine Gjøsæter, PhD-candidates Peter Joachim Gogstad and Biraj Singh Thapa and Phd Mette Eltvik. The design software use classical calculations to make easily portable designs of Francis turbines. The results are easily transferred to programs like Ansys Turbogrid and Creo 2.

The system used in this thesis is an older version of the program due to the interest for using the guide vane design. This is not completely finished in the latest version and the program in use here is therefore of simpler stature.

The tool is tab based, and walk the user through the needed steps. The first tab define the nature of the project, either if it is a new project or is from earlier defined paramters, as shown in figure C.1.

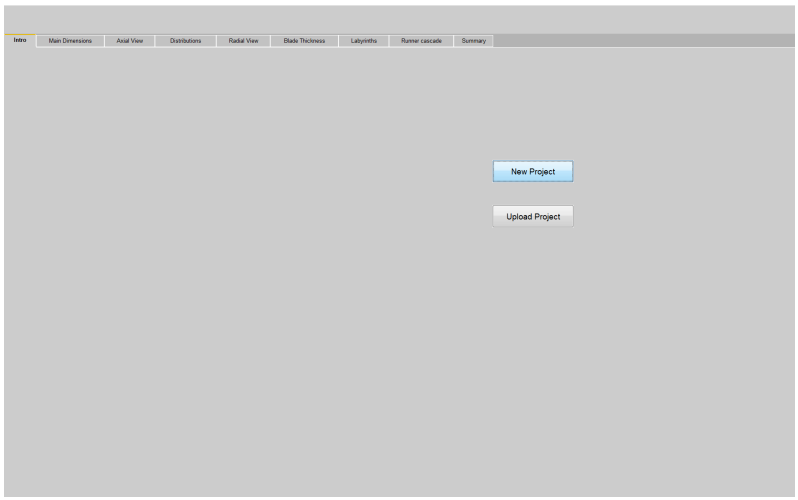

Figure C.1: First tab of Khoj.

The second tab of the program defines the main dimensions of the turbine, as shown in figure C.2. These specifications are used to calculate the coarse outline of the turbine. This definition is used further in the third tab, where the axial view of the stream lines are calculated. This tab is constructed to help the user visualize the calculations so far and makes it possible to alter the design along the process. The tab is shown in figure C.3. The axial view is a simplistic way of viewing the runner of the turbine, as it only show the curvature in a 2D perspective. To construct the runner a 3D visualization is necessary, and that is achieved by using the GH-plane. The plane is an abstract link between the axial view and the radial view, which makes it

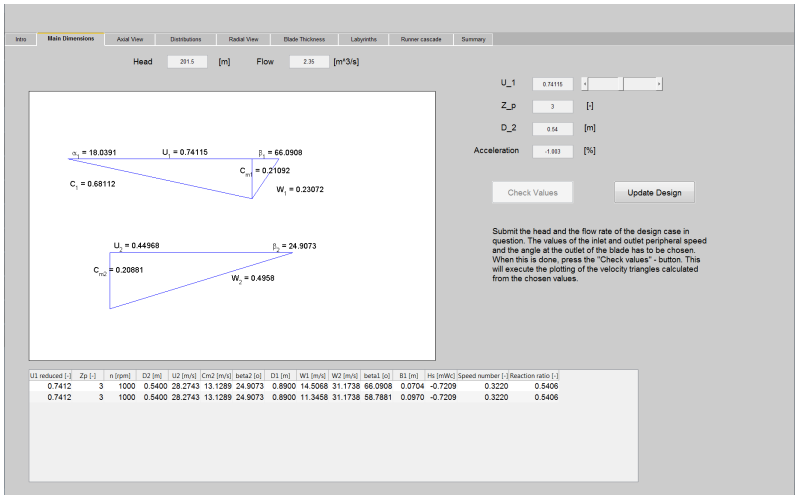

Figure C.2: Second tab of Khoj: Main Dimensions.

possible to calculate one by using the other. The plane is defined as in figure C.4

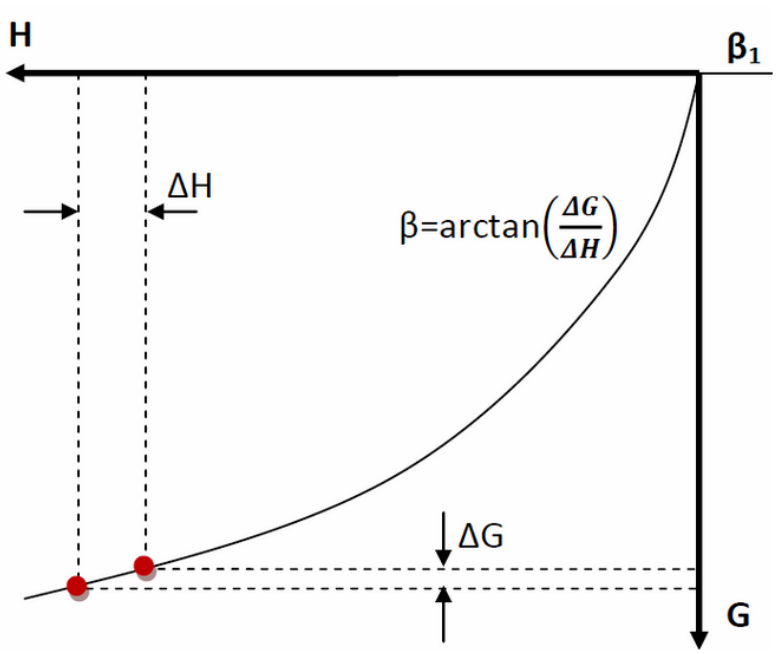

Figure C.4: Definition of the GH-plane.

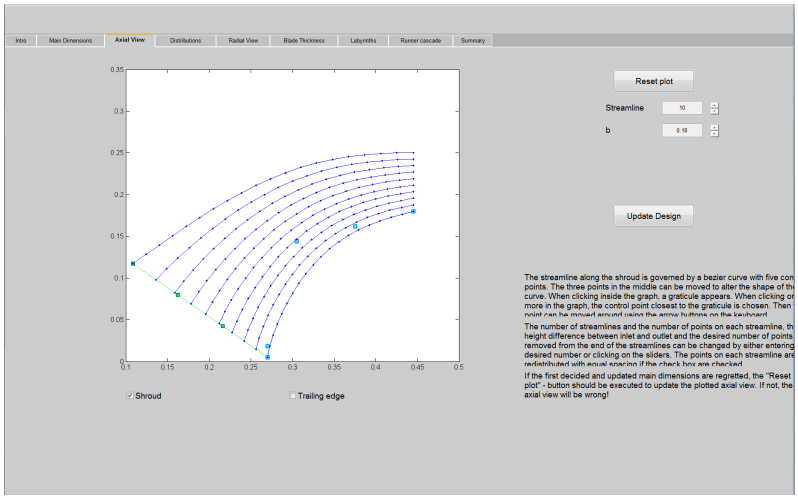

Figure C.3: Third tab of Khoj: Axial View.

The definition is used to calculate the radial view of the turbine, but first the distribution of load along the blade must be defined. This is done in the Distribution tab of the program, the fourth tab. This is shown in figure C.5

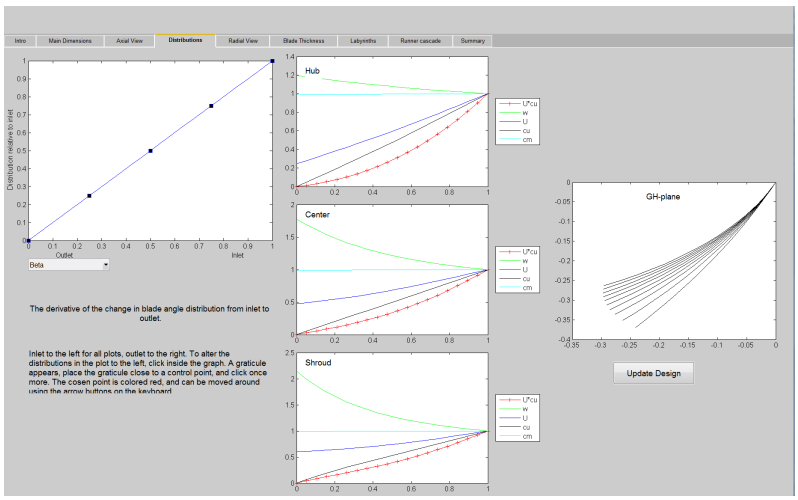

Figure C.5: Fifth tab of Khoj: Distribution.

The load of the blade is defined by either defining the blade angle β or the distribution of $U \cdot C_u$ along the blade. Both options are possible in the program.

From here the number of blades of the runner is defined, which is done

in the Radial View tab. The tab is shown in figure C.6

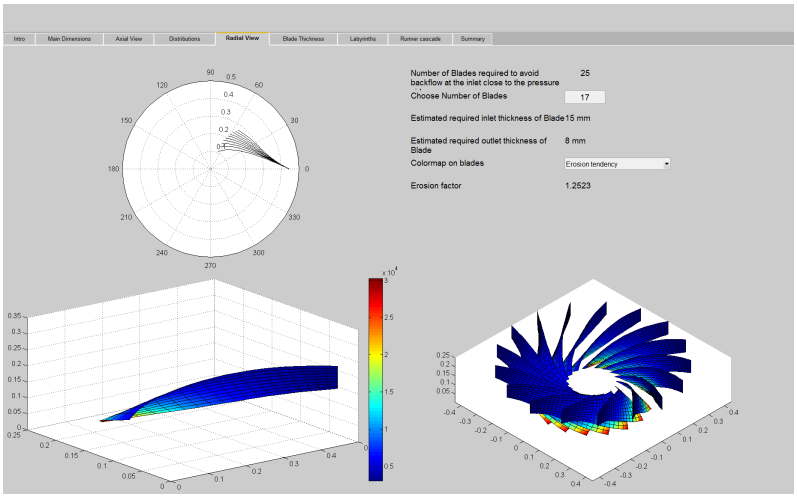

Figure C.6: Sixth tab of Khoj: Radial View.

From here the rest of the design, defining blade thickness, labyrinth seals and guide vanes should be done by using tab seven, eight and nine. These features are not included in the GUI of the used version of the program and are therefore only roughly covered in this chapter. The design of the guide vanes was in this report done by manually entering the wanted data in the code rather than using any unfinished program. The tabs are nevertheless shown in figure C.7, C.8 and C.9.

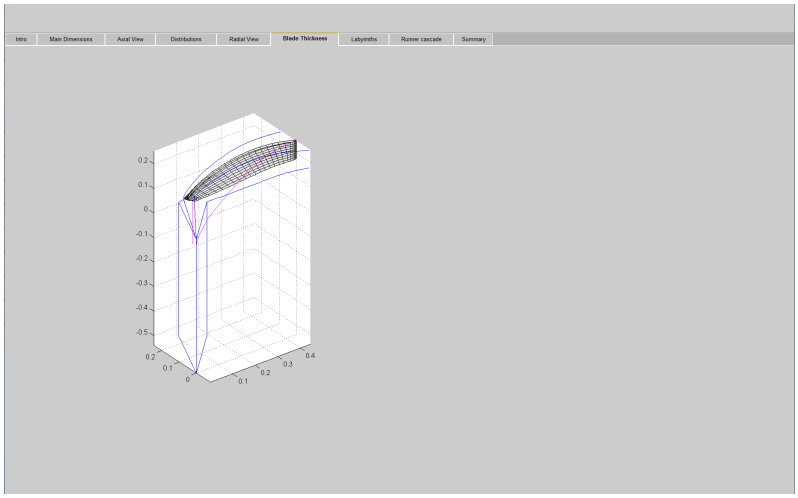

Figure C.7: Seventh tab of Khoj: Blade Thickness.

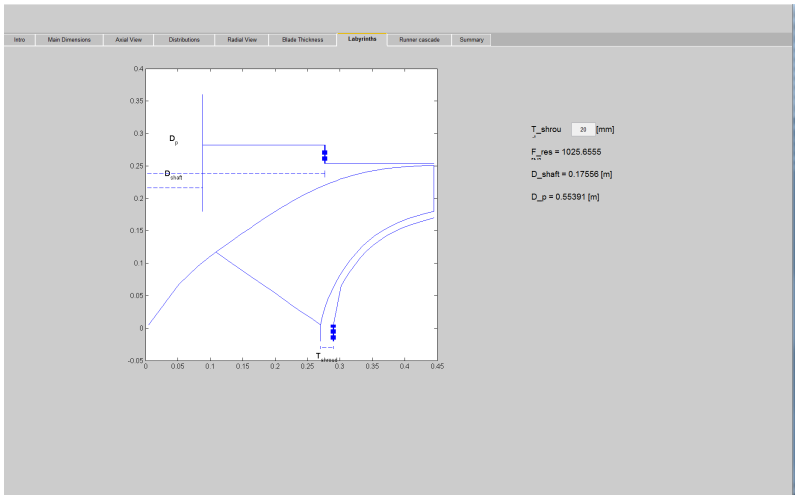

Figure C.8: Eight tab of Khoj: Labyrinths.

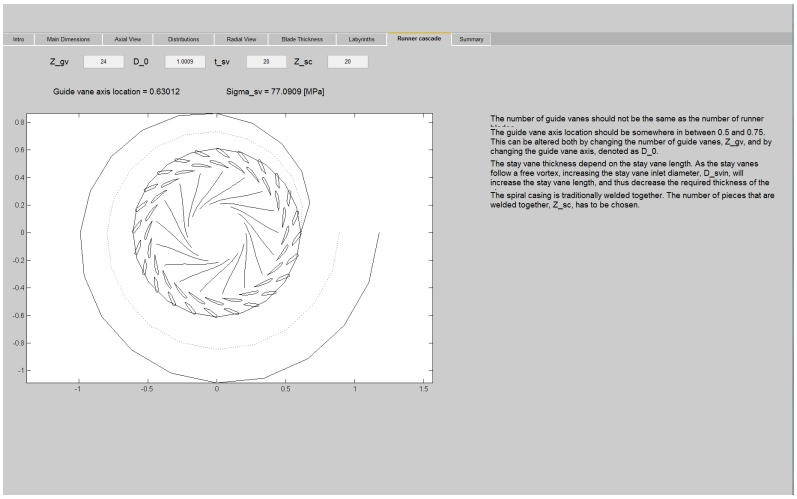

Figure C.9: Ninth tab of Khoj: Runner Cascade.

Finally, the last tab summarize the design parameters and export the design details to file formates used by the meshing software Ansys Turbogrid. Later versions of the program also convert the files compatible to the 3D-modeling program Creo 2. The final tab is shown in figure C.10

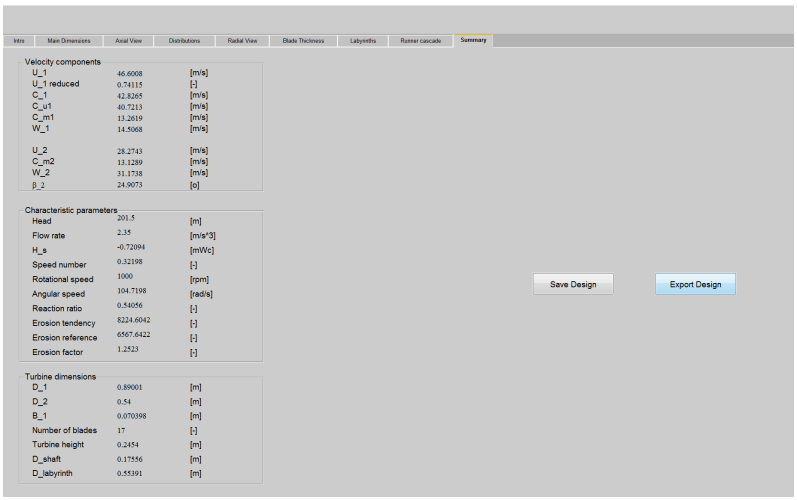

Figure C.10: Tenth tab of Khoj: Summary.

D Erosion models

This section is from the Master thesis of Kristine Gjøsæter

According to Truscott [14], several authors have given simple expressions for erosion rate as a function of velocity and particle properties based on wear test results. The most often quoted expression is as shown in equation D.1

$$Erosion \propto Velocity^i \tag{D.1}$$

where i may vary depending on material properties, but are commonly close to three.

D.1 Bergeron's model

Not all models considered by Truscott are suitable for hydraulic machinery, as they were developed for other conditions. However, Truscott also presents a more complicated expression of wear rate adjusted for hydraulic machinery which was developed by Bergeron, shown in equation D.2.

$$Erosion \propto \frac{W^3 \cdot (\rho_p - \rho_w) \cdot D^3 \cdot p \cdot K}{D} \qquad [-] \tag{D.2}$$

K in equation D.2 is an experimental coefficient dependent on the abrasive nature of particles.

D.2 Tsuguo's model

Another relation of erosion rate worth mentioning is the one established by Tsuguo. This model is based on 8 years of erosion data from 18 hydro power plants, while most of the other models are based on laboratory tests. Tsuguo's model gives the erosion rate measured as loss of thickness per unit time.

$$Erosion = \lambda \cdot K_{con.}^x \cdot K_{size}^y \cdot K_{shape} \cdot K_{hardness} \cdot K_{material} \cdot W^i [\frac{mm}{year}] \tag{D.3}$$

In equation D.3 K is coefficient of respectively concentration, size, shape, hardness and the abrasive resistance of the material. All K's are non-dimensional constants.

D.3 The IEC model

The International Electrotechnical Commission (IEC) recommends the following theoretical model of abrasion rate in order to demonstrate how different critical aspects influence the particle erosion rate in the turbine.[44]

$$\frac{dS}{dt} = f(particlevelocity,\ concentration\ and\ physical\ properties,\ flow\ pattern,\ turbine\ material\ properties\ and\ other\ factors) \tag{D.4}$$

However, it is not known how the listed variables interact with each other and thus several simplifications are introduced. Most importantly, all the variables in the model are considered independent. This simplification is not proven, but based on literature studies and experience. For hydraulic machinery, IEC suggest the expression shown in equation D.5.

$$S = W^3 \cdot PL \cdot K_{material} \cdot K_{flow} \quad [mm] \tag{D.5}$$

$K_{material}$ is the turbine material factor and K_{flow} is the flow factor.

D.4 Tabakoff's model

The Tabakoff model gives the erosion rate as the eroded wall material divided by the mass of the particles.[38] A non-dimensional mass M is found as in equation D.6.

$$M = k_1 \cdot f(\gamma) \cdot V_p^2 \cdot cos^2\gamma \cdot (1 - R_T^2) + f(V_{PN}) \tag{D.6}$$

where

$$f(\gamma) = (1 + k_2 \cdot k_5 \cdot sin(\gamma \frac{\pi/2}{\gamma_0}))^2 \tag{D.7}$$

$$R_T = 1 - k_4 \cdot V_P \cdot sin\gamma \tag{D.8}$$

$$f(V_{PN} = k_3 \cdot (V_P \cdot sin\gamma)^4 \tag{D.9}$$

k_1 to k_5 and γ_0 are model constants which depend on the particle/wall materials combined. V_p is the particle impact velocity and γ is the impact angle in radians.

Tabakoff's erosion model is implemented in the Ansys CFX solver and might thus be used to predict the erosion rate in the CFD analyses. The total erosion rate found from CFX is defined as:

$$TotalErosionRate = M \cdot \dot{N} \cdot m_p \quad [kg/m^2s] \tag{D.10}$$

E Mesh Independency

For the simulation to be realistic the mesh must be independent, which means that the results would be the same even when using more nodes in the mesh. This can only be achieved by testing the different meshes and comparing the result.

This test is defined by using four points on the blade, measuring the absolute pressure. The blade is shown in figureE.1.

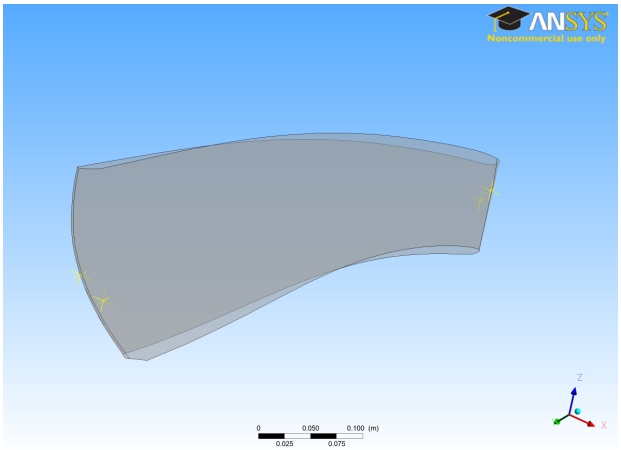

Figure E.1: Independency test nodes

The result of this test is shown in table E.1.

Table E.1: Independence test

Nodes	Pressure leading edge 1 [kPa]	Pressure leading edge 2 [kPa]	Pressure trailing edge 1 [kPa]	Pressure trailing edge 2 [kPa]	Imbalance within 1%	RMS convergence
20000	1413	1420	-40	230	yes	yes
100000	1235	1367	220	230	yes	yes
250000	1230	1332	200	128	yes	yes
1000000	1233	1340	122	184	yes	no
1500000	1235	1340	110	190	no	no

The grid dependency is shown in figure E.2.

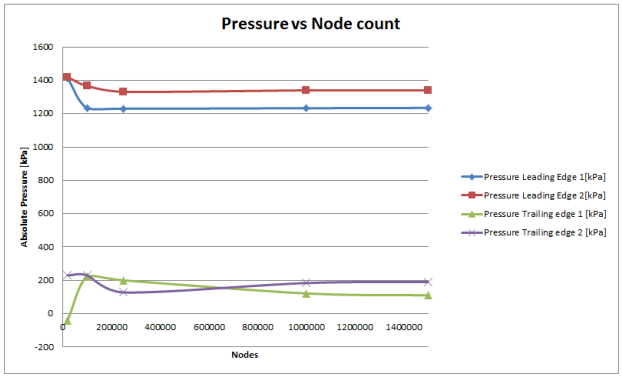

Figure E.2: Simulated pressure by node count

As one can see from figure E.2 the results are divided. The pressure on the leading edge stabilize itself on approximately 250 000 nodes, which is according to the literature. The trailing edge show some variance until stabilizing around 1 000 000 nodes. The variance from 250 000 nodes is however negligible[45], and the result are therefore according to theory. The y^+ value at the hub and shroud is for 250 000 nodes given as ~ 16, which is within the acceptable values given in the theory.

It should be noted that the result for 1 500 000 nodes in this report is not dependable, given that it fails the convergence criteria listed in the theory. This is shown in table E.1.

Similar independency tests have previously been done by Biraj Singh Thapa and Mette Eltvik.[14, 16] These tests are done based on the size of y^+. The results are given in figure E.3.

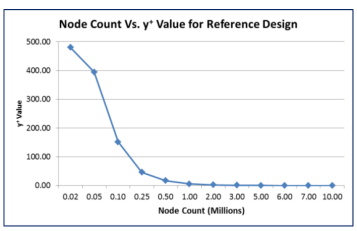

(a) Dependency of y^+ on node count (Thapa, 2011)

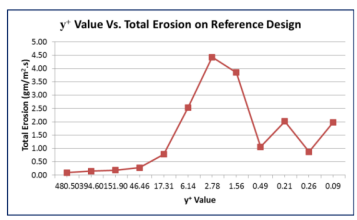

(b) Total erosion dependant on y^+ (Thapa, 2011)

Figure E.3: Independence test(Thapa, 2011)

According to these results, it is plausible to assume that a mesh coarseness of approximately 250 000 nodes will yield a sufficient accurate result, and

this mesh size is used in the simulations.

Certain parameters must be specified in TurboGrid to define the mesh.[13] The parameters are specified in table E.2.

Table E.2: Boundary layer refinement control data, TurboGrid

Proportional refinement	
Factor ratio	1,1
Near wall element size specification	
Method Reynolds number	y^+ 250 000

The parameter factor is defined as the expansion ratio of the mesh cells size from the wall. According to Gogstad[17] a small size of approximately 1.25 is recommended. Gogstad implies that a value of 1.25 is impossible to achieve due to insufficient computer memory when meeting the y^+-criteria, and therefore choose a factor of 2 in his report.[17] The computational capacity is at present sufficient to use a parameter factor for 1.1 when meeting the criteria, which has been chosen based on literature and response from TurboGrid concerning limit values.[46]

F Guide for sediment definition in CFX-Pre

This guide is written in order to save time, as the implementation and usage of the different softwares in Ansys may be difficult to comprehend in the beginning. With this one should be able to save valuable time

F.1 Defining environment

This tutorial assume a working mesh for each part is already made using Ansys Turbogrid

1. Start Ansys CFX-pre
2. Select Tools > Turbo Mode

This is the basic setup when simulating hydro machinery. The setup consists of four different steps, each described under. It is assumed in this tutorial that no interconnection from the Ansys workbench is present (otherwise, step one may be ignored).

Tab	**Setting**	**Value**
Basic Settings	Machine Type	Radial Turbine
	Axes > Coordinate frame	Coord 0
	Axes > Rotaion Axes	Z
	Axes > Axis Visibility	(marked)
Component Definition	1. Right-click Add Domain 2. In fold-down menu, select Stationary 3. (Optional) Name your domain (like Guide Vane). Default is S1 for stationary, R1 for rotating	
	Components > S1 >Component Type	Stationary
	Components > S1 > Mesh > File	Load mesh file
	Components > S1 > Mesh > File > Available volumes	Define wanted volume, for GV this is default
	Components > S1 > Passages and Alignment	(select)

Tab	Setting	Value
	Components > S1 > Passages and Alignment > Passages/Mesh > Passages per Mesh	1
	Components > S1 > Passages and Alignment > Passages to Model	1
	Components > S1 > Passages and Alignment > Passages in 360	24[a]
	Components > R1 >Component type	Rotational
	Components > R1 > Mesh > file	Load mesh file
	Components > R1> Mesh > file > Available volumes	Define wanted volume for runner
	Components > R1 > Passages and Alignment	(select)
	Components > R1 > Passages and Alignment > Passages/Mesh > Passages per Mesh	1
	Components > R1 > Passages and Alignment > Passages to Model	1
	Components > R1 > Passages and Alignment > Passages in 360	17[a]
	Region Information	(select)
	Region Information	Define regions
Physics Definition	Fluid	Water
	Model Data > Reference Pressure	1 [atm]
	Model Data > Heat Transfer	None
	Model data > Turbulence	Shear Stress Model (SST)
	Inflow /Outflow Boundary Templates	Mass Flow Inlet P-static Outlet
	Inflow /Outflow Boundary Templates > Inflow > Mass Flow	Per Machine
	Inflow /Outflow Boundary Templates > Inflow > Mass Flow Rate	(Define)[a]
	Inflow /Outflow Boundary Templates > Inflow > Inflow Direction	Cylindrical Coordinates
	Inflow /Outflor Boundary Templates > Inflow > Inflow Direction > Axial	0[-]
	Inflow /Outflor Boundary Templates > Inflow > Inflow Direction > Radial	0.5505[-][a]

Tab	Setting	Value
	Inflow /Outflor Boundary Templates > Inflow > Inflow Direction > Tangential	0.8348[-][a]
	Inflow /Outflor Boundary Templates > Outflow > P-Static	1 [atm]
	Interface > Default type	Frozen Rotor
	Solver Parameters	(none)
Interface Definition	Interfaces > R1 to R1 Periodic 1[b]	(select)
	R1 to R1 Periodic 1 > Side 1	Passage PER1[a]
	R1 to R1 Periodic 1 > Side 2	Passage PER2[a]
	Interfaces > R1 to S1[c]	(select)
	R1 to S1 > Side 1	Passage INFLOW[a]
	R1 to S1 > Side 2	OUTLET[b]
[a]Default for this particular case, may be defined differently for other cases. [b]Identically defined for cases like S1 to S1 Periodic and S2 to S2 Periodic, with different locations. [c]Identically defined for cases like S2 to R1, with different locations of course.		

Table F.1: Turbo mode

Press finish.

Now the general flow should be defined. The sediment definition is next.

F.2 Defining the Properties of Quartz

The material properties of quartz particles used in the simulation need to be defined. Heat transfer and radiation modeling are not used in this simulation, so the only property that needs to be defined is the density of the quartz particles.

To calculate the effect of the particles on the continuous fluid, between 100 and 1000 particles are usually required. However, if accurate information about the particle volume fraction or local forces on wall boundaries is required, then a much larger number of particles needs to be modeled.

When you create the domain, choose either full coupling or one-way coupling between the particle and continuous phase. Full coupling is needed to predict the effect of the particles on the continuous phase flow field but has a higher CPU cost than one-way coupling. One-way coupling simply

predicts the particle paths during post-processing based on the flow field, but without affecting the flow field.

It is possible to combine the two ways of modelling the sediments, choosing a small part of the sediment flow as fully coupled while the larger part is one-way coupled. This will not be covered in this tutorial, as the technique is the same for one sediment group.

1. Click *Material*, then create a new material named Quartz
2. Apply the following settings:

Table F.2: Sediment definition.

Tab	**Setting**	**Value**
Basic Settings	Material Group	Particle Solids
	Thermodynamic State	(Selected)
Material Properties	Thermodynamic Properties > Equation of State > Density	2.65 [g/cm3]
	Thermodynamic Properties > Molar mass	60.08 [g/mole]
	Thermodynamic Properties >Specific Heat Capacity > Specific Heat Capacity	0 [J/kg K][d]
	Thermodynamic Properties > Reference State	(Selected)
	Thermodynamic Properties > Reference State > Option	Automatic
[d] This value is not used because heat transfer is not modeled in this tutorial.		

3. Click **OK**.

F.3 Defining the flow

1. Right click Simulation in the **Outline** tree view. The domains defined earlier should now appear under the Simulation branch.
2. Double click domain S1 and apply the following settings

Table F.3: Defining sediment in flow, table 1.

Tab	**Setting**	**Value**
General Options	Basic Settings > Fluids List	Water
	Basic Settings > Particle Transportation Fluid	(Selected)
	Basic Settings > Particle Transportation Fluid > Material	Quartz
	Domain Models > Pressure > Reference Pressure	1 [atm]
Fluid Models	Heat Transfer > Option	None
	Turbulence > Option	SST[e]
Fluid Details	Quartz	(Selected)
	Quartz > Morphology > Option	Solid Particles
	Quartz > Morphology > Specific diameter	(Selected)
	Quartz > Morphology > Particle Diameter Distribution > Option	Specific diameter
	Quartz > Morphology > Particle Diameter Distribution > Option > Define diameter	0.1 [mm]
	Quartz > Erosion Model	(Selected)
	Quartz > Erosion Model > Option	Tabakoff
	Quartz > Erosion Model > K12 Constant	0.585
	Quartz > Erosion Model > Reference Velocity 1	159.11 [m/s]
	Quartz > Erosion Model > Reference Velocity 2	194.75 [m/s]
	Quartz > Erosion Model > Reference Velocity 3	190.5 [m/s]
	Quartz > Erosion Model > Angle of Max Erosion	25 [°]
	Quartz > Particle Rough Wall Model > Option	(none)

[e] The turbulence model only applies to the continuous phase and not the particle phases.

3. Apply the following settings

Table F.4: Defining sediment in flow, table 2.

Tab	**Setting**	**Value**
Fluid Details	Water	(Selected)
	Water > Morphology > Option	Continuous Fluid[f]
Fluid Pairs	Fluid Pairs	Water|Quartz
	Fluid Pairs > Water|Quartz > Particle Coupling	One-Way Coupled
	Fluid Pairs > Water|Quartz > Momentum Transfer > Drag Force > Option	(Schiller Naumann)
[f] The different ways of modeling the sediments is done by using fully coupled flow, which is CPU expensive for part of the flow, for a small part of the sediment flow and One-Way Coupled for the rest of the sediments. This is done by defining secondary sediments in the flow.		

4. Click **OK**.

5. Next, go to the **Outline** tree view. Double-click the **Inlet** boundary of your guide vane (in this tutorial called **S1 Inlet**) and follow the steps

Table F.5: Defining sediment in the flow, table 3.

Tab	**Setting**	**Value**
Basic Settings	Boundary Type	Inlet
	Location	Inlet
Boundary Details	Mass And Momentum > Option	Mass Flow Rate
	Mass And Momentum > Mass Flow Rate	97.9167 [kg/s][g]
	Flow Direction > Option	Cylindrical Components
	Flow Direction > Axial Component	0 [-][h]
	Flow Direction > Radial Component	0.5505 [-][h]
	Flow Direction > Theta Component	0.8348 [-][h]
	Axial Definition > Option	Coordinate Axis

Table F.5: Defining sediment in the flow, table 3.

Tab	**Setting**	**Value**
	Axis Definition > Rotation Axis	Global Z
	Turbulence > Option	Medium (Intensity = 5%)
Fluid Values[b]	Boundary Conditions	Quartz
	Quartz > Particle Behavior > Define Particle Behavior	(Selected)
	Quartz > Mass and Momentum > Option	Zero Slip Velocity
	Quartz > Particle Position > Option	Uniform Injection
	Quartz > Particle Position > Number of Positions > Option	Direct Specification
	Quartz > Particle Position > Number of Positions > Number	5000
	Quartz > Particle Mass Flow > Mass Flow Rate	3 [kg/s]
[g]This flow rate is defined by total flow rate divided by number of passages [h]These velocities should already be defined by the turbo mode setup.		

6. Do **NOT** specify the Particle Diameter Distribution in Fluid Values from the last tab. This value is already specified in the flow conditions and changing it here may cause complications.

G Parameters from Khoj

Table G.1: Turbine data, Khoj.

Velocity components	
U_1	46,600775
$U_{1,reduced}$	0,74115
C_1	42,826474
C_{u1}	40,721348
C_{m1}	13,261923
W_1	14,506766
U_2	28,274334
$U_{2,synchronous}$	28,274334
C_{m2}	13,128906
W_2	31,173805
$Beta_2$	24,907331
Turbine dimensions:	
Blades	17
D_1	0,890009
D_2	0,54
B_1	0,070398
b	0,18
D_{shaft}	0,175558
$D_{labyrinth}$	0,553909
Characteristical parameters	
Head	201,5
Flow rate	2,35
Rotational speed	1000
Angular velocity	104,719755
Speed number	0,321982
Submergence req,	-0,720942
Reaction ratio	0,54056
Erosion tendency	8224,604216
Erosion reference	6567,6422
Erosion factor	1,252292

Table G.2: CFX data, Khoj.

Blades	17
Flow rate	2,35
Rotational speed	-1000
Velocity components:	
Between runner and guide vanes:	
C_{theta}	0,95305
C_r	0,302814
C_z	0
Between guide vanes and stay vanes:	
C_{theta}	0,833683
C_r	0,552244
C_z	0
At stay vane inlet:	
C_{theta}	0,851614
C_r	0,524169
C_z	0

H Figures from CFX

H.1 Reference blade pressure

H.1.1 Positive design

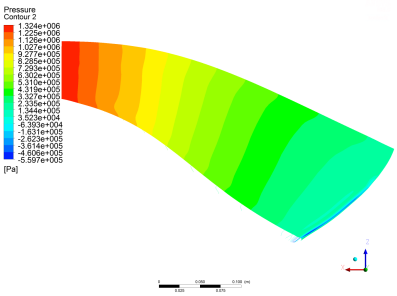

(a) NACA 0012 (reference)

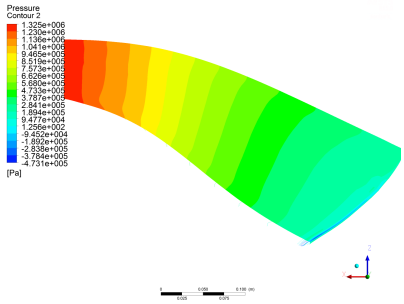

(b) NACA 1412

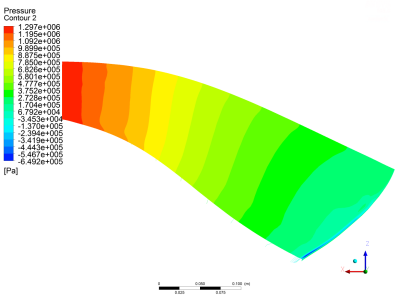

(c) NACA 2412

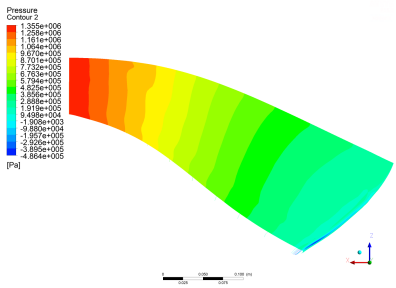

(d) NACA 4412

Figure H.1: Pressure distribution at runner blade, pressure side, positive designs.

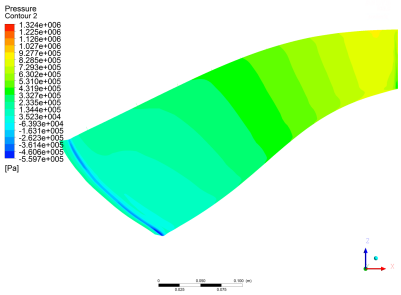

(a) NACA 0012 (reference)

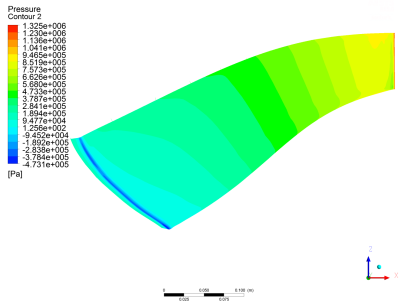

(b) NACA 1412

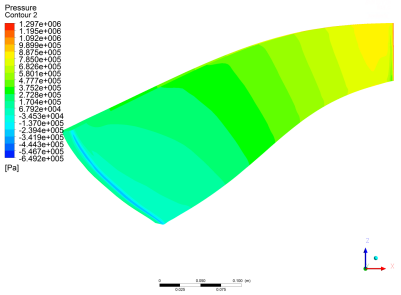

(c) NACA 2412

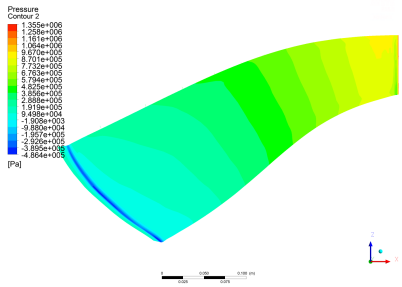

(d) NACA 4412

Figure H.2: Pressure distribution at runner blade, suction side, positive designs.

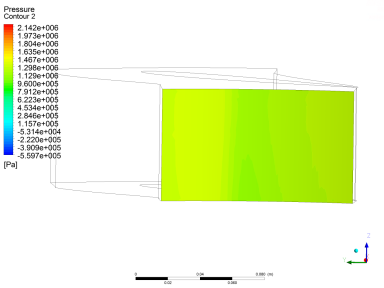

(a) NACA 0012 (reference)

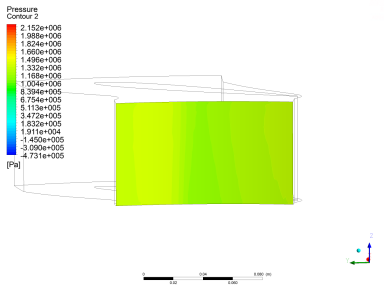

(b) NACA 1412

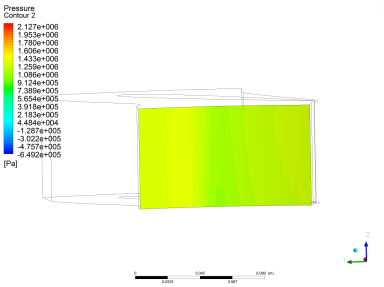

(c) NACA 2412

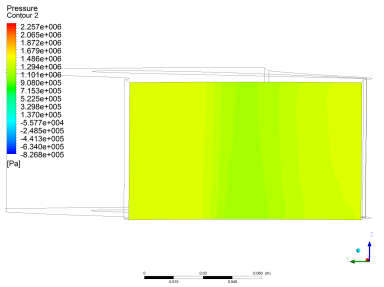

(d) NACA 4412

Figure H.3: Pressure distribution at guide vane outlet, standard label, positive design changes.

H.1.2 Negative design

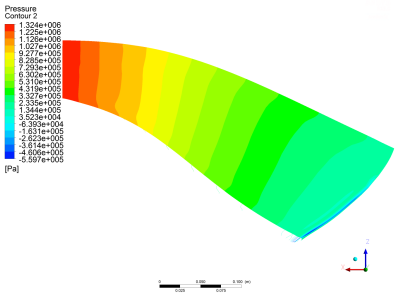

(a) NACA 0012 (reference)

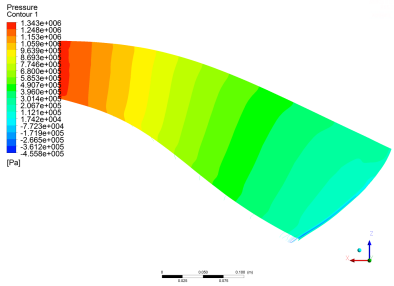

(b) NACA 1412

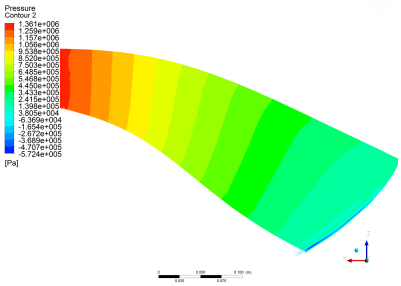

(c) NACA 2412

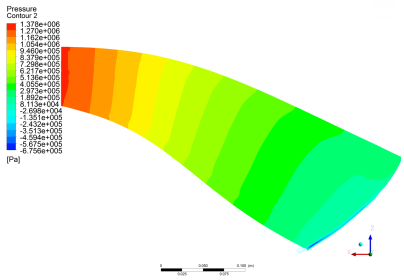

(d) NACA 4412

Figure H.4: Pressure distribution at runner blade, pressure side, negative designs.

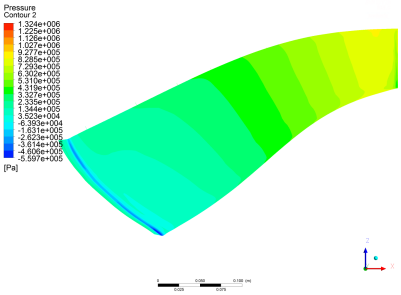

(a) NACA 0012 (reference)

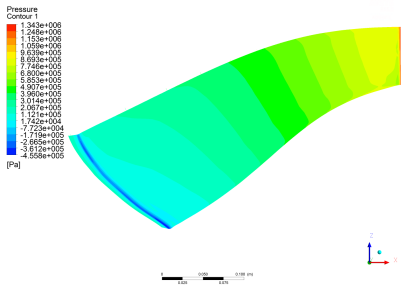

(b) NACA 1412

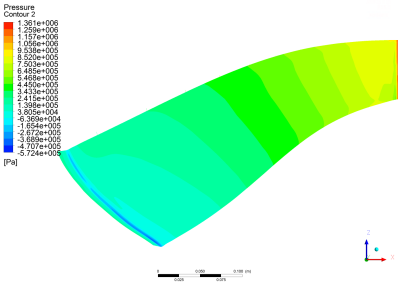

(c) NACA 2412

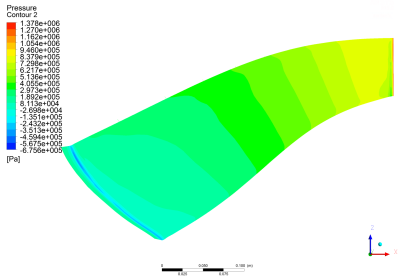

(d) NACA 4412

Figure H.5: Pressure distribution at runner blade, suction side, negative designs.

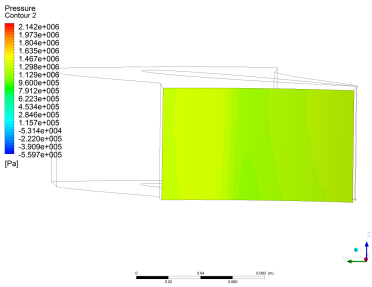

(a) NACA 0012 (reference)

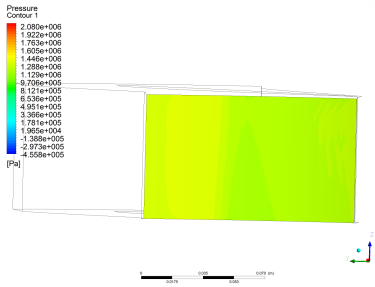

(b) NACA 1412

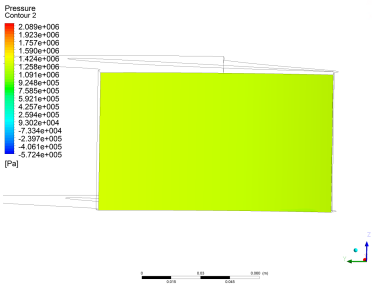

(c) NACA 2412

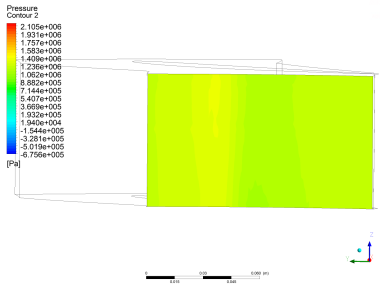

(d) NACA 4412

Figure H.6: Pressure distribution at guide vane outlet, standard label, negative design changes.

H.2 Optimal design streamlines

H.2.1 Positive design

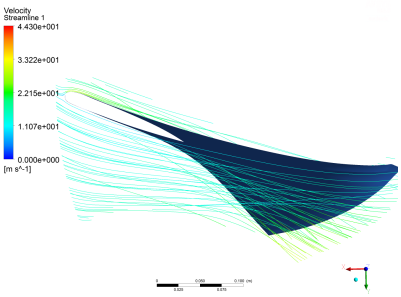

(a) NACA 0012 (reference)

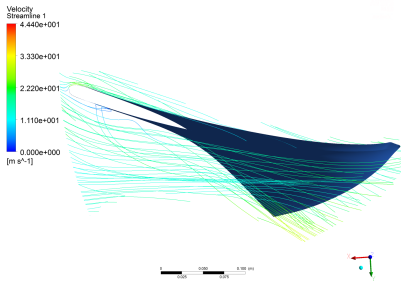

(b) NACA 1412

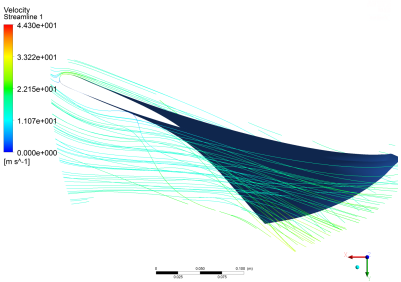

(c) NACA 2412

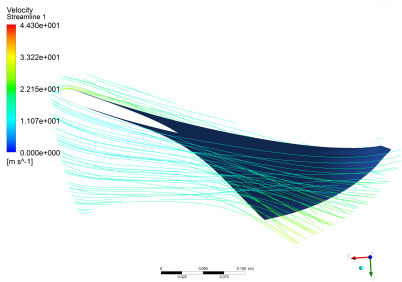

(d) NACA 4412

Figure H.7: Velocity streamlines at optimal blade, radial view.

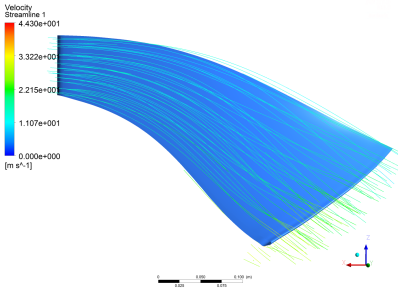

(a) NACA 0012 (reference)

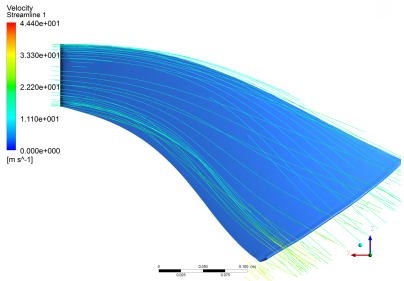

(b) NACA 1412

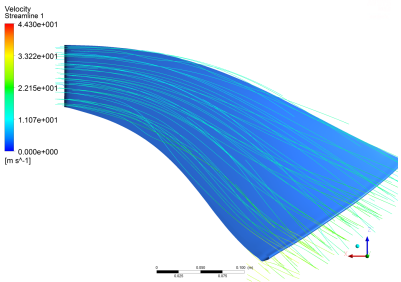

(c) NACA 2412

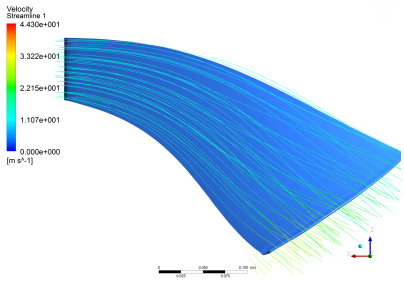

(d) NACA 4412

Figure H.8: Velocity streamlines at optimal blade, pressure side.

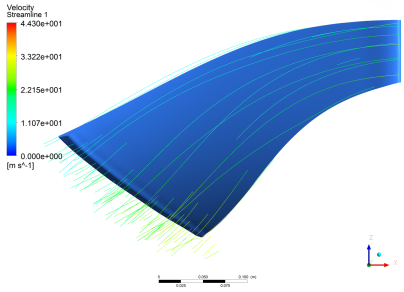

(a) NACA 0012 (reference)

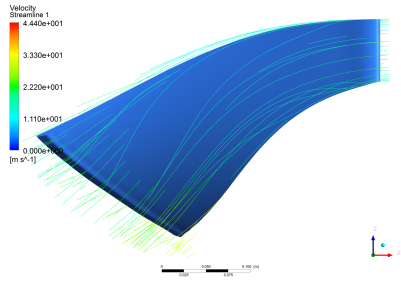

(b) NACA 1412

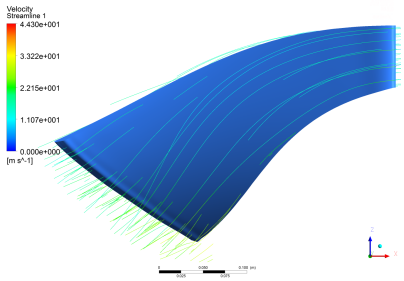

(c) NACA 2412

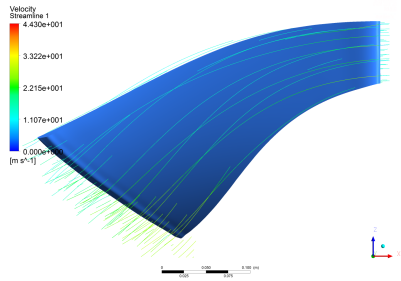

(d) NACA 4412

Figure H.9: Velocity streamlines at optimal blade, suction side.

H.2.2 Negative design

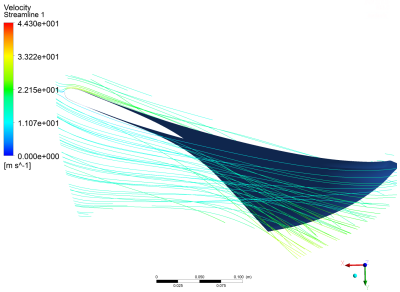

(a) NACA 0012 (reference)

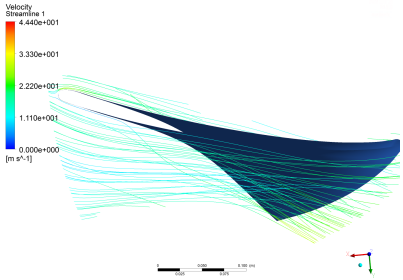

(b) NACA 1412

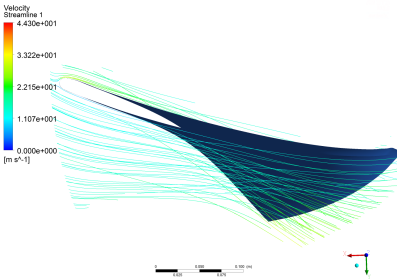

(c) NACA 2412

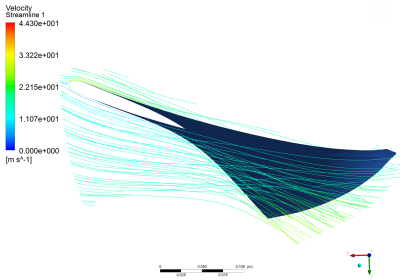

(d) NACA 4412

Figure H.10: Velocity streamlines at optimal blade, radial view.

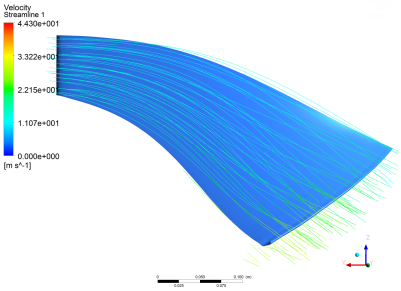

(a) NACA 0012 (reference)

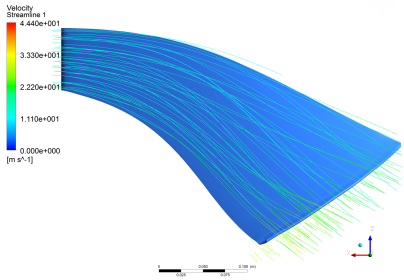

(b) NACA 1412

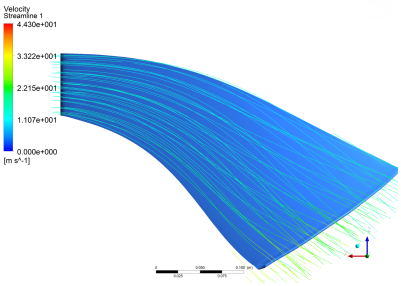

(c) NACA 2412

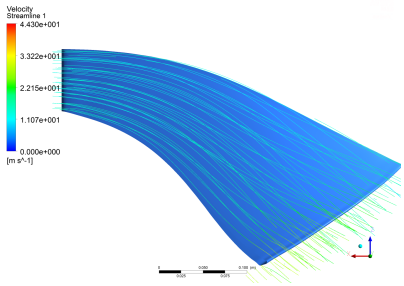

(d) NACA 4412

Figure H.11: Velocity streamlines at optimal blade, pressure side.

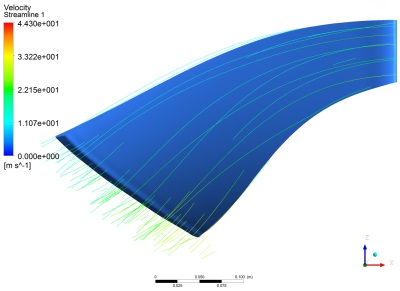

(a) NACA 0012 (reference)

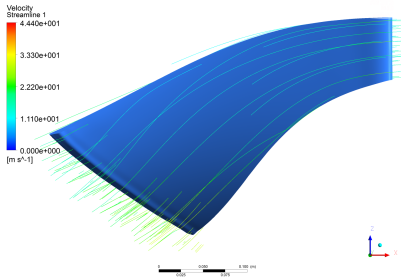

(b) NACA 1412

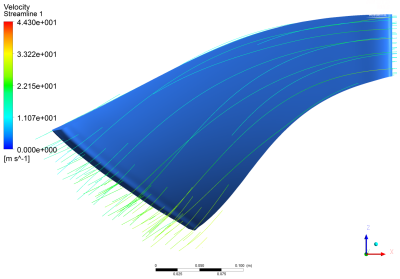

(c) NACA 2412

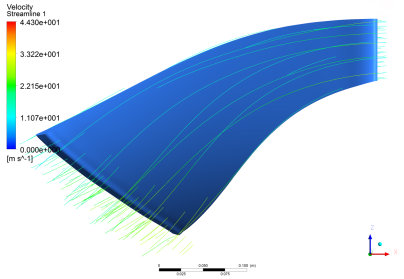

(d) NACA 4412

Figure H.12: Velocity streamlines at optimal blade, suction side.

H.3 Velocity vector direction

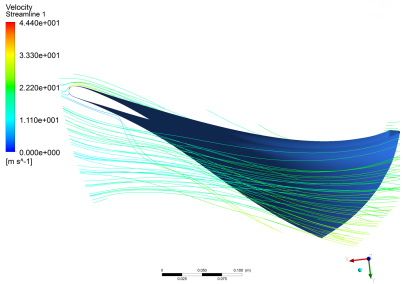

(a) NACA 0012 velocity, correct boundary vector

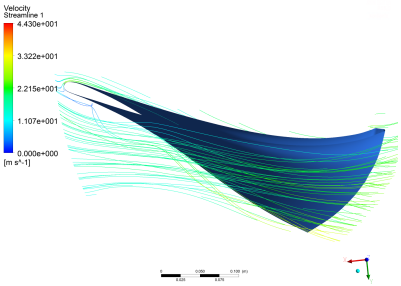

(b) NACA 4412 velocity, positive design, correct boundary vector

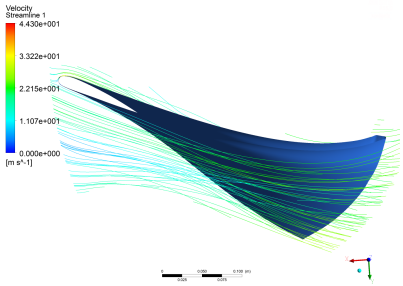

(c) NACA 4412 velocity, negative design, correct boundary vector

Figure H.13: Velocity result for correct boundary vector.

I Efficiency calculations

Table I.1: CFX Results for optimal blade design

	Reference	Positive design			Negative design			
	NACA 0012	NACA 1412	NACA 2412	NACA 4412	NACA 1412	NACA 2412	NACA 4412	unit
Rotation Speed	-104,72	-104,72	-104,72	-104,72	-104,72	-104,72	-104,72	rad/s
Inlet Volume Flow Rate	2,36	2,36	2,36	2,36	2,36	2,36	2,36	m^3/s
Reference Density	997,00	997,00	997,00	997,00	997,00	997,00	997,00	kg/m^3
Reference Diameter	0,20	0,20	0,20	0,20	0,20	0,20	0,20	m
Output Power	4,30	4,55	4,33	4,35	4,36	4,36	4,36	MW
Capacity Coefficient	2,73	2,72	2,73	2,73	2,72	2,72	2,73	
Head Coefficient	4,23	4,50	4,26	4,28	4,29	4,30	4,29	
Power Coefficient	11,12	11,75	11,21	11,25	11,29	11,28	11,29	
Total-to-Total Head	193,11	205,92	194,45	195,53	196,13	196,70	196,23	m
Total-to-Total Efficiency %	0,979	0,962	0,969	0,970	0,967	0,964	0,965	
Nozzle Loss Coefficient	0,21	0,21	0,18	0,22	0,16	0,14	0,14	
Nozzle Efficiency %	95,26	95,82	96,26	95,45	96,64	97,18	97,09	

The head of the optimal designs are reduced due to sediment load, as shown in table I.1. The low head is of little relevance for this thesis and is thus deemed satisfactory.

Table I.2: Manual efficiency calculation

Fixed Parameters	
Flow rate $[m^3/s]$	2,3571
Rotational Speed [rad/s]	104,72
Density $[kg/m^3]$	997

	Design	Profile	Torque [Nm]	Total to Total Head [m]	Total to Total Pressure [Pa]	Total Torque[Nm]	Efficiency [-]
	Reference	NACA 0012	2506,15	200,58	1961786,731	42604,55	0,964841145
Reference blade	Positive	NACA 1412	2533,5	201,53	1971078,272	43069,5	0,970772768
		NACA 2412	2555,69	203,126	1986688,062	43446,73	0,971581057
		NACA 4412	2554,99	205,41	2009026,884	43434,83	0,960514673
	Negative	NACA 1412	2461,75	199,94	1955527,166	41849,75	0,950781319
		NACA 2412	2535,97	201,67	1972447,552	43111,49	0,971044639
		NACA 4412	2542,33	201,844	1974149,371	43219,61	0,972640747
	Coarse	NACA 0012	2506,18	200,53	1961297,702	42605,06	0,965093271
Optimal blade	Reference	NACA 0012	2420,47	190,88	1866915,202	41147,99	0,979209593
	Positive design	NACA 1412 pos	2564,11	205,92	2014014,974	43589,87	0,961555827
		NACA 2412 pos	2441,11	194,45	1901831,837	41498,87	0,969428501
		NACA 4412 POS	2449,52	194,95	1906722,122	41641,84	0,970273414
	Negative design	NACA 1412 neg	2456,88	196,12	1918165,388	41766,96	0,967382979
		NACA 2412 neg	2454,7	196,68	1923642,508	41729,9	0,963772665
		NACA 4412 NEG	2458	196,6	1922860,062	41786	0,965461025

J ANSYS report

This appendix include the Ansys hydraulic turbine report for the reference design NACA 0012.

Title

Hydraulic Turbine Report

Date

2014/06/05 16:37:40

Contents

1. Introduction
   - Figure 1 Complete meridional view of the flow passage and blades
2. Performance Results
   - 2.1. Overall Performance Results
     - Table 1 Overall Performance Results Table
   - 2.2. Stage Performance Results
     - Table 2 Stage 1 Performance Results
3. Component Summary Data
   - Table 3 Component 1 Summary Data Table
   - Table 4 Component 2 Summary Data Table
   - Table 5 Component 3 Summary Data Table
4. Meanline 1-D Charts
   - Chart 1 Chart showing streamwise, area averaged Cm versus averaged normalized M.
5. Stage Plots
   - 5.1. Stage 1 Plots
     - Figure 2 Stage 1 meridional view of the flow passage and blades
     - Figure 3 Stage 1 contours of P at 50% span
     - Figure 4 Stage 1 velocity vectors at 50% span
     - Figure 5 Stage 1 contours of Ptr at 50% span
     - Figure 6 Stage 1 contours of circumferentially area-averaged P
     - Figure 7 Stage 1 contours of circumferentially area-averaged Cm
6. Component Charts
   - 6.1. Blade Loading Charts
     - Chart 2 Component 1 blade loading chart
     - Chart 3 Component 2 blade loading chart
   - 6.2. Spanwise Charts
     - Chart 4 Component 1 chart showing circumferentially averaged flow angle at the LE
     - Chart 5 Component 1 chart showing circumferentially averaged flow angle at the TE
     - Chart 6 Component 1 chart showing circumferentially averaged Cm at the TE
     - Chart 7 Component 2 chart showing circumferentially averaged flow angle at the LE
     - Chart 8 Component 2 chart showing circumferentially averaged flow angle at the TE
     - Chart 9 Component 2 chart showing circumferentially averaged Cm at the TE

---

1. Introduction

This report summarizes the results of a CFD analysis performed for the turbine geometry shown in Figure 1. In the following sections both quantitative and qualitative results are presented in the form of tables, charts and plots.

Figure 1. Complete meridional view of the flow passage and blades

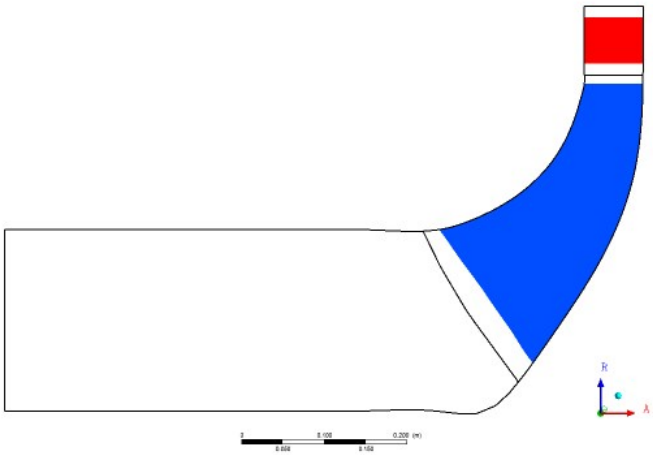

2. Performance Results

The quantitative results are summarized in the following tables. The first table shows the overall performance. The next series of tables shows the performance results for each stage.

2.1. Overall Performance Results

The following table gives the overall performance for the machine.

Table 1. Overall Performance Results Table

Inlet Volume Flow Rate	2.3571	[m^3 s^-1]
Reference Density	997.0000	[kg m^-3]
Head	205.6260	[m]
Output Power	4576570.0000	[W]

2.2. Stage Performance Results

The following table(s) give a summary of the performance results for each stage.

Table 2. Stage 1 Performance Results

Rotation Speed	-104.7200	[radian s^-1]
Inlet Volume Flow Rate	2.3571	[m^3 s^-1]
Reference Density	997.0000	[kg m^-3]
Reference Diameter	0.2022	[m]
Output Power	4576570.0000	[W]
Capacity Coefficient	2.7222	
Head Coefficient	4.4866	
Power Coefficient	11.8225	
Total-to-Total Head	205.1510	[m]
Total-to-Static Head	211.5930	[m]
Total-to-Total Efficiency %	103.3300	
Total-to-Static Efficiency %	106.5190	
Nozzle Loss Coefficient	0.1402	
Nozzle Efficiency %	97.1760	

3. Component Summary Data

The table(s) below give a summary of the mass or area averaged solution variables and derived quantities computed at the inlet, leading edge (LE Cut), trailing edge (TE Cut) and outlet locations. The flow angles Alpha and Beta are relative to the meridional plane.

Table 3. Component 1 Summary Data Table

Quantity	Inlet	LE Cut	TE Cut	Outlet	TE/LE	TE-LE	Units
Density	997.0000	997.0000	997.0000	997.0000	N/A	N/A	[kg m^-3]
Pstatic	2022030.0000	1998060.0000	1292080.0000	1245700.0000	N/A	-705983.0000	[Pa]
Ptotal	2178440.0000	2184670.0000	2138510.0000	2156520.0000	N/A	-46155.8000	[Pa]
Head	222.8070	222.7430	221.0970	220.7460	N/A	-1.6456	[m]
Static Head	206.8100	202.8950	132.2490	127.2880	N/A	-70.6467	[m]
Cm	9.7428	10.2331	11.2384	11.6938	1.0982	1.0053	[m s^-1]
Cu	14.7931	15.2157	39.3747	40.9774	2.5878	24.1591	[m s^-1]
C	17.7133	19.0664	41.0473	42.6524	2.1529	21.9809	[m s^-1]
Distortion Parameter	1.0001	1.0773	1.0212	1.0130	0.9479	N/A	
Flow Angle	56.6302	54.4712	74.2422	74.0429	N/A	19.7710	[degree]

Table 4. Component 2 Summary Data Table

Quantity	Inlet	LE Cut	TE Cut	Outlet	TE/LE	TE-LE	Units
Density	997.0000	997.0000	997.0000	997.0000	N/A	N/A	[kg m^-3]
Pstatic	1245560.0000	1185510.0000	92394.1000	110236.0000	N/A	-1093120.0000	[Pa]
Ptotal	2156360.0000	2142170.0000	192799.0000	172148.0000	N/A	-1949370.0000	[Pa]
Ptotal (rot)	204963.0000	209825.0000	166456.0000	178165.0000	N/A	-43369.2000	[Pa]
Head	220.7140	219.7890	18.7218	17.6567	N/A	-201.0680	[m]
Static Head	127.2650	119.4730	8.6221	11.2141	N/A	-110.8500	[m]
U	47.7657	46.6142	21.1757	19.9693	0.4543	-25.4384	[m s^-1]
Cm	11.6987	12.4273	12.3811	10.4473	0.9963	-0.0461	[m s^-1]
Cu	40.9764	41.5779	0.6030	-1.0531	0.0145	-40.9748	[m s^-1]
C	42.6530	43.5105	13.9228	11.0790	0.3200	-29.5877	[m s^-1]
Wu	-6.7893	-5.0365	-20.5728	-21.0224	4.0847	-15.5363	[m s^-1]
W	13.7698	14.1854	24.1599	23.5346	1.7031	9.9745	[m s^-1]
Distortion Parameter	1.0129	1.0437	1.1025	1.0359	1.0563	N/A	
Flow Angle: Alpha	74.0489	70.1687	-5.5229	-6.2078	N/A	-75.6916	[degree]
Flow Angle: Beta	-29.6649	-24.8025	-61.6301	-63.7060	N/A	-36.8276	[degree]

Table 5. Component 3 Summary Data Table

Quantity	Inlet	Outlet	Out/In	Out-In	Units
Density	997.0000	997.0000	N/A	N/A	[kg m^-3]
Pstatic	110315.0000	101208.0000	N/A	-9107.5600	[Pa]
Ptotal	172248.0000	165906.0000	N/A	-6341.3800	[Pa]
Head	17.6682	17.1816	N/A	-0.4866	[m]
Static Head	11.2236	10.2538	N/A	-0.9698	[m]
Cm	10.4460	10.6748	1.0219	0.2288	[m s^-1]
Cu	-1.0621	-0.7555	0.7113	0.3067	[m s^-1]
C	11.0803	11.1999	1.0108	0.1196	[m s^-1]
Distortion Parameter	1.0361	1.1144	1.0756	N/A	
Flow Angle	-6.0909	-1.6799	N/A	4.4110	[degree]

4. Meanline 1-D Charts

The following charts show streamwise mass or area averaged quantities from the inlet to the outlet of the full machine.

Chart 1. Chart showing streamwise, area averaged Cm versus averaged normalized M.

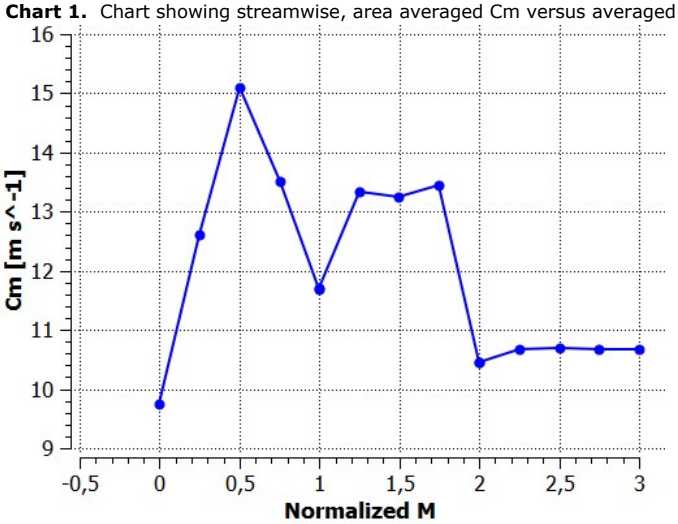

5. Stage Plots

The following plots show, for each stage, a meridional view of the geometry, blade-to-blade contour and vector views, and circumferentially averaged meridional views.

5.1. Stage 1 Plots

Figure 2. Stage 1 meridional view of the flow passage and blades

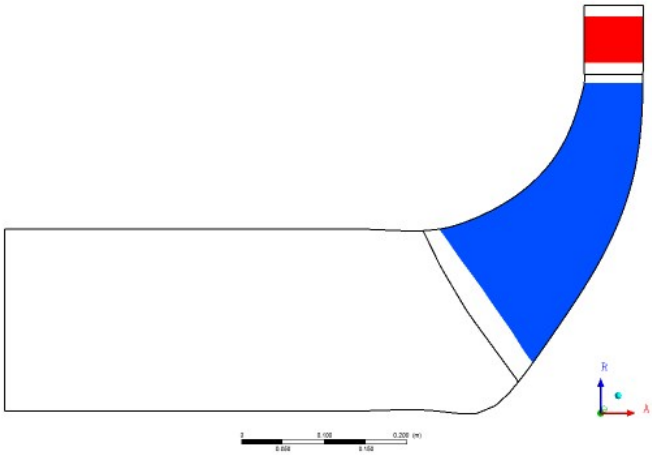

Figure 3. Stage 1 contours of P at 50% span

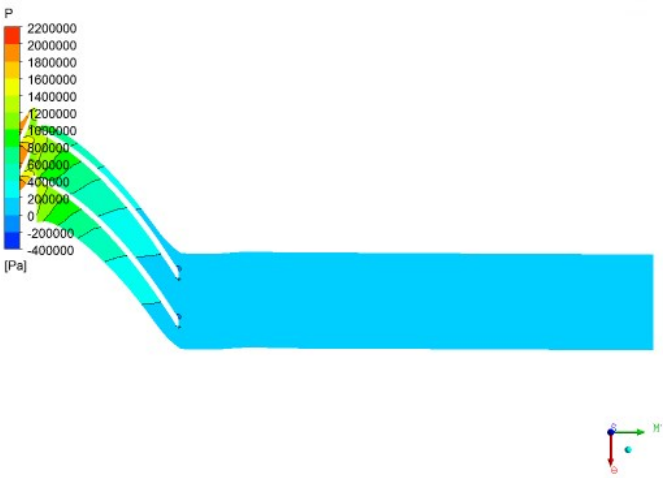

Figure 4. Stage 1 velocity vectors at 50% span

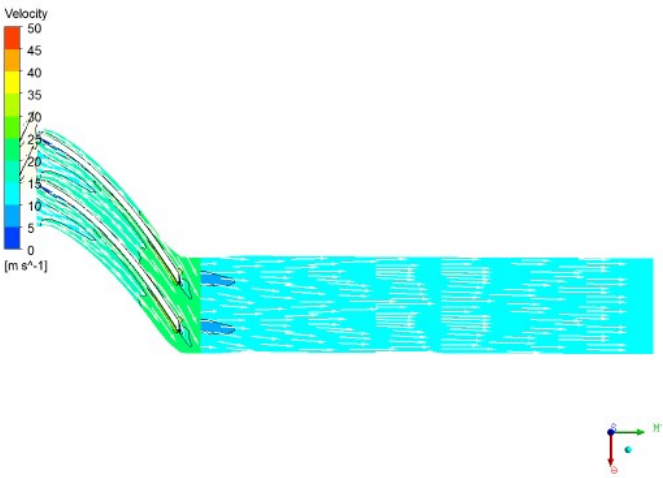

Figure 5. Stage 1 contours of Ptr at 50% span

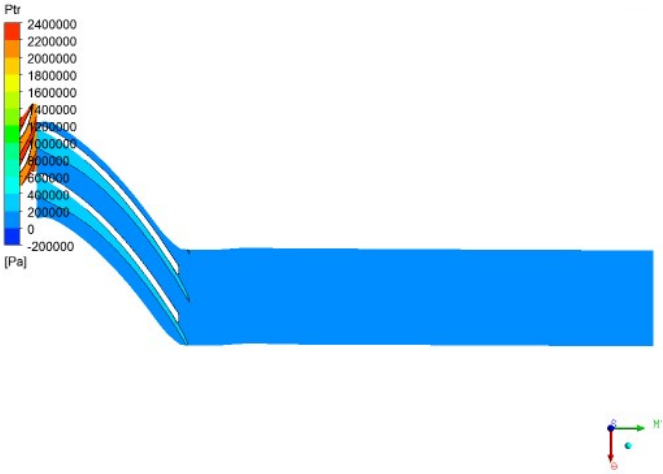

Figure 6. Stage 1 contours of circumferentially area-averaged P

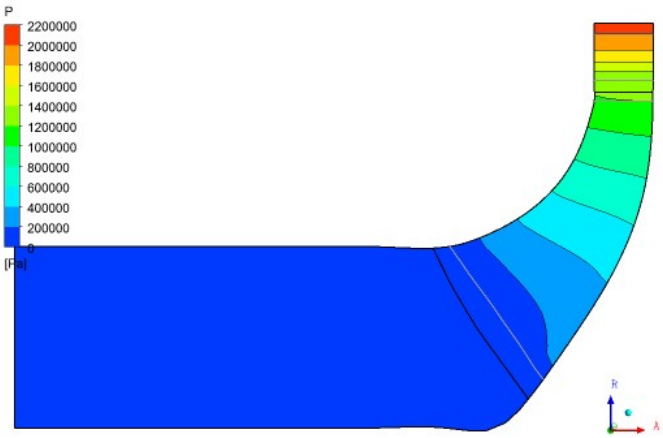

Figure 7. Stage 1 contours of circumferentially area-averaged Cm

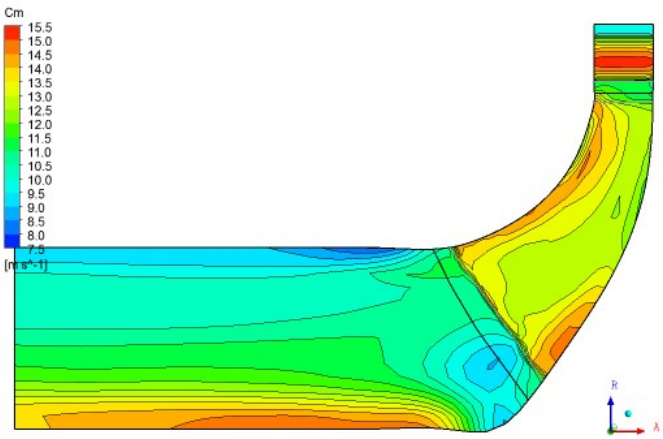

6. Component Charts

The following charts show blade loading and spanwise-averaged quantities for each component.

6.1. Blade Loading Charts

The following charts show the blade loading for each component.

Chart 2. Component 1 blade loading chart

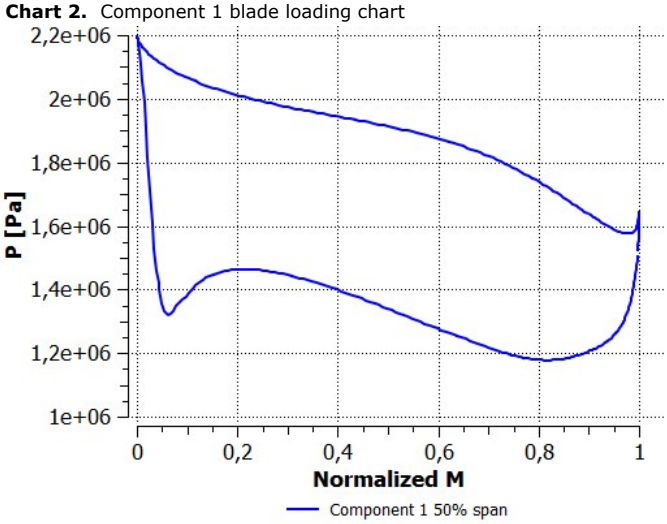

Chart 3. Component 2 blade loading chart

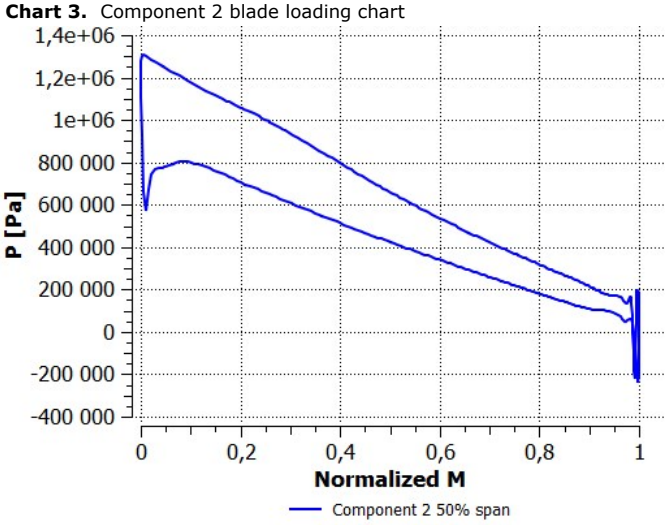

6.2. Spanwise Charts

The following charts show circumferentially averaged quantities along hub-to-shroud lines located at the leading and trailing edges of the blade.

Chart 4. Component 1 chart showing circumferentially averaged flow angle at the LE

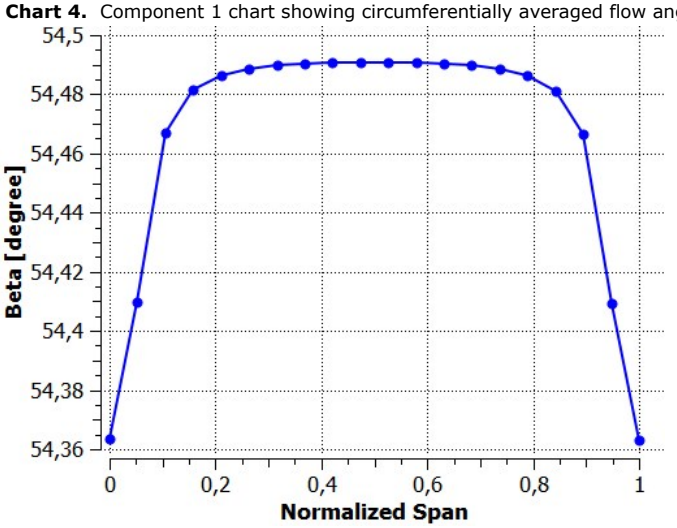

Chart 5. Component 1 chart showing circumferentially averaged flow angle at the TE

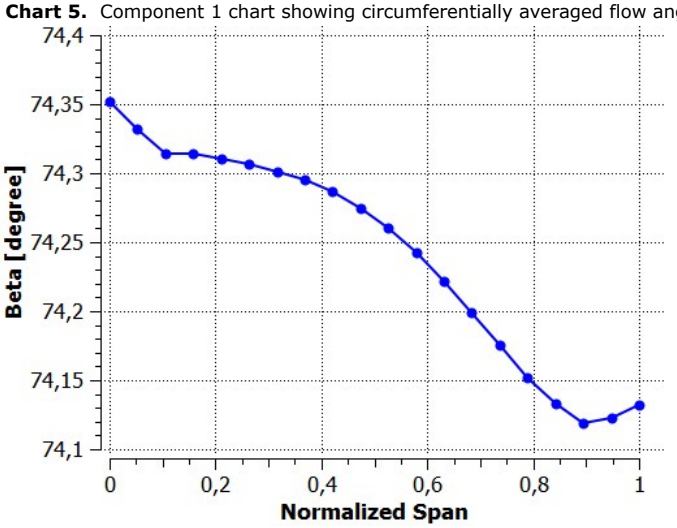

Chart 6. Component 1 chart showing circumferentially averaged Cm at the TE

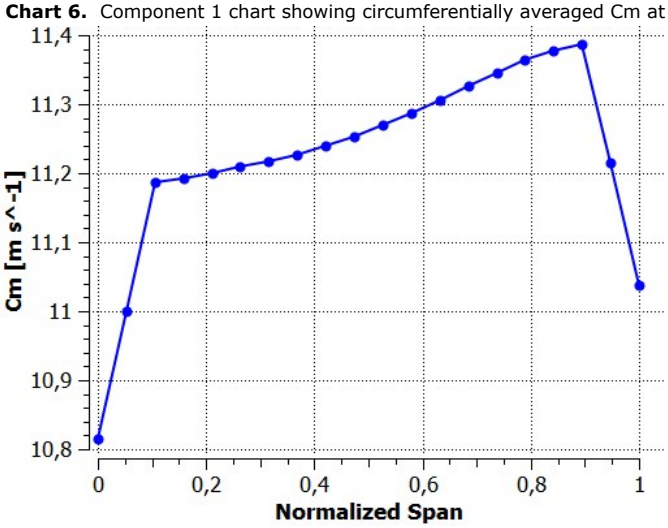

Chart 7. Component 2 chart showing circumferentially averaged flow angle at the LE

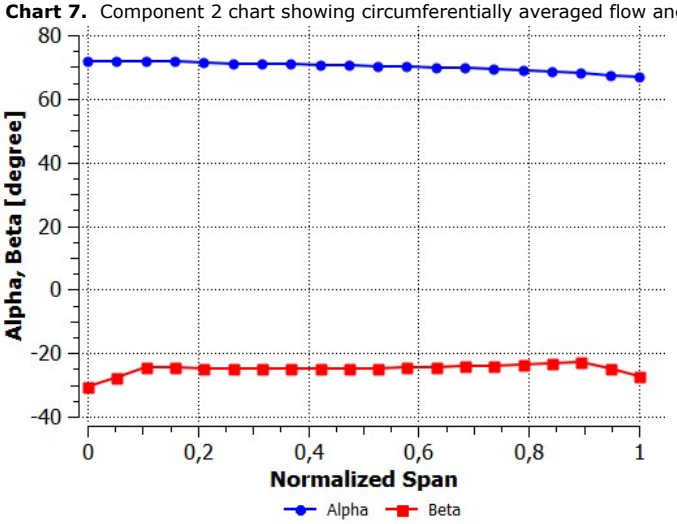

Chart 8. Component 2 chart showing circumferentially averaged flow angle at the TE

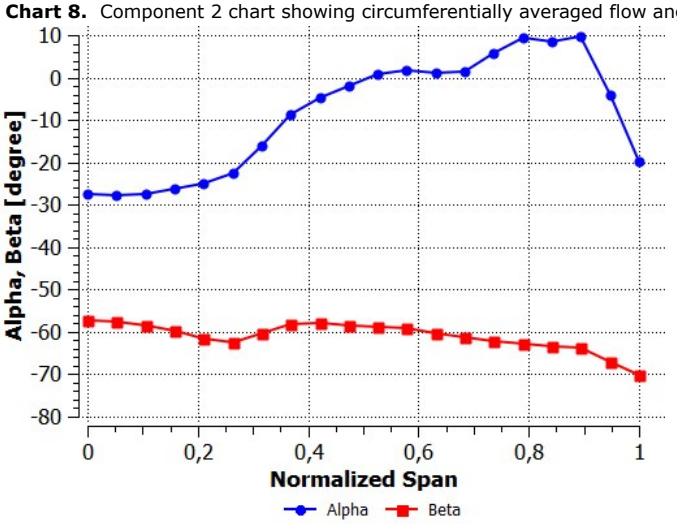

Chart 9. Component 2 chart showing circumferentially averaged Cm at the TE